GRANT NO. DE-FG03-97ER 41020
DOE/ER/41020--T1

ANNUAL REPORT

Nuclear Physics Laboratory

University of Washington

April, 1996

Sponsored in part by the United States Department of Energy under Grant DE-FG06-90ER40537

INTRODUCTION

The Nuclear Physics Laboratory of the University of Washington has for over 40 years supported a broad program of experimental physics research. The current program includes 'in-house' research using the local tandem Van de Graaff and superconducting linac accelerators and non-accelerator research in solar neutrino physics at the Sudbury Neutrino Observatory in Canada and at SAGE in Russia, double beta decay and gravitation as well as user-mode research at large accelerator and reactor facilities around the world.

Our tandem and linac accelerators continue to work very well. In the past year we upgraded our tandem/linac bunching system with the installation of a new high energy buncher which operates at 13/12 of the linac fundamental. The new buncher, which is now being used in experiments, provides much cleaner time spectra by suppressing spurious 'satellite' beam bunches by an additional factor of 10 or more. We are also upgrading our capability for high energy gamma ray detection with the installation of 2 additional large NaI spectrometers (for a total of 3) in Cave 2. This project involves the construction of a new support platform, new detector carts which move on air pads, an upgraded vacuum system and detector electronics, and will be ready for experiments beginning in late Spring.

Some highlights of our research activities during the past year are given below.

Work continues at a rapid pace toward completion of the Sudbury Neutrino Observatory in January 1997. Following four years of planning and development, installation of the acrylic vessel began last July and is now 50% complete, with final completion scheduled for September. The 'miniSNO' array of 95 photomultipliers has been assembled in the old water-shield room of the former UW Cyclotron, and is providing realistic event signals for exercising SNO electronics and data acquisition software. The Neutral-Current Detector project has also made great strides in the last year, with successful production of prototype ultrapure nickel tubing by the CVD process. Completion of very low-noise preamplifier prototypes, logarithmic amplifiers, delay lines, cable design, anchor prototyping, and endcaps for proportional counters has been carried out in parallel with commissioning of a Class-1000 cleanroom and a complex array of assembly equipment for the production phase. Design of the remotely operated submersible vehicle to be used to deploy the neutral current detectors in the acrylic vessel has been completed.

The Russian-American Gallium Experiment (SAGE) has completed a successful ^{51}Cr neutrino source experiment. The results indicate that the efficiency of the gallium detector for detection of neutrino induced events is in agreement with the efficiency determined from chemistry based methods.

The first data from ^{8}B decay have been taken in the Mass-8 CVC/Second Class Current study. The ^{8}B nuclei were produced with 15 microamps of beam from the new terminal ion source which was designed, constructed and installed this past year. The new terminal ion source will produce ^{3}He beams of up to 30 microamps and energies of up to 7.5 MeV.

The analysis of our measured barrier distributions for Ca-induced fission of prolate ^{192}Os and oblate ^{194}Pt has been completed. In addition to the expected shape signatures, a splitting due to octupole excitation of the projectile has been identified. We have also determined sensitivities to the diffuseness of the nucleus-nucleus potential.

In a collaboration with a group from the Bhabha Atomic Research Centre we have shown that fission anisotropies at energies well above the barrier are not influenced by the mass asymmetry of the entrance channel relative to the Businaro-Gallone critical asymmetry. We also have preliminary evidence at higher bombarding energy that noncompound nucleus fission scales with the mean square angular momentum, in contrast to previous suggestions.

We have measured proton and alpha particle emission spectra from the decay of A ~ 200 compound nuclei at excitation energies of 50 - 100 MeV, and used these measurements to infer the nuclear temperature. Our temperatures are in disagreement with the results of recently published experiments, but are consistent with calculations which take into account the temperature dependence of the effective mass of nucleons inside hot nuclear matter.

We have developed a stable and reliable beam of C_{60} and are starting to use it for fragmentation studies.

Our investigations of multiparticle Bose-Einstein interferometry have led to a new algorithm for putting Bose-Einstein and Coulomb correlations of up to 6th order into Monte Carlo simulations of ultra-relativistic collision events, and to a new fast algorithm for extracting event temperatures. We have shown that 3-particle correlations are not useful for single-event Hanbury-Brown, Twiss analysis, and we have found that high-order Bose-Einstein correlations amplify 'Fourier-ripple' effects arising from non-Gaussian asymmetric sources.

Preparation and construction of the detector to be used by the emiT Collaboration for a search for time reversal invariance in neutron beta-decay is nearly complete. Work at NPL has concentrated on development of the proton segment detectors and electronics as well as vacuum systems. Measurements are expected to commence in the coming year at the National Institute of Standards and Technology cold neutron facility in Gaithersburg, MD on this experiment and also on our parity-violating neutron spin rotation experiment.

As always, we encourage outside applications for the use of our facilities. As a convenient reference for potential users, the table on the following page lists the vital statistics of our accelerators. For further information, please write or telephone Professor Derek W. Storm, Director, Nuclear Physics Laboratory, University of Washington, Seattle, WA 98195; (206) 543-4085 (e-mail; STORM@NPL.WASHINGTON.EDU).

We note the retirement of Professor William Weitkamp, after serving the Laboratory for over 27 years as Technical Director.

We close this introduction with a reminder that the articles in this report describe work in progress and are not to be regarded as publications or to be quoted without permission of the authors. In each article the names of the investigators have been listed alphabetically, with the primary author to whom inquiries should be addressed underlined.

We thank Karin M. Hendrickson for her help in producing this report.

Kurt Snover
Editor

Barbara Fulton
Assistant Editor

TANDEM VAN DE GRAAFF ACCELERATOR

A High Voltage Engineering Corporation Model FN purchased in 1966 with NSF funds; operation funded primarily by the U.S. Department of Energy. See W.G. Weitkamp and F.H. Schmidt, "The University of Washington Three Stage Van de Graaff Accelerator," Nucl. Instrum. Meth. **122**, 65 (1974).

Some Available Energy Analyzed Beams

Ion	*Max. Current* (particle μA)	*Max. Energy (MeV)*	*Ion Source*
H^1 or H^2	50	18	DEIS or 860
He^3 or He^4	2	27	Double Charge-Exchange Source
He^3 or He^4	30	7.5	Tandem Terminal Source
Li^6 or Li^7	1	36	860
B^{11}	5	54	860
C^{12} or C^{13}	10	63	860
* N^{14}	1	63	DEIS or 860
O^{16} or O^{18}	10	72	DEIS or 860
F	10	72	DEIS or 860
* Ca	0.5	99	860
Ni	0.2	99	860
I	0.01	108	860

* Negative ion is the hydride, dihydride, or trihydride.

Additional ion species available include the following: Mg, Al, Si, P, S, Cl, Fe, Cu, Ge, Se, Br and Ag. Less common isotopes are generated from enriched material.

BOOSTER ACCELERATOR

We give in the following table maximum beam energies and expected intensities for several representative ions. "Status of and Operating Experience with the University of Washington Superconducting Booster Linac," D.W. Storm *et al.*, Nucl. Instrum. Meth. A **287**, 247 (1990).

Available Energy Analyzed Beams

Ion	*Max. Current* (pμA)	*Max. Practical Energy* MeV
p	>1	35
d	>1	37
He	0.5	65
Li	0.3	94
C	0.6	170
N	0.03	198
O	0.1	220
Si	0.1	300
^{35}Cl	0.02	358
^{40}Ca	0.001	310
Ni	0.001	395

TABLE OF CONTENTS

1.0 FUNDAMENTAL SYMMETRIES, WEAK INTERACTIONS AND NUCLEAR ASTROPHYSICS

1.1 Measurements of the $\alpha - \beta$ angular correlations in the beta decays of ^{8}Li and ^{8}B

M. Beck, D.T. Corcoran, L. De Braeckeleer, M. Felton, H. Lawler, J.P.S. van Schagen, H.E. Swanson, D.W. Storm, D. Wright and Z. Zhao

The $\alpha - \beta$ angular correlation in beta decays of ^{8}Li and ^{8}B are being studied as part of a test of CVC or a search for second class currents. As has been explained previously,[1] in each of these beta decays the angular correlation has the form

$$W(\theta_{\beta-\alpha}) = 1 + a_1 \cos(\theta_{\beta-\alpha}) + a_2 \cos^2(\theta_{\beta-\alpha}).$$

The coefficient a_2 results from induced weak currents. The a_1 coefficient results from the recoil of the ^{8}Be produced in the beta decays. Both of these coefficients are expected to be roughly proportional to the energy of the beta particle. For 10 MeV beta particles the kinematic term, a_1, should be 10% and the term resulting from induced currents, a_2, is expected to be around ± 3 to 4%, where the + sign is for ^{8}Li decay. Because the decaying states in ^{8}B and ^{8}Li are members of an iso-triplet, when the a_2 values obtained in each decay are subtracted, the difference results from weak magnetism, weak electricity, and from possible second class currents. If CVC holds and there are no second class currents, this term can be related to the isovector M1 and E2 widths of the decay of the corresponding member of the isotriplet in ^{8}Be. This photon measurement is discussed elsewhere in this Annual Report, and our results have been published.[2]

Our measurement of the angular correlation in the decay of ^{8}Li has been reported previously[1,3] where an upgrade of the apparatus involving two more beta detectors was mentioned. In addition, the mylar windows of the α-particle counters were changed from 200 to 140 μg/cm^2 thickness. In order to do the ^{8}B measurement effectively, the terminal ion source was developed[4] for intense ^{3}He beams. During the previous year the system with the new beta counters was first tested with ^{8}Li and then, using the terminal ion source, we carried out test runs with ^{8}B, followed by a long run with ^{8}B. We had to change the targetry for the ^{8}B production, because the intense ^{3}He beams overheated the nickel foil target wheel. (The ^{8}B is produced by the ^{6}Li(^{3}He,n) on a rotating wheel coated with ^{6}LiF. The ^{8}B activity recoils into a carbon catcher foil.) Copper, mounted on a black painted wheel, withstood the beam power and the LiF did not evaporate. While analyzing the new ^{8}B data, a new beta detector calibration technique was developed (see the following section).

Because of the symmetry of the experiment, we make two simultaneous measurements of the angular correlation with either of two alpha counters providing the reference. From the ^{8}B test run we obtained values for a_{1u}/E_β of $(-9.7 \pm 1.4) \times 10^{-3}$ MeV^{-1} and for a_{1d}/E_β of $(-9.1 \pm 0.9) \times 10^{-3}$ MeV^{-1}, while a_{2u}/E_β was $(-5.2 \pm 0.9) \times 10^{-3}$ MeV^{-1} and a_{2d}/E_β was $(-4.9 \pm 1.0) \times 10^{-3}$ MeV^{-1}. The subscripts *u* and *d* refer to the alpha particle counter upstream or downstream of the catcher, respectively. The agreement between the two pairs of values is encouraging. Although not strictly proportional to beta energy, the values of a_1 do exhibit the expected beta energy dependence, except for the case of a_{1d} at the highest energies.

The measurement of ^{8}B requires more running time than ^{8}Li, in spite of the higher ^{3}He beam intensity we have obtained, because of the lower production rate. We now have 2.2×10^7 events, compared to the total of 1.6×10^8 for ^{8}Li. The final analysis of these data is presently underway.

---

[1] Nuclear Physics Laboratory Annual Report, University of Washington (1995) p. 27.

[2] L. De Braeckeleer *et al.*, Phys. Rev. C **51**, 2778 (1995).

[3] K. Swartz, "Measurement of the $\beta - \alpha$ angular correlation in the decay of ^{8}Li," Ph.D. Thesis, University of Washington, 1996.

[4] Nuclear Physics Laboratory Annual Report, University of Washington, p. 61 (1995); G. Harper *et al.*, *Proc. Seventh Int'l. Conf. on Heavy Ion Accel. Tech.* (1995), to be published in Nucl. Instrum. Methods.

1.2 Calibration method for the β-counters in the Mass-8 experiment

J.P.S. van Schagen, K.B. Swartz and D. Wright

To obtain the coefficients a_1 and a_2 in the $\alpha-\beta$ angular correlation (see Section 1.1) as measured with the Mass-8 apparatus,[1] an accurate knowledge of the calibration of the β-counters is necessary.

This calibration must be obtained *in situ*, since no natural mono-chromatic β-sources of sufficient energy are available. However, the β-decay feeds a broad final state in ^{8}Be which subsequently decays into two α-particles.[2] A Si-counter placed at 90° with respect to all seven β-counters measured the α-particle kinetic energy T_α with high resolution. This energy, corrected for the energy loss in the catcher foil, can be related to the (total relativistic) β-endpoint energy E_0 by:

$$E_0 = Q^{+/-} + Q_{^8Be\rightarrow 2\alpha} + m_e c^2 - 2T_\alpha, \tag{1}$$

In measuring β-particles in coincidence with an α-particle in the Si-counter, spectra for different endpoint energies were obtained. These spectra were then fitted *simultaneously* to the theoretical spectral distribution for the electron/positron decay in a χ^2-minimization procedure. Only the values for the offset a_{cal}, the linear coefficient b_{cal} and the normalization constant N_{norm} for each value E_0 were varied. The spectral distribution is given by:

$$w(E_\beta, E_0)dE_\beta = \left[N_{norm} \int_{m_e c^2}^{E_0} R(E_\beta, E'_\beta) F(Z, E'_\beta, \beta^{+/-}) E'_\beta pc (E_0 - E'_\beta)^2 dE'_\beta \right] dE_\beta, \tag{2}$$

which is valid for allowed transitions and includes folding with the β-counter response. $F(Z, E'_\beta, \beta^{+/-})$ is the Fermi-function, *pc* the electron/positron momentum. For the lineshape $R(E_\beta, E'_\beta)$ a Gaussian peak with an exponential tail is used.[3]

As a typical example, Fig. 1.2-1 shows the results of the fit for an endpoint energy E_0 = 14.262 MeV where both the data and the fit have been converted to a Kurie-plot for easy comparison. The data in between the two markers were included in the region. Excellent agreement can be observed.

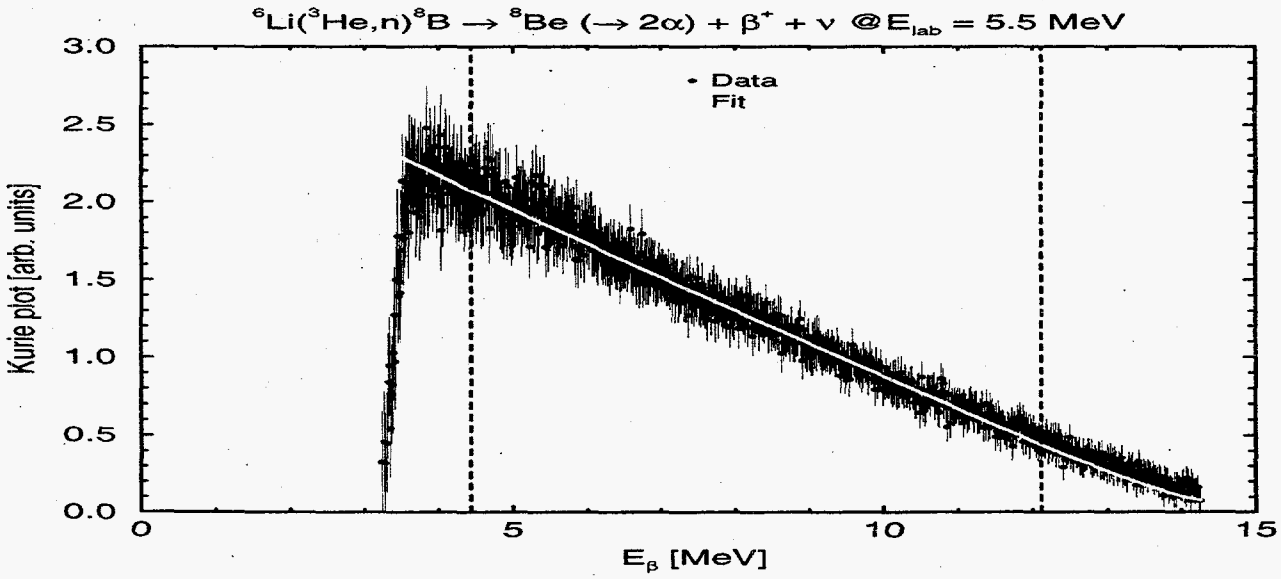

Fig. 1.2-1. Data and theoretical spectral distribution plotted as a Kurie-plot for E_0 = 14.3 MeV. The calibration coefficients are given by a_{cal} = 1.43 MeV, b_{cal} = 0.0135 MeV/CH.

[1] Nuclear Physics Laboratory Annual Report, University of Washington (1994) p. 19.
[2] Nuclear Physics Laboratory Annual Report, University of Washington (1994) p. 21.
[3] A.M. Sandorfi and M.T. Collins, Nucl. Instrum. Methods in Phys. Res. **222**, 479 (1984).

1.3 Effect of the energy loss of the α -particles on the α – β angular correlation in Mass-8

M. Beck, L. De Braeckeleer and K. B. Swartz

We developed a Monte Carlo program for the beta-decay part of the Mass-8 experiment (see Section 1.1) in order to investigate the effect of a threshold for detecting the α -particles. The threshold arises from the finite thickness of the windows of the α -counters and the thickness of the catcher foil. The simulated $\beta-\alpha$ angular correlation used the allowed GT form for the $\beta-\alpha-\nu$ angular correlation of $\omega = 1-\cos\theta_{\beta\alpha}\cdot\cos\theta_{\alpha\nu}$ and includes the kinematic boost by the recoiling ^{8}Be. Other weak form-factors were included by a generic a_2-coefficient of $a_2 = k\cdot E_\beta$ with E_β the kinetic β-energy and $k = 0.0033/\text{MeV}$ for ^{8}Li.[1]

The thicknesses of the windows and catcher foils were approximately $200\mu g/cm^2$ and $100\mu g/cm^2$ for the ^{8}Li measurements and $140\mu g/cm^2$ and $90\mu g/cm^2$ for the ^{8}Be measurements. These correspond to a total energy loss of 0.74 MeV and 0.6 MeV for an α-particle that passes through the window and the entire catcher foil.

In Fig. 1.3-1 the result of the simulation together with measured data (see Ref. 1) for the kinematic coefficient a_1 is displayed for ^{8}Li for different energy thresholds. The two data sets correspond to two different α -counters. It can be clearly seen that for higher β -energies the simulated a_1 with energy threshold deviates systematically from the a_1 without energy threshold. This deviation seen in the simulation corresponds to the measured deviation of the a_1 coefficient and lies in between the deviation of the two detectors. The reason for the difference of the a_1 coefficients for the two α–counters is not yet understood (see Ref. 1).

In the future we plan to include a realistic α -energy loss computation in the catcher foil and the window instead of applying an energy cut.

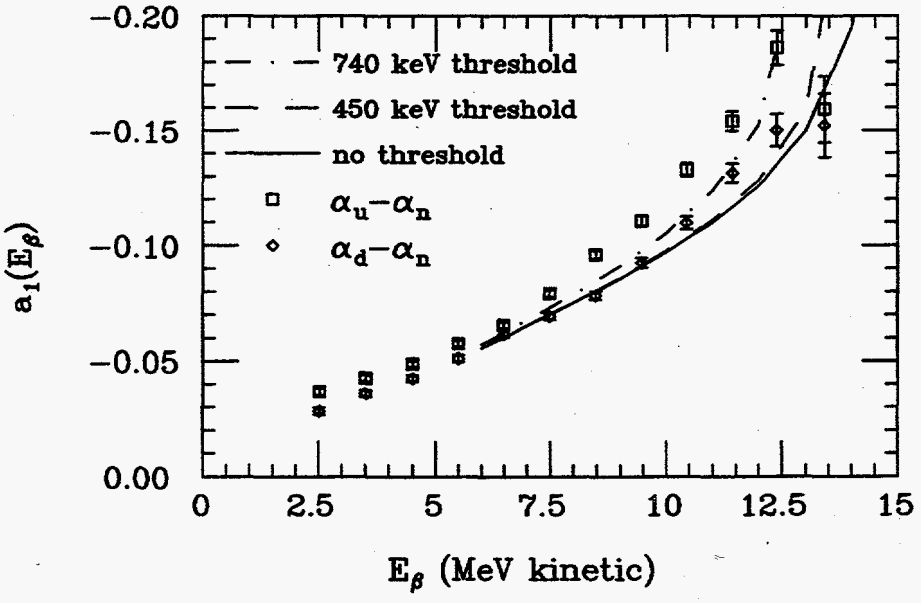

Fig. 1.3-1. Measured and simulated a_1-coefficients. $\alpha_u-\alpha_n$ is the a_1 extracted from the upstream α-counter, $\alpha_d-\alpha_n$ for the downstream α -counter. The simulation shows a systematic deviation of the a_1 depending on the α -energy threshold in the data.

[1] K.B. Swartz, Measurement of the $\beta-\alpha$ angular correlation in the decay of ^{8}Li, Ph.D. Thesis, University of Washington (1996).

1.4 The $\beta\beta$ decay of ^{100}Mo to the first excited 0^+ state of ^{100}Ru

L. De Braeckeleer, A.W.P. Poon and M. Felton

Recently, two groups have attempted to observe the $\beta\beta$ decay of ^{100}Mo to the first excited 0^+ state of ^{100}Ru (see Fig. 1.4-1). Assuming similar matrix elements as the ones governing the transition to the ground state, one expects a partial half-life of 10^{21} years. Presently the two groups report conflicting results: $6.1^{+1.8}_{-1.1} \times 10^{20}$ years[1] and a null result at the level of 2×10^{21} years.[2] Previous experiments have focused on approaches to creating a very low background by using special materials or by conducting the experiments in underground laboratories. We are currently investigating a different approach. The detection in coincidence, of the two γ -rays following the $\beta\beta$ decay of ^{100}Mo to the first excited 0^+ state of ^{100}Ru.

A lower limit of 2×10^{20} years has already been obtained.

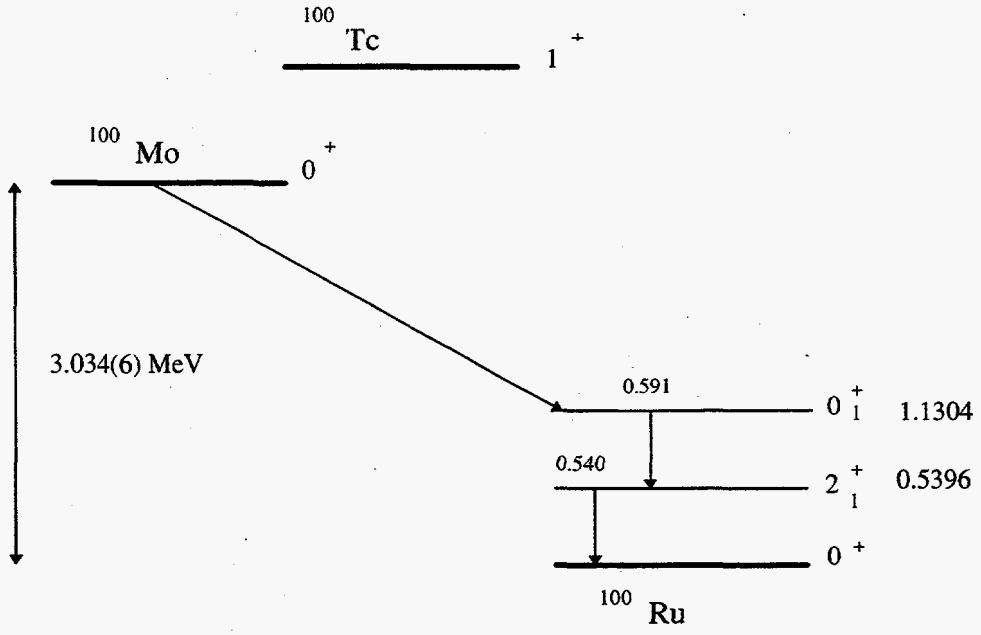

Fig. 1.4-1. Partial $\beta\beta$ decay scheme of ^{100}Mo.

[1] A.S. Barabash *et al.*, Phys. Lett. B **345**, 408 (1995).
[2] D. Blum *et al.*, Phys. Lett. B **274**, 506 (1992).

1.5 The $e-\nu$ correlation in the superallowed decays of ^{32}Ar and ^{33}Ar

E.G. Adelberger, M. Beck, A. Garcia,* N. Koloskamis,* H.E. Swanson, Z. Zhao and the ISOLDE Collaboration†

Precision studies of the $e-\nu$ correlation provide an unbiased probe for rare weak processes involving scalar or tensor interactions.[1] Because of experimental limitations, very little information on this correlation is available for $0 \rightarrow 0$ Fermi transitions;[1,2] these are particularly sensitive to scalar decays that could occur, for example, if a massive scalar boson were exchanged instead of the usual $W^{\pm}$. We have recently studied the $e-\nu$ correlation in the superallowed decays of ^{32}Ar and ^{33}Ar by measuring the effect of lepton recoil on the line shapes of the narrow ($\Gamma \leq 150$eV) delayed-proton groups following these decays.

The experiment was performed at the ISOLDE General Purpose On-line Isotope Separator at CERN. Short-lived Ar activities were produced by bombarding CaO targets with 1 GeV protons and ionized in a plasma ion source. The Ar ions were stopped in a $25\mu g/cm^2$ carbon foil. Delayed protons were counted using a PIN diode detector setup described elsewhere in this report. Two 8192-channel energy spectra with gains of approximately 0.5 and 1.0 keV/channel were recorded along with the time delay of the event after the proton burst.

Data were taken in a sequence where long ^{32}Ar runs alternated with shorter ^{33}Ar runs (the intensity of the ^{33}Ar beam was 40 times greater than that of the ^{32}Ar beam). The ^{33}Ar data provided the energy calibration, as well as being interesting in their own right. A total of 9×10^4 and 1.1×10^6 superallowed decays of ^{32}Ar and ^{33}Ar, respectively, were observed. The low-gain spectra are shown in Figs. 1.5-1 and 1.5-2. An expanded high-gain spectrum showing the superallowed group from ^{32}Ar decay is shown in Fig. 1.5-3. A very preliminary analysis of the ^{32}Ar data yields an $e-\nu$ correlation coefficient consistent with the standard model value of unity with an uncertainty of 0.026.

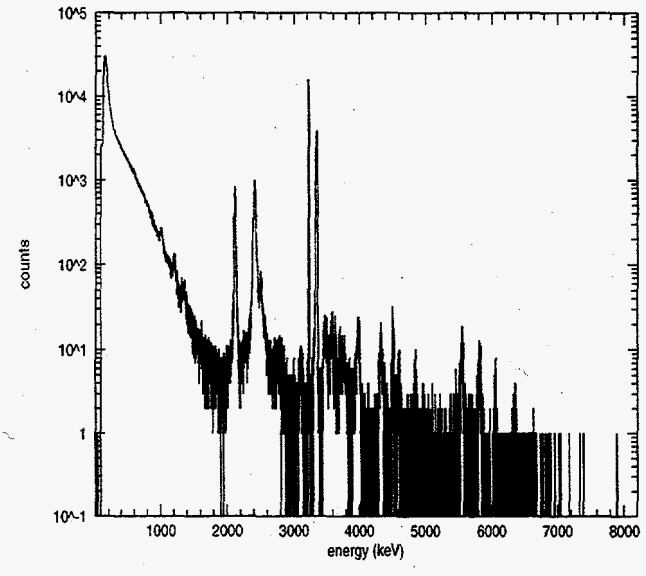

Fig. 1.5-1. ^{32}Ar delayed proton spectrum.

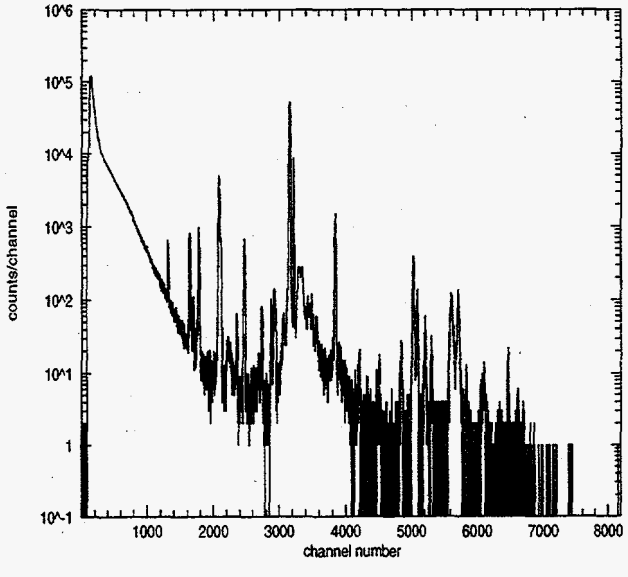

Fig. 1.5-2. ^{33}Ar delayed proton spectrum.

*Dept. of Physics, University of Notre Dame, South Bend, IN.
†ISOLDE collaboration, PPE-Division, CERN, CH-1211, Geneva 23, Switzerland.

[1]E.G. Adelberger, Phys. Rev. Lett. **70**, 2856 (1993).
[2]D. Schardt and K. Riisager, Z. Phys. A **345**, 265 (1993).

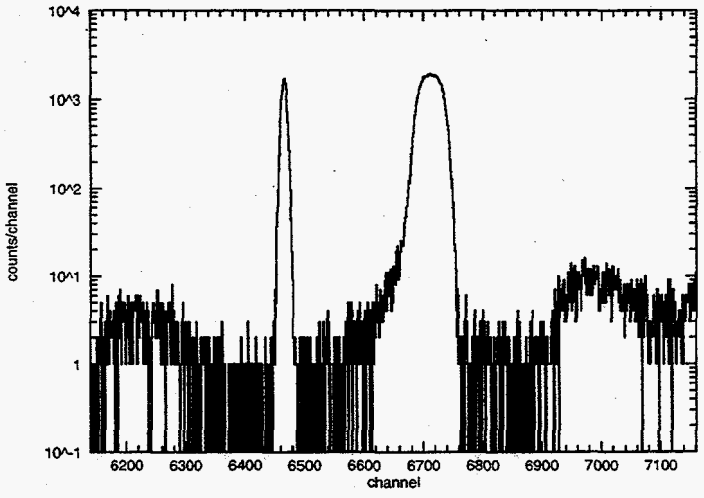

Fig. 1.5-3. Expanded ^{32}Ar delayed proton spectrum showing superallowed proton group. The peak in ch 6466 is a pulser.

1.6 The $e-\nu$ correlation in ^{8}Li decay

E.G. Adelberger, A. Cronin, L. De Braeckeleer, G.B. Franklin,* H.E. Swanson, K.B. Swartz and Z. Zhao

The $e-\nu$ correlation in ^{8}Li decay can be used to determine the induced tensor contribution to the decay. We made preliminary attempts to measure this correlation by detecting, in coincidence, the two α's from the decay of the ^{8}Be daughter state. We used the target transfer system of the 'mass 8' apparatus at the UW tandem accelerator. The energies E_1 and E_2 of the two α's were registered in pairs of thin surface-barrier detectors. These counters were backed by large surface-barrier VETO counters to identify events where the counter was struck by both the β and one of the α's from a given decay. The sum energy, $\Sigma=E_1 + E_2$, of an event gave the excitation energy of the daughter state, while the difference energy $\Delta=E_1 - E_2$ (which ranges up to $\pm$400 keV) was sensitive to the lepton recoil (and therefore to the $e-\nu$ correlation). The energy response of the surface-barrier detectors was measured on-line using an $E_\alpha = 3183$keV ^{148}Gd source and (at a variety of energies) in subsequent runs using elastically scattered α's from the UW tandem accelerator. These preliminary measurements proved the usefulness of the technique. However, we did not obtain a final result because of problems with gain drifts and with a coincidence efficiency of only 99%. We intend to cure these problems in future runs.

*Carnegie Mellon University, Pittsburgh, PA.

1.7 Target composition studies relevant to a proposed $^{7}Be(p,\gamma)^{8}B$ cross section measurement

E. G. Adelberger, L. De Braeckeleer, S. M. Graff,* K. A. Snover and Z. Zhao

We propose to carry out a remeasurement of the astrophysically interesting $^{7}Be(p,\gamma)$ cross section in the energy range $E_p \leq 1$ MeV. The experiment will be a collaboration between NPL and TRIUMF. The radioactive ^{7}Be target will be fabricated at TRIUMF and the cross section measurements will be carried out here. We plan to use a ^{7}Be target of approximately 10^{17} atoms/cm^2 with an area of about 3 mm^2, and a proton beam which is swept in x and y coordinates to ensure a uniform beam flux on target. In this report we describe layered target composition studies relevant to the proposed experiment.

The ^{7}Be activity will be produced by the $^{7}Li(p,n)^{7}Be$ reaction, chemically separated and evaporated onto a solid backing at TRIUMF. The total number of ^{7}Be atoms will be determined by radioactive counting of the 478-keV gamma ray from the decay of the first excited state of ^{7}Li, following electron capture by ^{7}Be. The idea of a layered target is to use a second material such as aluminum, which has a narrow resonance in the (p,γ) reaction at a convenient proton energy, as a monitor of the energy thickness of the Be target. To this end, we tested several targets consisting of 5 - 7 μg/cm^2 Al evaporated onto solid Cu backings, with 45 μg/cm^2 natural Be evaporated onto the Al. Both the shift of the 992 keV resonance in $^{27}Al(p,\gamma)$ and the width of the 1083 keV resonance in $^{9}Be(p,\gamma)$ were used to deduce the Be thicknesses, with good agreement. The bare Al resonance was about 1.5 keV wide, due to beam energy spread and target thickness, while the shifted Al resonance was 5 - 6 keV wide, due mainly to straggling. With a spot (3 mm^2) Be on Al/Cu target approximately 35% of the beam was focused onto the Be, and the shifted Al resonance was clearly visible above the high energy tail of the unshifted Al resonance due to beam striking outside of the spot area.

These tests clearly demonstrate the feasibility of the proposed technique. Two other methods are currently being considered as alternatives to the layered target: (1) the 1083 keV $^{9}Be(p,\gamma)$ resonance could serve as a good energy thickness monitor if the ^{7}Be target is fabricated with at least 10% ^{9}Be. (2) The narrow 1376 keV $^{7}Be(\alpha,\gamma)$ resonance would also be an excellent monitor, but would require a modification of our terminal ion source to permit a rapid change from proton to alpha beams.

*Formerly of TRIUMF, Vancouver, B.C., Canada.

1.8 An apparatus to measure the PNC spin rotation of cold neutrons in a liquid helium target

E.G. Adelberger, J.H. Gundlach, B.R. Heckel, D.M. Markoff, S.D. Penn and H.E. Swanson

An apparatus to measure the parity non-conserving (PNC) spin rotation of transversely polarized neutrons through a 46 cm liquid helium target with an error of 5×10^{-8} radians, has been completed and is now being tested. Our neutron spin rotation is predicted to lie between 1.2×10^{-7} and 2.2×10^{-7} radians.[1,2] The predicted range is dominated by uncertainties in the value of the isovector pion-exchange amplitude, F_π, which is sensitive to the neutral current contribution to the weak nucleon-nucleon interaction. F_π is currently bounded by the circular polarization of the 1082 keV γ-ray measured in ^{18}F.[3] The neutron spin rotation in helium, $\phi_{PNC}(\vec{n}+\alpha)$, in conjunction with the longitudinal analyzing power of polarized protons in helium, $A_L(\vec{p}+\alpha)$,[4] will determine F_π, the weak pion-exchange amplitude with an uncertainty much smallr than that from ^{18}F.

We have improved the liquid helium target filling system which alternately fills the front and back targets. We have eliminated the liquid helium valves and replaced them by an open system with two 'walking pipes.' One end of each pipe is raised above the height of the chamber for filling and subsequently lowered for emptying the connected target chambers. These pipes are controlled with strings pulled by air-actuated pistons located outside of the cryostat. The liquid helium pump has been built, installed and tested. We have demonstrated that this system successfully fills, holds and drains liquid helium from the target chambers.

During the final testing of the apparatus, we encountered a number of set-backs. The Oxford Instruments cryostat developed a cold-sensitive leak in a vacuum joint which we successfully repaired in house. Our insert container which houses the liquid helium target chambers, also developed cold-sensitive vacuum leaks. After several iterations of unsatisfactory repairs and testing, we identified an inherent problem with our electrical feedthrough wires. We have implemented a new design consisting of anodized aluminum threaded rods that are glued into our aluminum flange using an improved epoxy.

Two tests of the neutron detector, a segmented ^{3}He ionization chamber described previously,[5] have been carried out to determine the operating parameters such as gas pressure and plate voltage. The first test was done with our tandem Van de Graff accelerator, using the ^{7}Li(p,n) reaction and wax to produce thermal neutrons. The second beam test was performed on a monochromatic cold neutron beamline at the Cold Neutron Facility at NIST in Gaithersburg. We found that a plate voltage of 2.5 kV will assure operating in the voltage plateau region for a pressure of 3 atm of Argon and 0.5 atm of ^{3}He. The detector output currents agree well with calculations and the average current noise is less than 5pA.

The data aquisition system is described elsewhere in this report (see Section 6.4).

---

[1] Y. Avishai, Phys. Lett. B **112**, 311 (1982).

[2] V.F. Dmitriev *et al.*, Phys. Lett. **125**, 1 (1983).

[3] S.A. Page *et al.*, Phys. Rev. C **35**, 1119 (1987).

[4] J. Lang *et al.*, Phys. Rev. C **34**, 1545 (1986).

[5] Nulear Physics Laboratory Annual Report, University of Washington (1995) p. 28.

1.9 Time reversal in neutron beta decay---the emiT experiment

S.R. Elliott, R.G.H. Robertson, T.D. Steiger, D.I. Will and J.F. Wilkerson

The emiT experiment is a search for a violation of time-reversal (T) invariance in the beta decay of free neutrons. The experiment will utilize a beam of cold (<10 meV), polarized neutrons from the Cold Neutron Research Facility at the National Institute of Standards and Technology (NIST) in Gaithersburg, MD. A sizable team of scientists has been assembled to perform this experiment from Los Alamos National Laboratory, NIST, the University of California at Berkeley/Lawrence Berkeley National Laboratory, the University of Michigan, the University of Notre Dame, and the University of Washington's Nuclear Physics Laboratory (NPL).

emiT will probe the T-odd triple correlation (between the neutron spin and the momenta of the neutrino and electron decay products) in the neutron beta-decay distribution.[1] The coefficient of this correlation, D, will be measured by detecting decay electrons in coincidence with recoil protons while controlling the neutron polarization. Technological advances in neutron polarization and proton detection---in addition to an improved detector geometry---will allow emiT to attain a sensitivity to D of 3×10^{-4}. This level of sensitivity represents a factor of five improvement over previous neutron T tests, and may permit restrictions to be placed on several extensions to the Standard Model that allow values of D near 10^{-3}.

emiT will be the first neutron T test to make use of a 'supermirror' neutron polarizer. Thus, emiT will achieve polarizations of > 95%, as opposed to the 65--85% polarizations typical in previous experiments. The emiT detector consists of four plastic scintillator paddles for electron detection and four arrays of large-area PIN diodes to detect the protons. The PIN diodes have been extensively tested and shown to be efficient and economical detectors of low-energy (~ 30 keV) protons.[2] The eight detector segments are arranged in an alternating octagonal array about the neutron beam so that each segment of one type lies at an angle of 135° relative to *two* segments of the other type. This geometry takes advantage of the fact that the electron--proton angular distribution is strongly peaked due to the disparate masses of the decay products. When compared to the 90° geometry used in previous experiments, this octagonal geometry results in an increase in signal rate which is the equivalent of a factor of seven increase in neutron beam flux.

During 1995 the emiT experiment was in an intensive building mode. Most of the major systems were constructed, assembled, and tested. The primary responsibilities of the NPL team include delivery of required cryogenics and vacuum systems as well as the production of the proton detector segments---including data acquisition electronics. The cryogenics and vacuum systems are complete and the PIN diodes are in hand. The electronics to run these diodes consist of custom-made precision on-board preamplifiers and a custom VME-based data acquisition board (see Section 1.10). These electronics have been designed and built and are currently undergoing final testing. It is expected that data collection will commence in the fall of 1996.

---

[1] J.D. Jackson, S.B. Treiman, and H.W. Wyld, Jr., Phys. Rev. **106**, 517 (1957).

[2] E.G. Wasserman, Time Reversal Invariance in Polarized Neutron Decay, Ph.D. Thesis, Harvard University, 1994.

1.10 A custom VME-based data acquisition system for the emiT experiment

M.C. Browne, A.W. Myers, T.D. Van Wechel and J.F. Wilkerson

A custom data acquisition system was designed for the proton detectors in the emiT experiment. This system enables interface of available VME hardware and software with a specially designed preamp, shaper, and discriminator. The proton data acquisition system is based on an 8 layer 6U VME board which is capable of monitoring 8 independent channels (1 channel = 1 proton detector). Design implementation included the use of a Field Programmable Gate Array (FPGA) as the interface and logic control unit. In the board design process, special emphasis was placed on maintaining a separation of digital and analog portions of the board in an attempt to minimize noise pick-up.

Commercial VME interfaces are readily available, yet offer little more than their name implies. The use of an FPGA to control the interface allows for several additional degrees of freedom in the acquisition system. The logic necessary to control the VME interface can be programmed directly into an Altera 7192 FPGA. In addition, the logic needed to run the acquisition board can also be programmed into the same chip. Since the FPGA is reprogrammable, many modifications can be performed to the board simply by reprogramming the Altera chip. This provides a one-time system capable of representing several levels of modifications without the need to produce a new board with successive generations.

The board is separated into an analog and digital portion, each being defined by its own ground plane. This is done in an attempt to minimize noise induced from the VME system. Analog signal inputs are sandwiched between analog ground planes, and further isolated from other inputs via ground strips. Each channel on the board consists of a three stage shaper, and a peak detect ADC. The Altera chip was programmed with a 28 bit scaler, as well as several monitors enabling constant access to the status of the board. The board is capable of being run in two different modes, as well as having the capability to run alone, or in series with other boards.

This board represents the first combined application of several packages purchased by NPL this past year. The original schematics were created using Cadence, a computer based design system enabling creation and simulation of electronic projects. The Altera chip is programmed with the use of Max + Plus II software, a system compatible with Cadence. Finally, the actual chip burning process is performed with a Data I/O chip burner. This project was completed in-house, with the exception of board fabrication.

The emiT data acquisition board has undergone preliminary testing of the analog section, and is expected to be completely operational in the summer of 1996.

1.11 Progress with a spin-polarized torsion pendulum

E.G. Adelberger, M.G. Harris and B.R. Heckel

We have built[1] a new electron spin polarized torsion pendulum to test for a spin-dependent interaction with the monopole-dipole form[2] $V(\vec{r}) = \alpha\vec{\sigma}\cdot\hat{r}[1/\lambda r + 1/r^2]e^{-r/\lambda}$, where $m = \hbar/\lambda c$ is the mass of a low-mass mediating boson. The torsion pendulum has been installed in the 'Eotwash' rotating apparatus.[3] Such an interaction would produce a field whose magnitude and direction depend on the range λ, and upon variations in the local topography. For our pendulum, a signal of 10 nrad would correspond to a measurement of 1.2×10^{-20}eV /electron spin.

To check for systematic errors, we have applied large gravity gradients (by reversing the compensators that normally cancel the gradients),[4] indicating an effect of at most 5 nrad of pendulum deflection under normal conditions. We have also investigated effects arising from the coupling of the remnant magnetic dipole moment of the pendulum to the lab-fixed magnetic field (reduced by a 3-axis Helmholtz coil, and 3 layers of mu-metal shielding). We installed a 'dummy' pendulum with a large, known magnetic dipole moment (about 1000 times larger than that of the spin-polarized pendulum). By observing the deflections of this pendulum both in the normal operating magnetic field, and in a large external field, we were able to establish a maximum magnetic systematic error also of about 5 nrad.

We observe spin pendulum signals of the order of hundreds of nrad, and (worse) a lack of reproducibility in measurements taken more than a week apart. We have recently isolated instabilities in the rotation rate of the apparatus, and in the electronics, which presumably caused the signals. The reproducibility problem has now been fixed. The remaining work which needs to be done involves making further and more careful measurements of the systematic errors mentioned above, as well as other minor ones (such as temperature effects), and a long-term collection of spin-potential data.

---

[1] Nuclear Physics Laboratory Annual Report, University of Washington (1993) p. 28.
[2] J.E. Moody and F. Wilczek, Phys. Rev. D **30**, 130 (1984).
[3] Y. Su *et al.*, Phys. Rev. D **70**, 3614 (1994).
[4] Y. Su, A new test of the Weak Equivalence Principle, Ph.D. Thesis, University of Washington, 1992.

1.12 Progress with the rotating-source torsion balance experiment

E.G. Adelberger, J.H. Gundlach, B.R. Heckel, G.L. Smith and H.E. Swanson

In this past year we have made several improvements, both to the apparatus and to our understanding of systematic effects.

We placed a hollow copper jacket surrounding the temperature sensitive torsion fiber inside the vacuum vessel. The very thin torsion fiber has a very small heat capacity, and comes into temperature equlibrium with the jacket quickly through radiation. This has two advantages: the large heat capacity of the copper jacket insulates the fiber from temperature changes outside the vacuum vessel, and we can control the temperature of the torsion fiber by controlling the temperature of the jacket. We use the temperature control feature to reduce the linear drift of the torsion fiber by temporarily warming it up. In the future, we plan to fill the jacket with liquid nitrogen and take data where the properties of the tungsten torsion fiber are believed to be superior.

We are able to position the composition dipole to within 0.05 mm of the turntable center in both the horizontal and the vertical planes using purely gravitational means -- an extraordinary accuracy considering the strength of the gravitational interaction. To find the vertical position, we place a large q_{21} moment on the pendulum and arrange the uranium to have a large Q_{31} field. When the pendulum is on the midplane of the uranium, the orthogonality of the multipole moments require the torque to be zero. Similarly for the horizontal position, the pendulum always has a large q_{44} moment and the source has a large Q_{55} field. When the pendulum is on the axis of rotation of the source, there again will be no torque. A theorem which describes how multipole moments transform under translations[1] allows us to measure the displacements.

We identified a previously unknown systematic effect coupled to our magnetic swing mode damper. The damper was connected to the vacuum vessel through a short (3 cm), thick (75 micrometer diameter) fiber, and connected to the pendulum through a long (90 cm), thin (20 micrometer diameter) fiber. We had always assumed the center of mass of the pendulum hung directly below the suspension point, and that the thick and thin fibers were colinear. We discovered that at our level of sensitivity this was not necessarily correct. The center of mass of the damper-pendulum system hangs below the suspension point, but if the center of mass of the damper is not colinear with the fiber attachment points, then the center of mass of the pendulum does not hang below the suspension point. A significant torque then arises about the thick fiber as the pendulum is attracted to the source mass. We improved the situation by reducing the mass of the damper by a factor of 3, and by increasing the torsional spring constant of the short, thick fiber by a factor of 16 by doubling its thickness.

We are currently taking composition dipole data, and expect to measure the differential acceleration between lead and copper towards uranium at the 5×10^{-13} cm/sec^2 level.

[1] Y. Su *et al.*, Phys. Rev. D **50**, 3614 (1994).

1.13 Construction of a new rotating torsion balance

E.G. Adelberger, J.H. Gundlach, B.R. Heckel, K. Mauldin, S.D. Penn and H.E. Swanson

We are currently building a new torsion balance designed to provide improved Equivalence Principle tests at length scales ranging from 1m to ∞. The design addresses the major statistical and systematic errors that limited our previous work[1] at the level $\Delta a \approx 10^{-12} \mathrm{cm}/\mathrm{s}^2$.

Statistical noise will be reduced by operating the torsion balance vacuum at pressures below 10^{-7} Torr. We are fitting the apparatus with a corotating 30 l/s ion pump, for which a rotating high voltage feedthrough has been built and is currently being tested in the old Eöt-wash apparatus. Torsion noise originating in the torsion fiber itself and in its attachments has been identified as a dominant noise source. Since it is known that low temperatures improve material properties we plan to surround all susceptible parts with a LN_2-cooled jacket. (We expect that systematic uncertainties will limit the achievable precision so it is not necessary to operate at liquid helium temperatures.)

A high-performance turntable consisting of an air-bearing, with a direct-drive eddy-current motor in a feedback loop with a high-quality shaft encoder will provide smoother rotation than our old turntable. The new turntable was developed together with, and built by, the Professional Instruments Company.[2] It is nearing delivery and promises to perform to specifications. A special test torsion pendulum designed to be extremely insenstive to gravity gradients will be used to verify the smoothness of rotation. For this test the old Eöt-wash balance will be suspended from the new turntable.

The largest systematic correction in our previous rotating torsion balance experiments resulted from a tilt of the turntable (due to the varying tilt of the laboratory floor) that induced a proportional change in equilibrium angle of the pendulum. This will be eliminated in the new apparatus by suspending the pendulum and autocollimator angle readout from a gimbal located inside the vacuum can.

The effects of residual gravity gradients were a significant systematic error in our previous measurements. We have developed a new pendulum containing 8 test bodies. The test bodies are mounted radially in two planes onto a tubelike holder. With this design most of the low-order multipole moments, q_{lm}, vanish. The lowest-order gravitational torque arises from the q_{44} moment of the pendulum (used to make a gravitational calibration); the lowest order effect at the signal frequency nominally occurs in l=7 multipole order. To reduce problems from non-repeatable test body placement, the test bodies are mounted with screws into conical receptors.

Gravitational gradients at the pendulum will be compensated with ≈ 1.5 tons of lead. These masses will be shaped to reduce the Q_{21}, Q_{31} and Q_{22} gradients separately. To measure and then minimize stray pendulum moments arising from mechanical imperfections, these compensators can be rotated by 180° to double the gradients instead of cancelling them. A stand for precisely positioning these massive compensators is completed.

We have constructed a hermetic thermal shield consisting of a double-walled cylinder with temperature-regulated water flowing between the layers and an insulating foam layer on the outside. A layer of μ-metal will be installed just inside the shields.

The electrical signals from the balance are led through a slip-ring assembly to the non-rotating side. This assembly is rotated by a feedback mechanism that follows the turntable and hence does not exert any torque on the main turntable.

---

[1] Y. Su *et al.*, Phys. Rev. D **50**, 3614 (1994).

[2] Professional Instruments Company, 4501 Highway 7, Minneapolis, MN 55416.

1.14 A new technique for measuring Newton's constant *G*

E.G. Adelberger, J.H. Gundlach, B.R. Heckel and H.E. Swanson

Three recent remeasurements of Newton's constant *G* have yielded values[1] that differ by up to 0.7% (52σ). A new determination that will resolve this puzzle is needed, preferably by a method that differs from those used previously and that is less susceptible to systematic error sources found or suspected[2] in previous measurements.

In last year's Annual Report[3] we proposed a method based on a continuously rotating torsion balance located in the field of a massive attractor. A feedback system controls the angular velocity of the turntable so that the torsion fiber does not twist. The rate of change of the turntable angular velocity directly yields the angular acceleration of the 'quasifree' pendulum. Expressed in multipole formalism, this acceleration is $\alpha = \Sigma\alpha_{lm} \propto G\sum\frac{q_{lm}}{I}Q_{lm}e^{im\phi}$ where q_{lm} and Q_{lm} are the multipole moments of the pendulum and attractor mass, respectively. The overwhelmingly dominant torque is $\alpha_{22} \propto G\frac{q_{22}}{I}Q_{22}$. If one uses a flat, two-dimensional pendulum its q_{22}-to-moment-of-inertia ratio becomes a constant $\frac{q_{22}}{I} = \sqrt{\frac{15}{32\pi}}$ i.e., is independent of the density distribution. For a rectangular pendulum with finite thickness, t, and width, w. this ratio becomes

$$\frac{q_{22}}{I} = \sqrt{\frac{15}{32\pi}}\frac{w^2 - t^2}{w^2 + t^2} \qquad (1)$$

i.e. it is only weakly dependent on the width and thickness. Furthermore, if the width-to-height ratio satisfies $10h^2 = 3(w^2 + t^2)$ then q_{42}=0. The next-to-leading order acceleration, arising from $\ell, m = 6,2$ coupling, is analytically calculable and small ($\alpha_{62}/\alpha_{22} \approx 10^{-5}$). To further reduce higher-order torques, the attractor will consist of 4 spheres located symmetrically on each side of the pendulum. They will be separated azimuthally by 45° ($\Rightarrow Q_{\ell 4} = 0$) and vertically by $\pm\sqrt{1/6},\rho$ where ρ is the horizontal distance to the torsion fiber ($\Rightarrow Q_{42} = 0$). The acceleration can be fitted with a harmonic series in the turntable angle, ϕ, to extract *G*. We will use a quartz plate for the body of the pendulum so that any non-uniformities can be minimized using optical methods. This plate will then be gold-coated so that its faces serve as mirrors for the angle read-out.

The attractor rotates on a second turntable to eliminate gravitational effects of background gravity gradients. To eliminate gravitational forces from the turntable itself, *G* will be derived from the difference of two measurements where the attractors are rotated by 90° on the turntable.

We have used numerical simulations to find a feedback scheme that most closely tracks the quasifree pendulum. This feedback method was then successfully implemented on our old Eöt-wash balance. From this test and the simulations, and the expected reduced systematic errors, we believe that our technique should permit a measurement to $\Delta G/G = 10^{-5}$.

---

[1] Physics Today, **48**, 9 (1995).

[2] K. Kuroda, Phys. Rev. Lett. **75**, 2796 (1995).

[3] Nuclear Physics Laboratory Annual Report, University of Washington (1995) p. 29.

2. NEUTRINO PHYSICS

2.1 Neutral current detector project at Sudbury Neutrino Observatory (SNO)

M.C. Browne, T.H. Burritt, P.J. Doe, C. Duba, S.R. Elliott, J.E. Franklin, J.V. Germani, K. Heeger, R. Meijer Drees, A.W. Myers, A.W.P. Poon, R.G.H. Robertson, T.D. Steiger, T. Van Wechel and J.F. Wilkerson

SNO will detect Čerenkov light emitted from electrons or positrons produced by charged-current neutrino interactions. These measurements will provide a measure of the flux of electron neutrinos from the sun. Neutrinos of any flavor, however, can produce free neutrons in the heavy water by neutral current interactions. Thus the measurement of the neutron production is a measurement of the total flux of neutrinos from the sun. Since solar burning produces only electron neutrinos, a comparison of the total neutrino flux to the electron neutrino flux could provide strong evidence for neutrino oscillations and therefore neutrino mass. The neutral current detectors (NCD's) are He-3 filled proportional counters designed to detect such neutrons.

This past year has seen the NCD project progress from the research-and-development stage, through a prototyping stage to imminent production. UW is playing a major role in the construction, testing, installation, and data analysis and acquisition segments of the project. The NCD project is a collaboration between UW, Los Alamos National Laboratory, Lawrence Berkeley National Laboratory, and Guelph University.

The final assembly of the NCD's and their initial testing will be done in the production facility that has been constructed at UW during the past year. The clean room was commissioned and is operating well. Major systems needed for construction such as the laser welder, the wire stringing apparatus, the vacuum bakeout, the gas handling system, and the acid etching system are all in place and are ready to go. We have nearly finalized the receiving and shipping logistics required to guarantee that the detectors will see a limited time above ground being activated by cosmic rays. We have identified a suitable Seattle-area underground storage site which can be used during any construction delays to safeguard counter parts from cosmic rays.

In addition to preparing the laboratory, we have also had a number of technical and production accomplishments during the year. A Ni tube has been produced by chemical vapor deposition on an anodized Al mandrel. Although the deposit did not meet our specifications with respect to thickness uniformity, the tube was leak tight. This is an improvement over the Teflon and the electroless-Ni coated mandrels previously used. Modifications to the process are being made to improve thickness uniformity.

All CVD Ni endcaps have been produced and are beginning to proceed through the production pipeline. They will be fabricated into parts with electronic and gas feedthroughs prior to being welded into detector tubes at the UW cleanroom.. We have verified that the endcap production process produces parts which are radioactively clean, electronically stable at HV, and have sufficient glass-to-metal seal strength. All of the commercial service providers have been selected and are ready to proceed with production.

The signal readout cable must be buoyant and extremely low in radioactivity as it will reside in the heavy water; the most sensitive region in SNO to radioactive impurities. A prototype cable has been produced and tested and the final order has been placed. The delay line design is still being finalized.

The preamp design has been tested and finalized, and production has commenced. Construction of the NCD electronics and acquisition system has been delayed in order to concentrate the DAQ group's efforts on SNO data acquisition. As a result, the data acquisition system used during the initial stage of underground storage will have a limited number of channels.

Full production of the NCD's should begin in June 1996 and is expected to last until about December. The counters will be stored underground at SNO until installation into the heavy water.

2.2 SNO NCD electronics

M.C. Browne, J.V. Germani, K. Heeger, A.W. Myers, R.G.H. Robertson, T.D. Van Wechel and J.F. Wilkerson

The SNO neutral current electronics is designed to extract pulse information from the ^{3}He proportional detectors in order to provide the necessary information required for SNO physics analysis. The information to be extracted consists of:

the particle energy
particle identification (including noise rejection)
position readout along the detector length
absolute time of event.

The extractable information is determined both by the physics of the ionization processes that take place within the detector, the selected detector operating parameters (gas mixture, pressure, anode wire diameter, detector radius), and special constraints of the SNO detector, in particular the minimization of radioactivity which has necessitated single ended readout of the counters. The need to acquire both the low-energy (700 keV) neutron induced events as well as the high-energy (5-8 MeV) alpha particle events requires an electronics system with both very low noise and large dynamic range. Extracting particle identification and position requires digitizing the pulse to record the information on the time development of the ionization. An overview of the electronic readout system follows.

Pulses generated in each detector string are first amplified by a current preamplifier. The output from the current preamplifier is then sent to both an energy measurement system and a digitization system. In the energy measurement system, a shaper discriminator circuit forms a trigger for the shaped pulse's sample and hold ADC. The sample and hold ADC allows one to make relatively fast, precise energy measurements. The digitization circuit consists of a fast discriminator, a logarithmic amplifier followed by delay cables, a multiplexer, and a digitizer unit. This circuit records the pulse time development information. In case of a burst of events (i.e. supernova), the digitizer system might not be able to keep up with the data rate, but the shaped pulse ADC and scaler would allow recording of pertinent information. High Voltage bias is provided by a single commercial HV supply.

Design, testing, and fabrication of the current preamplifier hybrid chip which is based on a Robertson design using an inverted cascode front end stage is complete. A number of prototype preamplifiers have been constructed and tested. Construction of production preamplifier modules is now starting.

Development of the logarithmic amplifier stage is complete, several 8 channel NIM based units have been constructed for initial data taking.

Design of the shaper discriminator circuit, the fast discriminator, and the multiplexer circuits are also complete and prototype units have been constructed and tested.

At this stage essentially all R&D is complete and we are now concentrating on the design and fabrication of the production NCD electronics.

2.3 SNO data acquisition system

Q.R. Ahmad, J.C. Beck, Y. Chan,* S.R. Elliott, M.A. Howe, M. Isaac,* R. Meijer Drees, F. McGirt,† A.W. Myers, T.D. Van Wechel and J.F. Wilkerson

Our group is responsible for providing the SNO data acquisition (DAQ) system which will be capable of reading out the signals from the nearly 9500 photomultiplier tubes used in SNO. The electronics and DAQ system must be able to handle modest background rates in excess of 1 kHz and burst rates in excess of 1 MHz. An additional goal is to keep the detector acquiring data essentially continuously throughout the life of the experiment, in case of a possible galactic supernova occurrence. The DAQ system is written in an object-oriented programming language (C++), supports the VME bus, and utilizes multiple VME embedded processors (Motorola MVME 167) for control of the experiment.

The DAQ software has been developed using an innovative approach that we term the Object Oriented Software Bus (OSB).[1] It utilizes the current techniques of Object Oriented Software Development (OOSD) to develop a set of data acquisition and analysis software tools according to a common specification, in a manner that is analogous to the way computer hardware has been developed since the advent of the bus structures of minicomputers and microcomputers. The approach allows one to write independent object oriented programming (OOP) based software objects that correspond directly to hardware objects, acquisition tasks, and analysis tools. Software objects have been written for numerous CAMAC, GPIB, and VME based hardware modules. These software objects are then utilized in acquisition task objects to meet a specific experiment's requirements.

The SNO DAQ system supports the readout of the 9500 individual channels via 19 custom 9U 'SNO Crates' each containing 16 32-channel front-end cards and a crate trigger card. Each SNO Crate is controlled via SNO Crate translator/controller cards that connect the SNO Crate backplane to a 6U VME card located in a standard VME crate, termed an interface crate.

The interface crate contains additional SNO translator/controller cards as well as VME embedded processors directing readout of each crate. Event information is shipped from these crates via VME-to-VME controllers to a VME embedded processor located in the primary VME data crate where event building, data recording, and shipment of data to the surface is handled. We are currently developing code using Metrowerks' CodeWarrior C++ compiler and the Symantec TCL 1.1.3 class library.

---

* Lawrence Berkeley National Laboratory, Berkeley, CA.
† Los Alamos National Laboratory, Los Alamos, NM.

[1] F. McGirt and J.F. Wilkerson, Invited paper, *Ninth Conference on Real Time Computer Applications in Nuclear, Particle and Plasma Physics*, Michigan State University, East Lansing, MI, May 1995.

2.4 SNO DAQ hardware module support

Q.R. Ahmad, J.C. Beck, M.A. Howe, R. Meijer Drees and J.F. Wilkerson

The SNO DAQ group is responsible for developing both the software needed for development and debugging of the SNO Front End Card (FEC32) readout electronics as well as the code necessary for data acquisition from the SNO detector. The final SNO DAQ code will initialize, control, readout data, and monitor the condition of the over 300 FEC32 cards that will be used in the SNO detector. Our group is working in close concert with the SNO Electronics and Calibration groups to design and implement a robust and complete acquisition system.

Software was written and used to perform low level debugging and testing of the VME-based prototype Front End Cards [pFECs]. These pFEC cards use the same custom Bipolar and CMOS integrated circuit chips that will be used in the production SNO electronics. Problems identified during this process were accounted and corrected for during the design of the FEC32 hardware.

Routines have also been written to initialize and take data using the pFEC system as the first step in developing code that will be used in the final SNO data acquisition system. We have successfully taken data using the pFEC system and the miniSNO test facility. At this point the software tools are in place to take raw data from the prototype electronics, write it to disk in the proper SNO format, and analyze it using both local tools and the collaboration's SNOMAN analysis package. We have also implemented on-line diagnostics, including the capability of performing on-line histogramming of desired quantities (e.g., charge and time, noise rates, etc.). Work continues in these areas to optimize our monitoring, diagnostic, and analysis tools. We have also recently performed an electronic calibration of the pFECs and miniSNO. This was a first attempt at checking the procedures and processes that will be used in the SNO detector calibration. Work has started on writing a task to automate this procedure for the final FEC32 based system.

Finally code has been written to support and test the development phase of SNO electronics. The software includes support of the FEC32 boards, as well as for the SNO translator cards that allow communication and control between the VME bus and the custom SNOBUS backplanes where the FEC32 hardware resides. This code is being tested and further developed as the electronics hardware becomes available.

2.5 The miniSNO detector and test facility

Q.R. Ahmad, J.C. Beck, R. Meijer Drees, M.A. Howe, K.T. Lesko,* M.E. Moorhead,* A.W. Myers, T.D. Van Wechel and J.F. Wilkerson

Last year, work began at NPL on a facility for software and hardware testing related to research on the Sudbury Neutrino Observatory (SNO). Construction of the facility was completed during the past year, and it is now providing valuable support for the commissioning and operation of the SNO detector.

The key component of the facility is a detector dubbed 'miniSNO' (Fig. 2.5-1). It was designed to be constructed quickly and at low cost from spare equipment and phototubes from the SNO detector. The detector is roughly spherical, with an inner diameter of 7 feet. It is capable of holding 128 SNO phototubes, though at the moment only 90 phototubes are available for use in the detector (Fig. 2.5-2). There are currently 42 channels of SNO prototype Front End Card (pFEC) electronics being used to read out the 42 phototubes of the equatorial panels of miniSNO. The miniSNO detector sits in an 18'x14' room capable of holding water to a depth of 12 feet. It was formerly used for neutron shielding of a detector room near the old NPL cyclotron. The water room has been coated with a black sealant, which gives us the option of filling the room and using miniSNO as a true water Cerenkov detector. The adjacent detector room has been converted to a laboratory for the SNO DAQ development and testing as well as maintenance of miniSNO.

The miniSNO test facility is useful to SNO in a number of ways:

1) Since miniSNO uses SNO hardware and produces SNO-format data, taking data with miniSNO allows us to more effectively develop data acquisition software for SNO.
2) MiniSNO is being used to develop and refine procedures, such as electronics calibration and detector monitoring, that will be used in the SNO detector.
3) MiniSNO's ease of access provides a place to test some hardware installation and use before it is attempted in the more restrictive underground environment of SNO.
4) Calibration sources for SNO can be tested with miniSNO .

Recently, miniSNO has been acquiring SNO-format data using a variety of light sources and triggers. Acquisition and analysis of this data has been invaluable for debugging software and better understanding hardware/software interactions. In the near future, NPL will be the site of many SNO Commissioning and Turn-on (CAT) preparations, including a test assembly of the SNO data acquisition system. The availability of the NPL test facility and the miniSNO detector makes possible a more complete preparation for the operation of the SNO detector, and allows us to identify and fix potential problems before they cause delays during underground installation and commissioning of SNO.

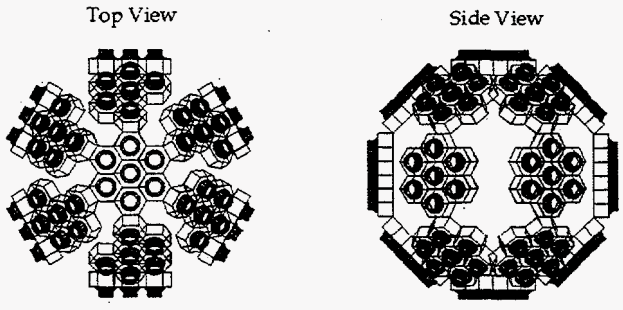

Fig. 2.5-1. Top and side views of the Mini-SNO detector.

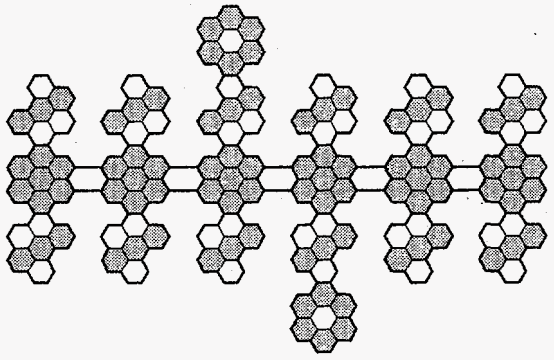

Fig. 2.5-2. A flattened view of Mini-SNO showing the 90 PMT locations (shaded).

* Lawrence Berkeley National Laboratory, Berkeley, CA.

2.6 Extensions to the SNO DAQ software

Q.R. Ahmad, M.A. Howe M. McGirt* and J.F. Wilkerson

The Sudbury Neutrino Observatory will use a data acquisition program that has been under development for several years by Frank McGirt and John Wilkerson. This program (SNO DAQ) is now undergoing extensive modifications here at NPL.

Written in C++, SNO DAQ runs on Macintosh computers. The object-oriented nature of C++ allows all possible operations associated with a particular hardware module to be encapsulated into an object class and for the hardware to have a corresponding software module that allows one complete control and testing of the functions supported by the hardware. A large number of VME, Camac, and NuBus based hardware modules are supported. Interactions between multiple hardware modules take place by way of software 'Tasks', which are also self-contained objects. Currently, 'Tasks' are hard-coded objects that must be compiled into the code by someone who is quite familiar with the object classes and C++ programming.

To overcome this limitation, the program is being converted into a data-flow model similar to the SControl[1] and GORDO[2] programs with a new user-interface that allows objects to be visually represented as icons. Data packets are directed from one object to another by drawing a line between the objects on screen using the mouse. The data packets are objects that contain either event data, header information, or run control information. Data processing objects developed include event filters, histograms, viewers and disk files. Complex hierarchies of interacting objects are constructed using container objects. The result is a dramatic improvement in the way that the user interacts with the program as well as an enhanced set of hardware development tools. Simple Tasks can be constructed at run time. In addition the user also has flexible control of data flow options.

Further upgrades include simplifying the process of adding new objects to the code. In the new version, a module is added by placing a configuration resource into a folder and registering the object itself in the code. The object's dialogs are automatically registered and the construction of the default configuration resource is done at run-time. While the addition of new modules must still be done by a programmer who is familiar with the code, it is much simpler than in the original version.

The SNO DAQ code is currently being tested and developed using the miniSNO facility at NPL.

---

* Los Alamos National Laboratory, Los Alamos, NM.

[1]Nuclear Physics Laboratory Annual Report, University of Washington (1995) p. 57.

[2]Nuclear Physics Laboratory Annual Report, University of Washington (1993) p. 89.

2.7 Progress on the acrylic vessel for the Sudbury Neutrino Observatory

P.J. Doe and the SNO Collaboration

A unique feature of the Sudbury Neutrino Observatory arises from the use of 1000 tonnes of heavy water which enables it to distinguish between different flavors of neutrinos. In order to satisfy the requirements for low radioactivity and excellent transmission of Cerenkov ligh, the heavy water will be contained in a 40' diameter acrylic sphere. An acrylic vessel of this size has never been constructed before, furthermore, loan of the heavy water by the Canadian government is contingent upon the integrity of the containment vessel. Personnel from the University of Washington have been leading an ongoing R&D program to ensure that the acrylic containment vessel satisfies all it's engineering and physics requirements.

The period 1995 to 1996 was a very exciting time, marked by the transition from R&D and component fabrication to installation in the underground laboratory. By July 1996, all 120 thermoformed acrylic panels from which the vessel is constructed had been fabricated and were on site awaiting installation. During the period June to July the five acrylic cylinders and two flanges which comprise the chimney of the vessel were shipped underground and bonded together to form the 6000lb, eight meter tall chimney. This was then hoisted to the top of the detector cavity while the main spherical shell of the vessel was constructed.

Construction of the shell takes place in three stages. In the first stage, a steel framework was erected on the construction platform on the floor of the underground cavity. The upper hemisphere is assembled "igloo fashion" from five rows of acrylic panels placed on the steel framework. The first row, the "equatorial row", consists of 20 panels. Ten of these panels contain the rope grooves from which the finished vessel will be suspended. Assembly of the equatorial row began in August. Once the panels were bonded into a ring, the 13 panels of the next row were positioned above the equatorial row and bonded to form a ring by making 13 vertical bonds between adjacent panels. This ring was then bonded to the equatorial row below it by making a single horizontal bond. The successful completion in early January of this first horizontal bond at the equator of the vessel was a milestone since at 125' it was the longest acrylic bond so far attempted in the world. Construction then continues towards the "north pole" of the vessel by bonding together the next ring of panels. As of the beginning of March 1996, the upper hemisphere of the vessel is now 80% complete.

The second stage is to bond the chimney to the upper hemisphere while it is still sitting on the construction platform on the floor of the cavity. The construction platform will then be raised from the floor of the cavity until the upper hemisphere is in its final location and the load is transferred to the 10 suspension ropes. This is scheduled to begin on 16 April.

The suspension ropes were originally to be made from kevlar fibers, however; accelerated aging tests (conducted by the Los Alamos National Laboratory) of the fibers in ultra pure water, similar to that which will be used in the experiment, showed that the strength of the fibers was reduced by approximately 44% over the 10 year life of the experiment. This was not acceptable and an expedited research program identified vectran fibers as a suitable replacement. Ropes of vectran have now been made, radioassayed and are on site awaiting installation.

The third and final stage, the assembly of the lower hemisphere of the vessel is begun by sequentially assembling rings of panels and bonding them to the suspended upper hemisphere. The vessel is scheduled for completion by mid September, after which it must undergo a series of acceptance tests, prior to completion of the detector.

2.8 Development of a compact 20 MeV gamma-ray source for energy calibration at the Sudbury Neutrino Observatory

M.C. Browne, N.P. Kherani,* A.W.P. Poon, R.G.H. Robertson and C.E. Waltham‡

We are developing a compact 20 MeV gamma-ray source for energy calibration at the Sudbury Neutrino Observatory (SNO). The gamma-rays are produced from the radiative capture reaction $^3H(p,\gamma)^4He$. The design and the operational characteristics of the proton source are described in a previous report.[1]

We have built a prototype gamma-ray source with a scandium deuteride (ScD_2) target. Scandium was chosen because of its good thermal stability[2]. We have designed and built an ultra-high vacuum system for the target evaporation process. We chose a molybdenum substrate for the target. Prior to the target fabrication process, the substrate was cleaned and etched in different solvents and acids to ensure a clean adhesion surface to accept the scandium film. The substrate and the evaporation system were baked extensively to ensure cleanliness. A scandium film of thickness of 7000Å was evaporated onto the substrate in the latest run. During the evaporation process, the pressure of the evaporation chamber did not exceed $3x10^{-7}$ torr despite the intense heat required to evaporate scandium. To ensure a good deuterium to scandium stoichiometric ratio, the scandium film was deuterated *in situ*. The substrate was heated up to 400°C by an internal heater installed in the evaporation system. Deuterium was let into the system and was pumped by the scandium film. Once the scandium film had been saturated by the deuterium, the temperature of the substrate was slowly brought down to anneal the film. Because of the extra care taken into ensuring a clean evaporation environment, the latest target has a scandium to deuteron atomic ratio of 1:2.2

The prototype source is being tested. A 12.7cm (Ø) x 15.2 cm NaI with an active annular cosmic-ray veto and lead shielding is used to detect the 5.5 MeV gamma-ray in the $^2H(p,\gamma)^3He$ reaction. A 12.7cm (Ø) x 5.1 cm liquid scintillator with active cosmic-ray veto is used to monitor the neutron production rate by pulse shape discrimination. The neutrons are produced from $^2H(d,n)^3He$, where the incident deuterons come from the naturally occurring deuterium in the hydrogen discharge gas and the exchange between the target deuterium with the ambient discharge gas.

Preliminary analyses show an increase of neutron and gamma event rates above background when the proton beam is turned on. In the pulse shape discrimination analysis of the liquid scintillator data, we found a (24±2)% increase in neutron production above background, and a (2.5±0.1)% increase in gamma-ray production. It is difficult to detect the $^2H(p,\gamma)^3He$ 5.5 MeV photopeak in the NaI detector because of the (n,γ) background in this energy region. In order to accurately determine the energy spectrum when the proton beam is on, we measured the beam-off background extensively (28-day real time equivalent). The background subtracted energy spectrum shows an increase in gamma-rays at 5 MeV (single escape) and at 5.5 MeV. From the single escape peak and the full energy peak in this spectrum, we estimated the $^2H(p,\gamma)^3He$ reaction rate in our prototype source to be 1 s^{-1} at a proton beam energy of 26 keV. The detection of the 20 MeV gamma-rays from the reaction $^3H(p,\gamma)^4He$ at the SNO detector will not be as difficult owing to the high primary gamma-ray energy, and the essentially unit efficiency for gamma-ray detection.

We are also in preparation of a second deuterium prototype run to familiarize ourselves with the target fabrication process. One improvement we plan to implement in this run is the use of isotopically pure hydrogen gas with less than 15 ppm HD. This will reduce the neutron production rate, and hence, the neutron capture background, in the energy region of interest. The final scandium tritide target will be fabricated in a similar evaporation system at the tritium facility at Ontario Hydro Technologies in Toronto, Canada. This tritiation run will be carried out in summer 1996.

---

* Ontario Hydro Technologies, 800 Kipling Avenue, Toronto, Ontario, Canada M8Z 5S4.

‡Department of Physics and Astronomy, University of British Columbia, Vancouver, B.C., Canada V6T 1Z1.

[1]Nuclear Physics Laboratory Annual Report, University of Washington (1994) p.10.

[2]J.H. Singleton and L. N. Yannopoulos, J. Vac. Sci. Technol., **12**, 414 (1975).

2.9 SAGE: The Russian American Gallium Experiment

S.R. Elliott and J.F. Wilkerson

The Russian-American Gallium Experiment (SAGE) is a radiochemical solar neutrino flux measurement based on the inverse beta decay reaction, $^{71}Ga(\nu_e,e^-)^{71}Ge$. The threshold for this reaction is 233 keV which permits sensitivity to the p-p neutrinos that comprise the dominant contribution of the solar neutrino flux. The target for the reaction is in the form of 55 tonnes of liquid gallium metal stored deep underground at the Baksan Neutrino Observatory in the Caucasus mountains in Russia. About once a month, the neutrino induced Ge is extracted from the Ga. ^{71}Ge is unstable with respect to electron capture ($t_{1/2}$=11.43 days) and, therefore, the amount of extracted Ge can be determined from its activity as measured in small proportional counters. The experiment has measured the solar neutrino flux in 31 extractions between January 1990 and October 1993 with the result; 69$\pm$10 (statistical) +5/-7 (systematic) SNU. This is well below the standard solar model expectation of 138 SNU. Additional extractions through the end of 1994 are awaiting analysis.

The collaboration has used a 518-kCi ^{51}Cr neutrino source to test the experimental operation. The energy of these neutrinos is similar to the solar ^{7}Be neutrinos and thus makes an ideal check on the experimental procedure. The extractions for the Cr experiment took place between January and May of 1995 and the counting of the samples lasted until fall. We have finished the bulk of the analysis of this data and presented preliminary reports at several meetings this past year. The result, expressed in terms of a ratio of the measured production rate to the expected production rate, is 1.0$\pm$0.15. This indicates that the discrepancy between the solar model predictions and the SAGE flux measurement cannot be an experimental artifact.

The University of Washington is playing a major role in the statistical analysis of the SAGE data and in the determination of systematic uncertainties. We are very active in the remaining analysis of the Cr experiment data as well as the solar neutrino data.

3. NUCLEUS-NUCLEUS REACTIONS

3.1 Entrance channel effects of light charged particle emission from the ^{156}Er compound nucleus

J.D. Bierman, P. Chan, M.P. Kelly, J.F. Liang, A.A. Sonzogni, R. Vandenbosch and J.P.S. van Schagen

As reported in last year's Annual Report,[1] the light charged particle decay of the ^{156}Er compound nucleus was measured for $^{12}C + ^{144}Sm$ and $^{60}Ni + ^{96}Zr$ reactions. The excitation energy and the spin distribution for the compound nucleus formation are matched in both systems. Comparisons of the light charged particle spectra, in coincidence with evaporation residues, show that the spectral shape of the ^{12}C induced reaction is harder than the ^{60}Ni induced reaction.

The experiment was repeated by varying the geometry of the electrostatic deflectors and detectors to look for possible bias in the measurement. The differences in the particle spectra between the two systems persist. Since this is not expected by the theory of compound nucleus decay, dynamical effects were investigated to try to resolve the discrepancies.

The amalgamation time for $^{60}Ni + ^{96}Zr$ is three to four times longer than that for $^{12}C + ^{144}Sm$, according to calculations performed by the one body dissipation model code HICOL.[2] Because of the high excitation energy of the reactions, the lifetime of the composite system $^{60}Ni + ^{96}Zr$ can be shorter than the amalgamation time. This may lead to particle and γ-ray emissions during formation which would remove energy from the system. Thus, the final excitation energy reached would be less than that of the $^{12}C + ^{144}Sm$ system. Statistical model calculations taking into account particle emission during formation were carried out. Fig. 3.1-1 presents the results of EVAP[3] calculations for both reactions using an amalgamation time estimated at spin $I = 30\hbar$. The solid curves are results including particle emission during formation and the dashed curves are results of no pre-compound (p.c.) emission. For the $^{12}C + ^{144}Sm$ reaction, the effect of pre-compound emission hardly changes the high energy slope of the particle spectrum. However, the inclusion of particle emissions during formation can almost account for the softer spectral shape of the $^{60}Ni + ^{96}Zr$ reaction. It should be pointed out that HICOL predicts that the formation time as a function of spin is not linear. The amalgamation time becomes significantly longer for higher spins.

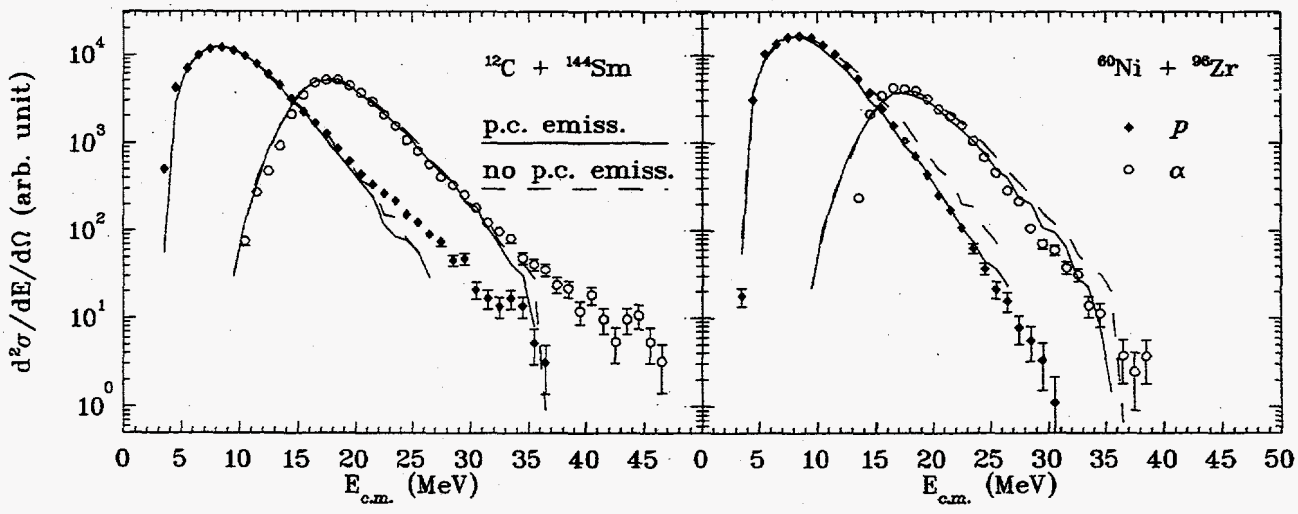

Fig. 3.1-1. Energy spectra of protons and α particles emitted from the decay of the ^{156}Er compound nucleus. See text for the explanations of curves in the figure.

[1]Nuclear Physics Laboratory Annual Report, University of Washington (1995) p. 21.

[2]H. Feldmeier, Rep. Prog. Phys. **50**, 915 (1987).

[3]N. G. Nicolis, D. G. Sarantities and J. R. Beene, computer code EVAP (unpublished).

3.2 The Giant Dipole Resonance and bremsstrahlung in $^{16,18}O+^{92,100}Mo$ reactions

J.D. Bierman, M.P. Kelly, J.F. Liang, K.A. Snover and A.A. Sonzogni

The GDR and bremsstrahlung observed in heavy-ion collisions, especially in the region of 1-3 MeV/u excitation energy, has been the subject of considerable experimental and theoretical study in recent years.[1,2] In particular, the behavior of the GDR width in the region of high temperature and spin is not understood and the treatment of bremsstrahlung in competition with GDR emission in reactions which populate this region of excitation energy has been cursory at best.

Our current studies of γ-rays produced in $^{16,18}O+^{92,100}Mo$ address these topics. The accurate determination of the bremsstrahlung cross section through angular distribution measurements is necessary if one is to extract reliable GDR parameters. Since GDR and nucleon-nucleon bremsstrahlung emission take place from different reference frames, their characteristic $a_1(E_\gamma)'s$ differ in an easily calculable way. Thus, the $a_1(E_\gamma)$ should allow an almost model independent separation of GDR and bremsstrahlung components.

Fig. 3.2-1 shows fold ≥ 4 γ-ray spectra obtained using the Seattle 10" x 15" NaI spectrometer for the reaction $^{18}O+^{100}Mo$ at 9.4 MeV/u bombarding energy. The left panel shows our 90° spectrum with a simultaneous fit of both statistical (CASCADE) and bremsstrahlung components (solid line), and the bremsstrahlung component alone, modeled by a simple falling exponential (dashed line). The center panel shows the same data with the phase space from the density of nuclear states divided out in an approximate way to give a pseudo absorption spectrum.[3] The right panel shows the measured a_1 coefficient and the predicted a_1(solid line) from the 90° cross section fit. A surprising result of this preliminary analysis is the narrow value of 8.4±0.5 MeV deduced for the GDR width. Further work including a simultaneous fit to both cross section and a_1 coefficient, investigation of possible contributions from pre-equilibrium emission, as well as further measurements at higher excitation energy will take place in the coming year.

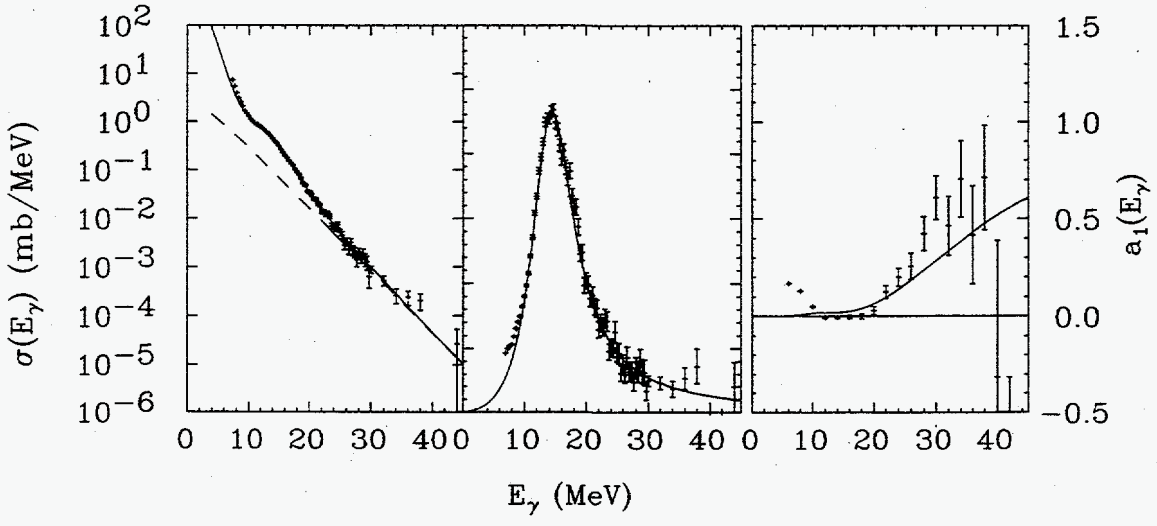

Fig. 3.2 -1. Fold ≥ 4 γ-ray spectra for $^{18}O+^{100}Mo$ producing ^{118}Sn at E*= 145 MeV.

[1]H.J. Hofmann *et. al.*, Nucl. Phys. A **571**, 301 (1994).
[2]A. Bracco *et. al.*, Phys. Rev. Lett. **74**, 3748 (1995).
[3]J.H. Gundlach *et. al.*, Phys. Rev. Lett. **65**, 2523 (1990).

3.3 Distributions of fusion barriers for systems involving targets with prolate and oblate static quadrupole deformation

J.D. Bierman, P. Chan, M.P. Kelly, J.F. Liang, A.A. Sonzogni and R. Vandenbosch

Our experiment to determine the distributions of fusion barriers for the systems $^{40}Ca + ^{192}Os, ^{194}Pt$ has been completed. The results have just recently been published.[1] In the Letter, coupled channel calculations were presented explaining which nuclear characteristics, oblate vs. prolate static quadrupole deformation, and couplings, projectile octupole and positive Q-value 2n transfer channels, were responsible for the structure present in the experimental results. While the calculations qualitatively agreed with the experimentally determined barrier distribution shapes, the calculations significantly overpredicted fusion at energies above the barrier and underpredicted fusion at energies below the barrier. We have since performed more coupled channel calculations attempting to improve agreement with the cross section data.

The new calculations include two significant modifications from those in the published letter. We have added a second transfer channel, 2n transfer from target to the first excited state in the projectile, the Q-value of which is still quite positive and of comparable coupling strength to transfer to the ground state. A second modification was to increase the nuclear diffuseness by approximately 35% over the default value. The need for a larger diffuseness has been noted in previous studies of barrier distributions.[2] The combination of these two changes results in calculations which are in much better agreement with the experimental results. The agreement with the barrier distributions is improved and the calculated fusion cross sections agree with the data far better than the previous results at energies both above and below the barrier region.

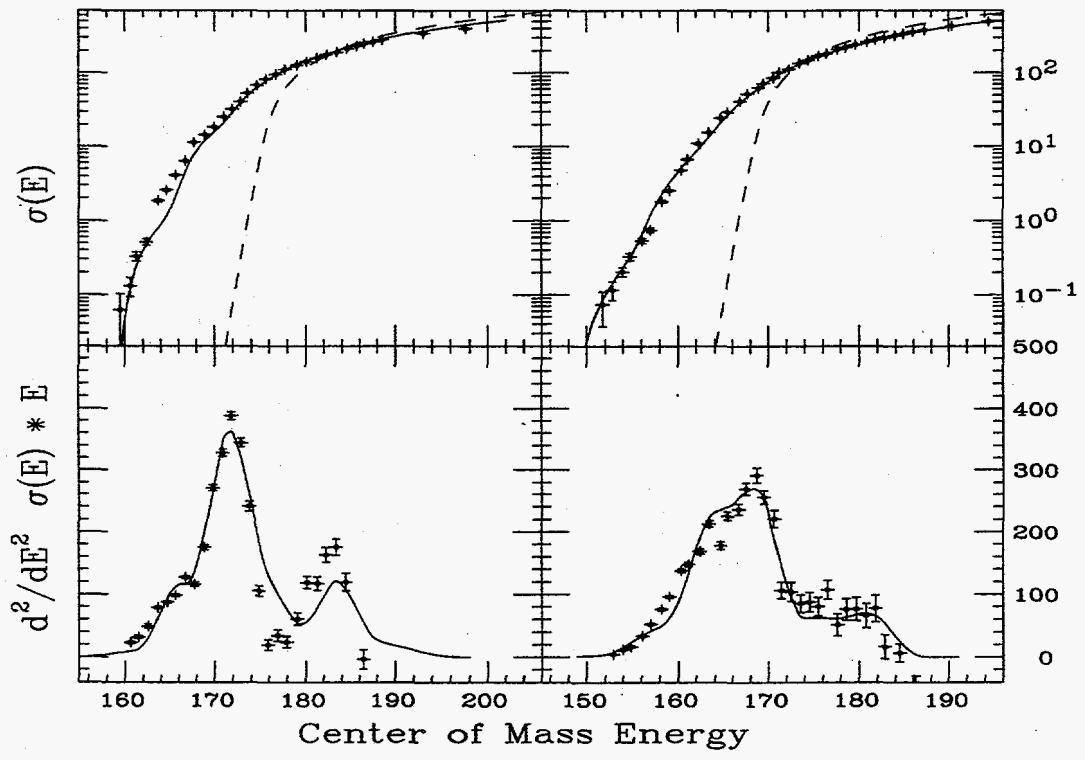

Fig. 3.3-1. Fusion cross sections and barrier distributions from both experimental work, data points, and coupled channels calculations for the systems $^{40}Ca + ^{194}Pt, ^{192}Os$. The left-hand panels are the platinum system results, osmium results are on the right. The full curve represents calculations including the deformations and couplings mentioned in the text. The dashed curve ignores these effects.

---

[1] J.D. Bierman *et al.*, Phys. Rev. Lett. **76**, 1587 (1996).

[2] R.C. Lemmon *et al.*, Phys. Lett. B **316**, 32 (1993).

3.4 Fusion reactions for $^{40}Ca + ^{46,48,50}Ti$ at energies close to the Coulomb barrier

J.D. Bierman, P. Chan, M.P. Kelly, J.F. Liang, A.A. Sonzogni and R. Vandenbosch

We have completed an experiment to obtain the fusion cross sections for the systems $^{40}Ca + ^{46,48,50}Ti$ at energies close to the Coulomb barrier. Description of the experimental technique as well as the motivation for the project can be found in the previous Annual Report.[1]

As an example of our results, we show in the figure below the cross sections and the corresponding barrier distributions for $^{40}Ca + ^{48}Ti$. The full line is from a coupled channel calculation, while the dashed line is from an uncoupled one.

By analyzing the fusion excitation functions, we found that $^{40}Ca + ^{50}Ti$ has a larger enhancement in the sub-barrier fusion cross section than $^{40}Ca + ^{48}Ti$, which in turn presents a larger enhancement than $^{40}Ca + ^{46}Ti$.

We used a coupled channel model[2] to separate inelastic and transfer contributions. We found that most of the enhancement for ^{46}Ti could be explained by the inelastic coupling alone, while ^{50}Ti required an important transfer contribution. A similar situation was observed when trying to fit the barrier distributions.

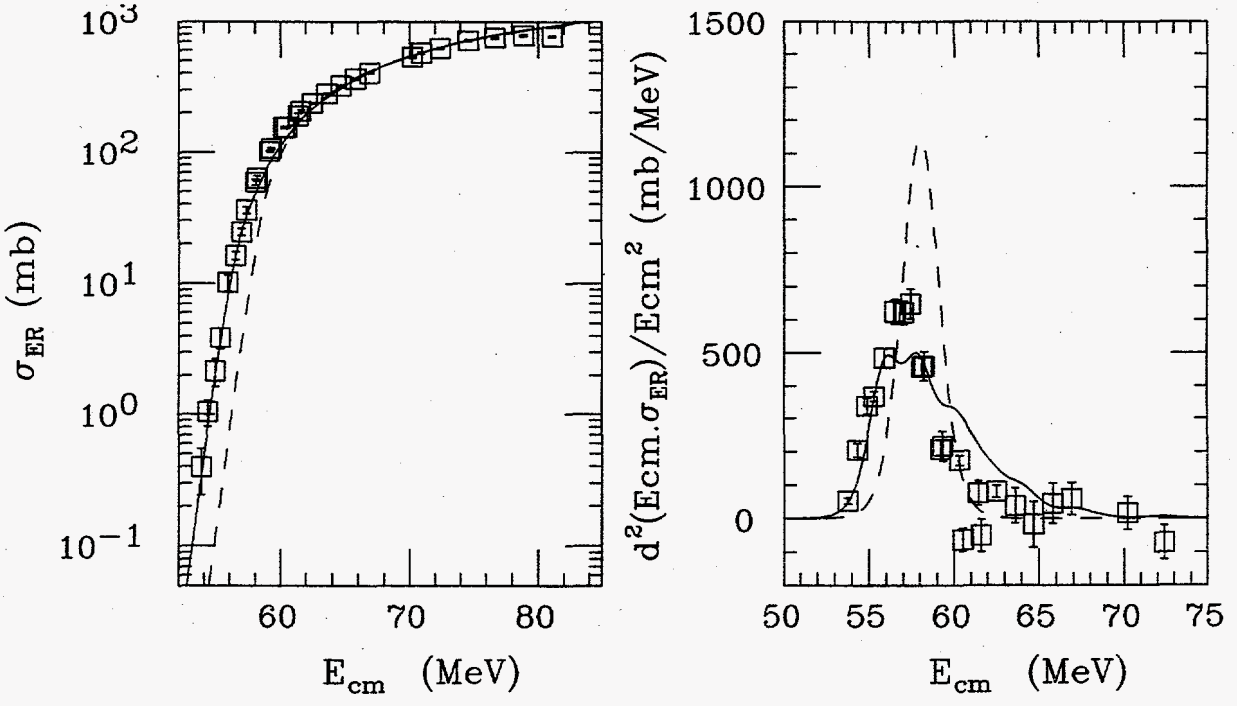

Fig. 3.4-1. The left panel shows the fusion excitation function for $^{40}Ca + ^{48}Ti$ as a function of the center of mass energy. The right panel shows the corresponding barrier distribution. The full line is from a coupled channel calculation while the dashed line is from an uncoupled one.

[1]Nuclear Physics Laboratory Annual Report, University of Washington (1995) p.19.

[2]J. Fernandez Niello *et al.*, Comp. Phys. Comm. **54**, 409 (1989).

3.5 Temperature dependence of the level density parameter

J.P. Lestone

The nuclear level density plays a central role in our theoretical modeling of the particle emission from, and fissioning of, hot compound nuclei. The density of nuclear levels as a function of thermal excitation energy $\rho(U)$ is often estimated assuming a weakly interacting Fermi-gas, and written as $\rho(U) \propto \exp(2\sqrt{aU}) / U^2$. Recent theoretical predictions of a temperature dependence of the Fermi gas level density parameter a have been obtained numerically using the Thomas-Fermi (TF) approximation.[1] This work included a spatial and temperature dependence of the effective nucleon mass. We have considered these complexities associated with the effective mass of nucleons in atomic nuclei and have used the local density approximation (LDA)[2] to obtain the following expression for the temperature dependence of the inverse level density parameter (K=A/a)

$$K(T) = 15.5\ \text{MeV} / [1.6 + 1.8A^{-1/3} - 0.5\{1 - \exp[-(\frac{TA^{1/3}}{21\ \text{MeV}})^2]\}]. \qquad (1)$$

The dashed lines in Fig. 3-5.1 show K(T) determined using Eq. (1) for systems with mass numbers 60 and 210. These results cannot be compared directly with the TF results shown in Fig. 1 of Ref. 1, since Shlomo and Natowitz adopted the definition $a_{\text{eff}}(T) = A / K_{\text{eff}}(T) = U / T^2$. The reflection $a \sim U / T^2$ is, however, only valid if $da / dU = 0$ (see Ref. 2) and thus $a \neq a_{\text{eff}}$. From Eq. (1) one can show that

$$\frac{1}{K_{\text{eff}}(T)} = \frac{1}{K(T)} - \frac{T^2 A^{2/3}}{6830\ \text{MeV}^3} \exp[-(\frac{TA^{1/3}}{21\ \text{MeV}})^2]. \qquad (2)$$

Fig. 3.5-1 shows numerical TF calculations of $K_{\text{eff}}(T)$ from Ref. 1 (solid lines) and $K_{\text{eff}}(T)$ obtained using equations (1) and (2) (dashed-dotted lines). The excellent agreement between these two sets of calculations leads us to conclude that the LDA adequately describes the temperature dependence of the TF calculations of the nuclear level density parameter.

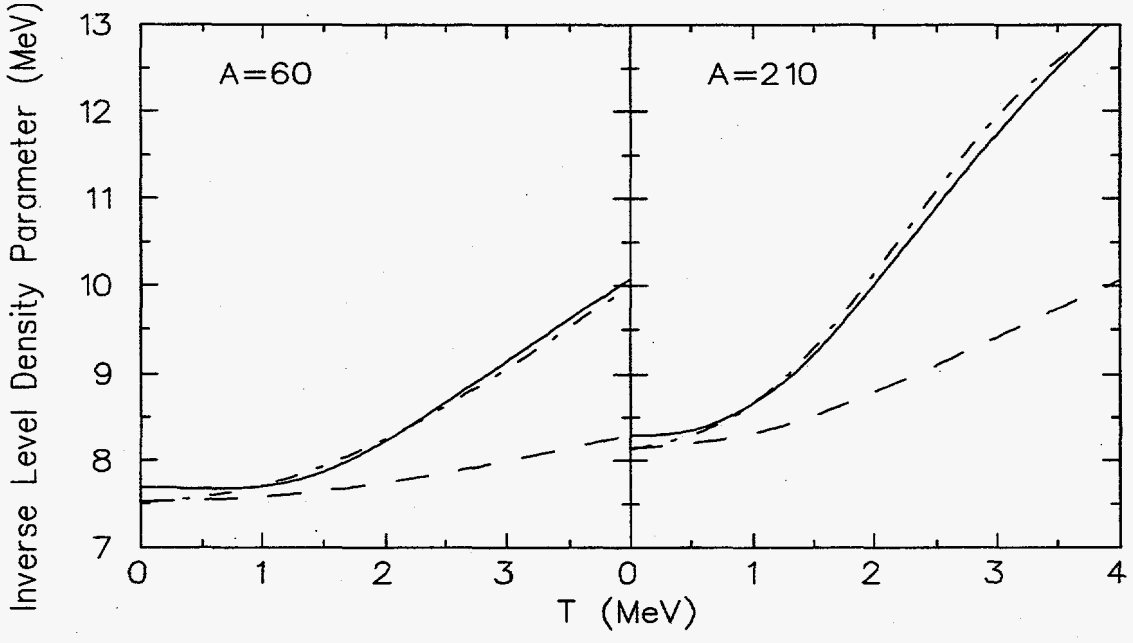

Fig. 3.5-1. K(T) determined using Eq. (1) (dashed lines); TF calculations of $K_{\text{eff}}(T)$ from Ref. 1 (solid lines) and $K_{\text{eff}}(T)$ obtained using equations (1) and (2) (dashed-dotted lines).

[1] S. Shlomo and J.B. Natowitz, Phys. Rev. C **44**, 2878 (1991).
[2] J.P. Lestone, Phys. Rev. C **52**, 1118 (1995).

3.6 Quasi-fission with A < 20 projectiles

J. P. Lestone

A long outstanding problem in fission physics has been the anomalously large fission fragment anisotropies obtained with A < 20 projectiles on actinide targets near and below the Coulomb barrier. Recently, experimental results of Hinde *et al.*[1] on the $^{238}U(^{16}O,f)$ reaction have led them to claim that they have "conclusive evidence" that the fraction of fission fragments coming from quasi-fission reactions increases as one drops through the Coulomb barrier. The precise mechanism by which this occurs is yet to be established but is believed to be associated with the large ground state deformation of actinide targets. To aid in the understanding of this problem, we have calculated fusion cross sections for A < 20 projectiles on actinides taking into account the deformed Coulomb and nuclear potentials around the actinide nuclei. These results are in good agreement with measured fusion cross sections. Once the fusion barrier is crossed (or penetrated) a one-dimensional symmetric mass split Langevin calculation is performed leading to an ensemble of fissioning times. Our Langevin calculations yield two distinct fission components, one fast and the other slow. The slow component is standard fusion-fission, i.e. with Langevin trajectories passing through the equilibrium deformation before processing to fission. The fast component is similar to, but not exactly the same as, quasi-fission observed with A > 20 projectiles. In order to describe this component let us consider the interaction of sub-barrier ^{16}O ions with ^{232}Th nuclei. Because the incoming ions are sub-barrier the ^{16}O will preferentially interact with the tips of the deformed ^{232}Th target. After the Coulomb barrier is penetrated, a hot deformed system is produced with a distance between the center of masses of the two halves, slightly less than that for the fission saddle point of this system. In a purely deterministic model, 100% of such systems would evolve towards the equilibrium deformation. If the Brownian forces associated with nuclear viscosity are included, then some fraction of the systems will be kicked across the fission saddle point without first proceeding to the equilibrium deformation. Fig. 3.6-1 shows our calculation of the percentage of fission due to quasi-fission as a function of beam energy relative to the fusion barrier. These calculations are qualitatively consistent with the conclusions of Hinde *et al.*, i.e. the quasi-fission increases as one drops through the fusion barrier.

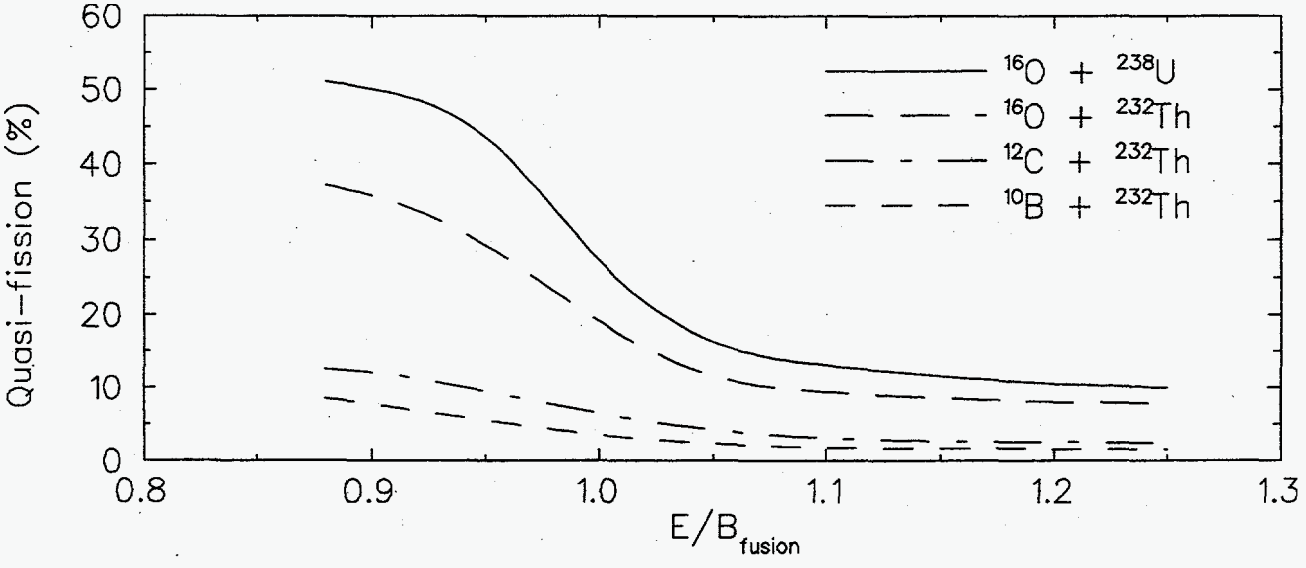

Fig. 3.6-1. Calculations of the percentage of fission due to quasi-fission as a function of beam energy relative to the fusion barrier.

[1]Hinde *et al.*, accepted for publication in Phys. Rev. C.

3.7 Light charged particles from $^{19}F + ^{181}Ta$ reactions leading to evaporation residues

J.P. Lestone, J.F. Liang, D.J. Prindle, A.A. Sonzogni, J.P.S. van Schagen and R. Vandenbosch

Recently, Fabris *et al.*[1] have measured α-particles in coincidence with evaporation residues (ER) in $^{19}F + ^{181}Ta$ reactions with beam energies from 90 to 140 MeV. From these α-data they concluded the Fermi-gas level density parameter decreases dramatically from $a = A / 8.3\ MeV^{-1}$ at a thermal excitation energy of U=20 MeV to $a = A / 12\ MeV^{-1}$ at U=100 MeV. Such a sharp drop in the level density parameter would give a much stronger increase in nuclear temperature, and thus particle emission rates, with increasing excitation energy than previously believed. If true, the claims of Fabris *et al.* would seriously affect the conclusions of many recent studies where the properties of particle emission from hot fissioning systems are used to estimate the time scales of heavy-ion fission reactions. We have measured the proton and α-emission spectral shapes at 90° and 160° to the beam direction in coincidence with ER from the reactions 150 MeV and 190 MeV $^{19}F + ^{181}Ta$. Our center of mass spectra are not consistent with the experimental results of Ref. 1. At 160° to the beam, the influence of non-equilibrium emission and ER detection efficiencies on our observed spectral shapes are expected to be small. Fig. 3.7-1 shows our 160° proton and α-spectra converted into the center of mass reference frame. The solid lines show statistical model calculations of the corresponding spectral shapes with an inverse level density parameter K=A/*a* which increases linearly with excitation energy from a value of K=8.1 MeV at U=0 MeV to K=9.2 MeV at U=100 MeV. The standard optical model emission barrier heights were lowered to reproduce the measured peak positions. The disagreement at the highest kinetic energies cannot be fixed with a simple change in the above-mentioned excitation energy dependence of the level density parameter without producing a significantly poorer fit to the data in the region several MeV above the peak positions. The dashed lines show calculations with the excitation energy dependence of the level density parameter as suggested by Fabris *et al.* The dependence of the level density parameter on excitation energy suggested by our data is consistent with recent theoretical calculations[2,3] while the results of Fabris *et al.* are not.

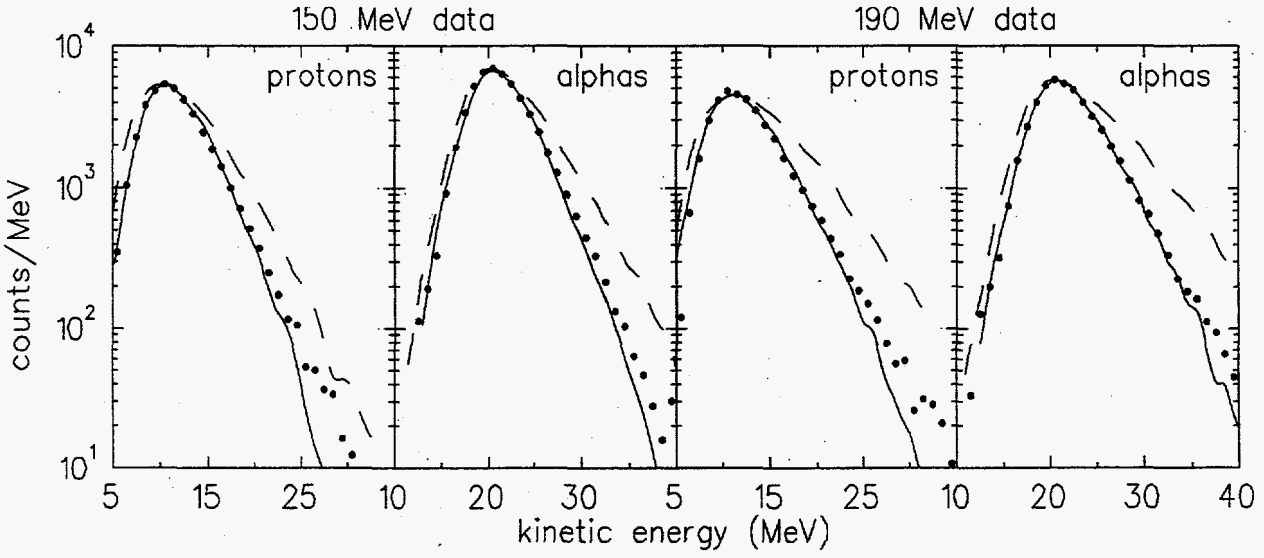

Fig. 3.7-1. Center of mass kinetic energy spectra for proton and α emission at $\theta_{lab} = 160°$ in coincidence with ER in 150 MeV and 190 MeV $^{19}F + ^{181}Ta$ reactions (solid circles). The solid and dashed lines shown statistical model calculations (see text).

[1] D. Fabris *et al.*, Phys. Rev. C **50**, R1261 (1994).

[2] J.P. Lestone, Phys. Rev. C **52**, 1118 (1995).

[3] S. Shlomo and J.B. Natowitz, Phys. Rev. C **44**, 2878 (1991).

3.8 Disappearance of entrance channel dependence of fission fragment anisotropies at above-barrier energies

J.D. Bierman, S. Kailas,* S.S. Kapoor,* J.P. Lestone, J.F. Liang, D.M. Nadkarni,* D.J. Prindle, A.A. Sonzogni and R. Vandenbosch

It has been observed[1] that the anisotropies for actinide targets are well accounted for by the transition state model for the lighter projectiles ^{12}C, ^{10}B and ^{9}Be but are larger than expected for the heavier projectiles ^{16}O and ^{19}F. These observations have been interpreted[1] as an entrance channel effect arising from contributions of fission-like events from pre-equilibrium fission expected to arise only in the case of the heavier projectiles, on the basis of the variation of the liquid drop model driving force at the saddle in the mass asymmetry degree of freedom. The target-projectile combinations having an entrance channel mass asymmetry $\alpha = (A_T - A_P)/(A_T + A_P)$ less than about 0.88 (^{16}O and ^{19}F) exhibit anomalous anisotropies. The Businaro-Gallone critical asymmetry (α_{BG}) value where the driving force changes direction has been estimated to be about 0.9 in this mass and charge region. For values of α greater than α_{BG}, the driving force favours amalgamation of the nascent partners (fusion and compound nucleus formation), whereas for smaller values the smaller partner gains in mass at the expense of the heavier, and the dinuclear system may reseparate as a fission-like event without K-equilibration and formation of a compound nucleus.

The above study,[1] however, involved formation of different compound nuclei and the data for the anomalous systems were at energies not very far above the fusion barrier. An alternative correlation with the energy relative to the barrier rather than with the entrance channel mass asymmetry has been offered.[2] We have performed a more definitive experiment by studying two entrance channels which lead to the same compound nucleus. The $^{12}C+^{236}U(\alpha = 0.903)$ entrance channel has α greater than the Businaro-Gallone critical asymmetry and the $^{16}O+^{232}Th(\alpha = 0.871)$, has α smaller than the critical asymmetry. At an excitation energy of 62 MeV (well above the fusion barrier for both entrance channels) one can also match the average angular momentum. The experiment was performed using beams from the tandem-booster accelerator. Inclusive single-fragment anisotropies were obtained from Si surface barrier detectors. We also used three large-area segmented gas detectors. These were primarily used for measurements of fragment-fragment coincidences in order to determine the folding angle distributions. We also determined inclusive (singles) fission fragment angular distributions from the gas detectors, and the anisotropies from these measurements agree well with the Si detector results. We report here the average value of the independent singles determinations with the two kinds of detectors. We focus here on the single-fragment anisotropies, as these were the kind of results that led to the motivation of the present measurement. Interpolating between the measured anisotropies gives 2.05 ± 0.1 for the O + Th system and 1.96 ± 0.1 for the C + U system at this excitation energy. As these two values are the same within the experimental error there is no evidence that the entrance channel mass asymmetry relative to the Businaro-Gallone critical asymmetry plays any role in determining the fission anisotropy at energies well above the fusion barrier.

---

* Nuclear Physics Division, BARC, Bombay-400085, India.

[1] V.S. Ramamurthy *et al.*, Phys. Rev. Lett. **65**, 25 (1990).

[2] R. Vandenbosch, "Advances in Nuclear Dynamics," W. Bauer and B. Back, eds, World Scientific, 1992, p. 25.

3.9 Scaling of high energy fission anisotropies

J.D. Bierman, J.P. Lestone, J.F. Liang, D.J. Prindle A.A. Sonzogni and R. Vandenbosch

In the previous article we have discussed some of the results of a collaborative experiment with a group from Bombay to measure fission fragment anisotropies. As part of that collaborative effort we measured anisotropies to bombarding energies considerably higher than for the data we discussed in the preceding report. These results are shown by the data points in Fig. 3.9-1. Here we discuss the interpretation of these higher energy anisotropies. We have noted that the anisotropies seem to scale with the mean square angular momentum. To demonstrate this we have arbitrarily taken the $^{12}C + ^{236}U$ data as a reference line (dashed), and scaled W(180)/W(90) -1 values by $< \ell^2 >$ to get the full and dotted lines for the other systems in the left panel of the figure. This simple scaling seems to adequately account for the difference in anisotropies for the different systems. This is expected to be the case for that fraction of the partial wave distribution where there is a finite fission barrier. The surprise is that the remaining fraction also scales as $< \ell^2 >$. This scaling is not expected in one model of non-equilibrium fission[1] where the anisotropy of this fraction is assumed to be independent of $< \ell^2 >$. This latter assumption has also been tested by finding the anisotropy of the non-equilibrium fraction required to account for the $^{12}C + ^{236}U$ anisotropy and using this anisotropy for the non-equilibrium fraction for the other systems. The results are shown in the right hand panel of the figure, and are seen to be incompatible with the data.

What might be the origin of the scaling of the anisotropies with $< \ell^2 >$ for ℓ values for which the fission barrier vanishes? One possible interpretation is that the anisotropy for these partial waves is determined at some shape of the fissioning nucleus in its evolution towards scission which is the same for all entrance channels.

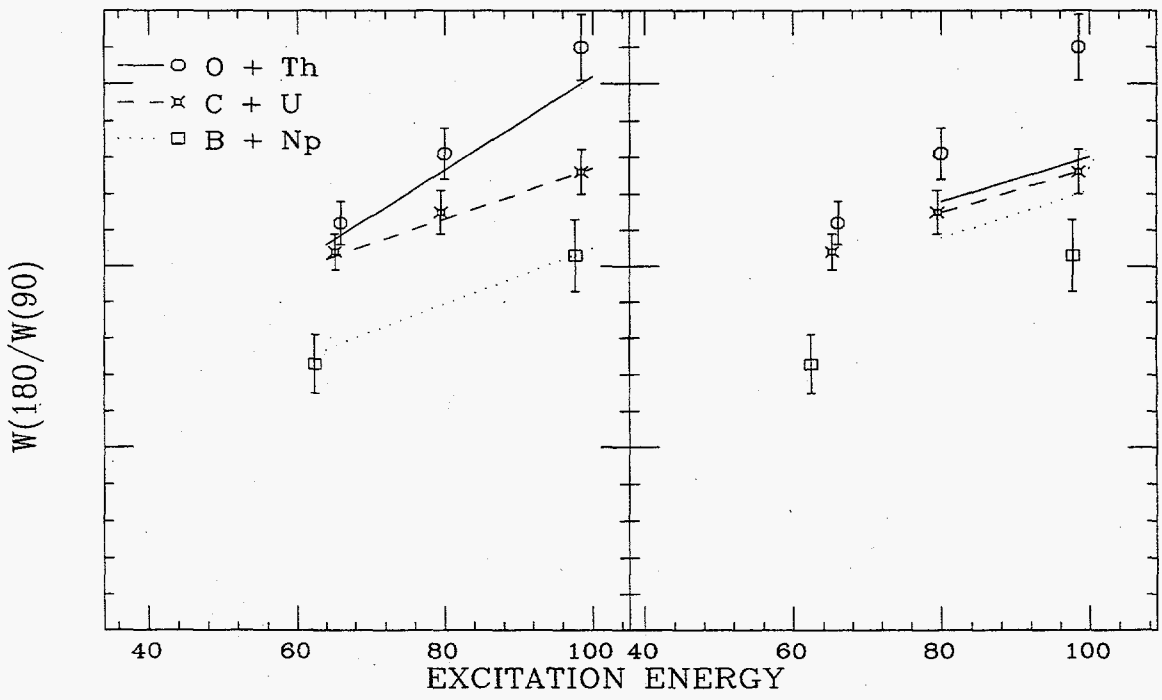

Fig. 3.9-1. In a) the full and dotted curves are obtained by $< \ell^2 >$ scaling. In b) it is assumed that the anisotropy is independent of $< \ell^2 >$ for that fraction of the cross section for which the fission barrier is less than 0.4 MeV.

[1] V.S. Ramamurthy and S.S. Kapoor, Phys. Rev. Lett. **54**, 178 (1985).

3.10 APEX recent results

T.A. Trainor and the APEX Collaboration

Narrow structures reported by GSI positron experiments EPOS and ORANGE first in positron singles energy spectra and later in electron-positron energy distributions associated with collisions of very heavy ions near the Coulomb barrier have been an outstanding puzzle in nuclear physics for nearly fifteen years. With CW uranium beams of 1-10 pnA intensity from the ATLAS accelerator at Argonne National Laboratory, a beam energy range matching the GSI experiments and a highly efficient apparatus providing a kinematically complete description of produced electrons and positrons APEX[1] was expected to provide a qualitative improvement in the understanding of this phenomenon.

In the initial operating period a program was begun to provide an accurate Monte Carlo (MC) representation of APEX. This representation has been extensively checked with radioactive source and heavy-ion beam studies.

A very stringent test of both APEX functioning and its MC representation has been the detection of Internal Pair Conversion (IPC) electron-positron pairs resulting from Coulomb excitation (in 5.95 MeV/u ^{206}Pb on ^{206}Pb collisions) of the 3^- level in ^{206}Pb followed by subsequent IPC of the E1 transition to the 2^+ first excited state. Since the IPC occurs in one of the moving collision partners the electron and positron detected energies must be Doppler corrected to narrow the line in the reconstructed electron-positron pair sum-energy spectrum. Because the identity of the source ion cannot be uniquely determined on an event-wise basis the Doppler correction is made with both velocity assumptions (one correct and one incorrect) for each event, resulting in a broader structure beneath a narrow peak, which is indeed quantitatively confirmed in the APEX electron pair sum-energy spectrum.

In a detailed systematic study of the ^{206}Pb data various cuts were made on both the heavy ion kinematics and lepton kinematics (opening angle) which should result in specific changes to both the peak-to-background ratio and the Doppler-corrected peak structure in the pair sum-energy spectrum. The agreement between measurement and simulation was found to be excellent.

A further result of the ^{206}Pb study was the first experimental determination of the branching ratio for IPC of $(4\pm1) \times 10^{-5}$, in agreement with the theoretical value of 4.17×10^{-5}. This detailed study of the IPC in ^{206}Pb clearly demonstrates that APEX has adequate sensitivity to observe narrow structures such as those reported by the GSI experiments and to elucidate their kinematic properties.

APEX has now been operational for two years. It has been thoroughly calibrated and has accumulated a very sizable data inventory for the HI collision systems U+Th and U+Ta (7000/μb for U+Th and 24,600/μb for U+Ta). No statistically convincing narrow structures have been observed by APEX in either the positron singles or electron-positron pair coincidence spectra.[2]

We conclude that the APEX results disallow the presence of any narrow structures in sum-energy spectra at a level which falls at least one order (~40σ for a strong HI energy dependence scenario and simple wedge cut), if not two orders (~300σ for no HI energy dependence and electron-positron pair kinematic restrictions to a back-to-back decay scenario) of magnitude (99% CL) below the levels reported by the GSI experiments. The conclusion seems inescapable that there is unresolvable disagreement between the APEX and GSI experimental results.

---

[1] I. Ahmad *et al.*, Nucl. Instrum. Methods **370**, 540 (1996).

[2] I. Ahmad *et al.*, Phys. Rev. Lett. **75**, 2658 (1995).

4. ULTRA-RELATIVISTIC HEAVY IONS

4.1 URHI overview

J.G. Cramer and T.A. Trainor

The University of Washington URHI group carries out collaborative experimental programs with two large-acceptance heavy ion experiments - STAR, a large solenoidal detector presently under construction and scheduled to commence operation at RHIC in 1999, and NA49, a fixed-target multi-TPC experiment that has been operating since 1994 at the CERN SPS. The Fall-1995 run of NA49 was the first in which all detector components were in operation, including four large TPCs using 180,000 electronics channels. About 10 Tbytes of data were recorded, representing about 700,000 central Pb-Pb events at 158 GeV/nucleon.

After a year of analysis the first NA49 physics results are becoming available. Surprises have appeared in several areas, including the high degree of nuclear stopping and the relative abundance of flow in central and peripheral collisions. One of the main goals of the NA49 and STAR experimental programs is event-by-event physics analysis. Much of the recent effort of the URHI group has been directed toward development of new event-by-event analysis techniques. In addition, with DOE capital equipment funds we have recently purchased two new HP 'Skyhawk' parallel-processor workstations providing greater computational power for extensive offline analysis of NA49 data.

The UW has had a leadership role in the production of main TPC tracking software for NA49. This software is completed and has passed through a quality assurance program. It is presently being used for full-scale production of data summary tapes for the 1995 NA49 data. This is the largest data volume ever processed at CERN, easily exceeding in a few weeks of detector operation the combined data volumes of all the LEP experiments to date.

A novel multitarget correlation analysis technique developed at the UW was used to determine the precise relative location of all NA49 detectors to about 100 micrometers and 100 microradians, thus virtually eliminating system geometry as a source of experimental error.

The main NA49 data display facility for tracking analysis and optimization, developed at the UW, permits one to 'fly' through a visual representation of the tracking data. It also facilitates direct access to data structures used by the tracking code. One of the images generated by this display was featured on the 1996 GSI calendar.

Investigations of multiparticle Bose-Einstein interferometry have advanced on several fronts in the past year. A new analysis procedure has been developed which offers the capability for distinguishing between the effects of source coherence and particle contamination. The 'ripples' produced by non-Gaussian source shapes have been investigated. A new Monte-Carlo event-generator code has been developed which can include Bose-Einstein and Coulomb correlation effects for up to order 6.

Work continues on STAR trigger algorithms, with a transition from level-1 algorithms emphasizing one-dimensional charged-particle multiplicity distributions on pseudorapidity to level-2 algorithms emphasizing two-dimensional EM calorimeter energy distributions applicable to jet and other high-p_t physics.

The slow control program SControl has been further improved and integrated into the NA49 detector systems and was used with good results in the Fall-95 run. We have completed an EPICS-based computer control system for the STAR TPC high voltage supply which interacts with the STAR slow controls system and stabilizes the TPC electron drift speed to about one part in 100,000.

4.2 First physics from NA49 lead beam operation at the CERN SPS

S.J. Bailey, J.G. Cramer, D.J. Prindle, T.A. Trainor and D. Weerasundara

Analysis of NA49 calorimetry data indicates that of the initial 33 TeV beam energy 1 TeV is converted into transverse energy in a central lead-lead collision, carried mainly by about 2500 hadrons. This transverse energy corresponds to about 60% of the total amount possible within kinematic constraints. Thus, although nuclear stopping is nearly complete at SPS energies, a significant fraction of the incident energy remains in directed longitudinal motion, either from incomplete stopping or from subsequent longitudinal expansion of the hot collision system.

The observed differential transverse energy of 450 GeV per unit pseudorapidity corresponds, by an estimating procedure due to Bjorken, to an energy density of 3 GeV/fm^3 in the initial reaction volume. Although there is some model uncertainty to this estimate this number compares favorably with lattice gauge estimates of a Quark-Gluon Plasma (QGP) phase transition at 1 GeV/fm^3 in terms of creating conditions for color deconfinement at the SPS.

Looking at the systematics of nuclear stopping in heavy ion collisions over a broad energy range, including the new lead-beam results, one observes that the participant particle rapidity shift is proportional to the total rapidity range available. This implies exponentially increasing stopping over the presently accessible energy range. Whether this trend continues to higher energies or whether a sufficient number of interactions in the nuclear medium finally strips partons of their ability to interact (leaving 'bare' quarks for example) is a very interesting question related to the possibility of a baryon-free region at mid rapidity at RHIC and LHC energies, which would facilitate more direct comparison with lattice gauge calculations.

Looking at the systematics of particle production in nucleus-nucleus collisions including the lead-beam data one observes that the number of produced hadrons per participant baryon does not increase significantly with stopped energy. This implies that the energy per produced hadron must increase. What is observed in the lead data are 'temperatures' or slope parameters for net baryon transverse mass spectra exceeding 250 MeV, and far exceeding the 150 MeV appropriate for a typical thermal or Hagedorn model. This suggests that a substantial part of the transverse energy in heavy nucleus-nucleus collisions is not thermal.

What is increasingly evident from the lead data analysis is that there is a surprisingly large transverse flow component to the momentum distribution of produced particles in heavy nucleus collisions. The large and mass-dependent apparent 'temperatures' for the hadron transverse-mass spectra are better interpreted as the consequence of radial flow. This can be interpreted as evidence that an initially thermalized hot prehadronic phase expands isentropically, cooling to 150 MeV and transferring some of the previously thermalized energy to directed radial flow with a beta of about 0.5. This combination leads to apparent temperatures for net baryons in the neighborhood of 250 MeV as observed.

In addition to radial flow there is now preliminary evidence from analysis of NA49 calorimeter data for directed transverse flow associated with peripheral collisions and correlated with the reaction plane.

In summary, preliminary analysis of NA49 lead data indicate formation of a substantial reaction volume with energy densities at or above that needed for substantial color deconfinement according to lattice gauge calculations. The analysis also indicates a surprising degree of nuclear stopping, and the persistence of a substantial radial flow field with beta as high as 0.5. The presence of flow in turn suggests that the hadronization process preserves considerable memory of earlier stages of the collision process, which may facilitate the detection and study of color deconfinement.

4.3 Event-by-event correlation analysis for NA49

S.J. Bailey, J.G. Reid and T.A. Trainor

Event-by-event analysis of multiparticle momentum distributions has been an important tool of high-energy physics for about two decades. The principal applications have been in the areas of jet physics at higher energies and collective flow of nuclear matter at lower energies. The concept becomes practicable when detector acceptance and particle multiplicities are sufficiently large to detect the correlation signals of interest above the statistical noise level.

The ultrarelativistic heavy ion programs at the CERN SPS, RHIC and LHC have as their object the study of QCD color deconfinement and the properties of deconfined colored matter, the so-called quark-gluon plasma. It is expected that one manifestation of color deconfinement may take the form of correlated structures in momentum distributions beyond those imposed by global kinematic constraints, and that these correlated structures, differing in form from event to event, would be largely washed out in any ensemble-averaged inclusive distributions. It is therefore essential to characterize each event in terms of its correlation structure in order to develop maximum sensitivity to color deconfinement phenomena.

The program that we have undertaken over the last few years is to develop a universal multiparticle correlation analysis system which can extract all possible information from each event. This system is based on the Renyi entropies, a system of topological measures of which the rank-1 Renyi entropy is identified with the Boltzman-Gibbs entropy of statistical mechanics.

In this work the Renyi entropies are defined as scale-dependent (scaled) quantities, and with each is associated a corresponding scaled dimension. For each event ensemble a reference entropy is determined. The arithmetic difference between the scaled entropy for an individual event and the reference entropy for the event ensemble is the scaled information for the event. The scaled information is then a sensitive measure of differential correlation. (This information is directly related to the Shannon-Wiener information of signal analysis.)

This system can be used in two complimentary ways, either as the basis for event selection, as in an online or offline trigger system, or to carry out a physics analysis on the dynamics of individual collision events. As an event selection mechanism the system would select the (presumably) small fraction of events that may contain an unusual correlation structure, possibly due to fluctuations associated with color deconfinement.

For the study and interpretation of these selected special events one can then use phenomenological event generators to produce simulated events with similar correlation structures, and in this way to sensitively test models of the collision process and aspects of QCD theory. Events from such a generator are passed through a Monte Carlo model of the experimental apparatus, and the resulting simulated particle distributions are passed through the correlation analysis chain. The resulting scaled information system provides a very sensitive measure of differential correlation, presenting a far more demanding test of event generators and physical models than simple ensemble-averaged inclusive distributions.

The correlation analysis system we have developed has been implemented in the C++ programming language and is compatible with the general data processing environment of the NA49 experiment. It has been tested with simulated events and is now being used to analyze real events from the Fall, 1995 NA49 lead beam run at CERN. We expect to analyze several hundred thousand events over the next several months. This analysis will form the basis for a first major search for color deconfinement correlation phenomena in lead-lead collisions at SPS energies.

4.4 Formalism and simulations of multiparticle Bose-Einstein correlations including coherence and contamination effects

J.G. Cramer, K. Kadija* and D. Weerasundara

In Bose-Einstein correlation analysis of two or more pions produced in ultra-relativistic heavy ion collisions, an empirical parameter λ is frequently used to reduce the strength of the correlation function, in order to take into account the possibilities that (a) the pion emission from the source may not be completely incoherent, and (b) the correlated particles assumed to be pions may be contaminated with other particles (kaons, electrons, protons, etc.) which will dilute the measured correlations. However, these two effects have different physical significance and qualitatively different consequences for the magnitude and shape of the correlation, and they should be treated separately.

In the recent literature of multiparticle Bose-Einstein correlations of pions there has been considerable interest in isolating the 'true' multiparticle correlations[1] that contribute to the overall correlation functions, e.g., correlations that are not representable as a product of lower-order correlations. For an incoherent source, this correlation arises from the simultaneous exchange of all particles in the correlated set. Such correlations must be present in an ideal quantum system of identical Bose-Einstein particles as a consequence of proper symmetrization of the multiparticle wave function, but demonstrating this has been an experimental challenge. Eggers *et al.*[2] have suggested using normalized cumulants to isolate the 'true' multiparticle correlation.

We have used the techniques of quantum optics to examine these effects for n = 2 to 6, where n is the number of correlated pions. In particular, we have derived expressions for correlation functions and normalized cumulants for n = 2 to 6, including the effects of coherence and contamination.

We have shown that in the presence of coherence the normalized cumulants no longer isolate the 'true' multiparticle correlation. We have also shown that the effects of coherence and contamination can be distinguished through their effects on the 'intercept' values of correlations and normalized cumulants, and we have proposed a way of analyzing multiparticle correlation data so as to reliably extract the coherence fraction present in the source. This work[3] has recently been published in Physical Review C.

As a continuation of this work, we have developed a Monte Carlo event generator program for simulating the pions produced in ultra-relativistic collisions. The program uses the formalism described in Ref. 3, together with a new Monte Carlo elimination algorithm, for 'building' Bose-Einstein and Coulomb correlations up to 6th order (n = 6) into the simulated event data. The program produces simulated data DST files that can be used as input to HBT analysis codes. We are presently using this new simulation program to investigate the effect of high-order Bose-Einstein and Coulomb correlation effects on conventional HBT analysis which implicitly assumes the presence only of two-particle Bose-Einstein and Coulomb effects.

---

* Max Planck Institute for Physics, Munich, Germany.

[1] N.M. Agababyan *et al.* (the EHS/NA22 Collaboration), Phys. Lett. B **332**, 458 (1994).
[2] H.C. Eggers, P. Lipa, P. Carruthers, and B. Buschbeck, Phys. Lett. B **301**, 298 (1993).
[3] J.G. Cramer and K. Kadija, Phys. Rev. C **53**, 908 (1996).

4.5 Multiparticle HBT for single event physics?

J.G. Cramer

If a relativistic heavy ion collision produces 10^3 final-state π^+ particles, there will be about 10^6 π^+ pairs and 10^9 π^+ triplets that can be used for Bose-Einstein interferometry. For single event physics it is of interest to extract an HBT radius for each event with the best possible statistical accuracy. This suggests that at some large pion multiplicity it may become statistically advantageous to perform single-event HBT analysis using three particles rather than two.

We have investigated this question using a Monte Carlo simulation of NA49 events with particles having a Gaussian distribution of width of 3.2 in rapidity y, a uniform distribution in the azimuthal angle ϕ, and a distribution in transverse-mass m_t that is an order 2 gamma distribution with a temperature of 140 MeV. We have made the following assumptions: (1) because of limited statistics, only the HBT radius R_{inv} corresponding to Q_{inv} in momentum space is of interest; (2) Coulomb effects can be ignored; (3) we wish to determine multiplicities and R_{inv} at which the statistics of pairs is equal to the statistics of triplets at the half-maximum point of the HBT correlation function. In defining condition (3), we note that for equal momentum differences the ratio of the 3-particle Q_{inv} to the 2-particle Q_{inv} at the correlation half-maximum is 1.59 and that the 3-particle HBT enhancement at half-maximum is twice as large as the 2-particle HBT enhancement.

Table 4.5-1. The results of these Monte-Carlo calculations

N_{tot}	dN/dy	Q_{crit} (MeV/c)	R_{crit} (fm)	R_{th} (fm)
20	4.161	223.24	0.5204	1.4476
50	10.403	150.23	0.7733	1.9647
100	20.806	112.61	1.0316	2.4754
200	41.611	88.350	1.3149	3.1187
500	104.03	64.810	1.7924	4.2328
1000	208.05	51.490	2.2561	5.3329
2000	416.1	40.155	2.8930	6.7191
5000	1040.3	29.898	3.8855	9.1193
10000	2080.6	23.518	4.9395	11.4896

Here N_{tot} is the total multiplicity of charged pions in the event (π^+ and π^-), dN/dy is the multiplicity at central rapidity of charged pions per unit rapidity, Q_{crit} is the value of 2-particle Q_{inv} at which 2- and 3-particle HBT enhancements have equal statistics at their half-maximum points, R_{crit} is the corresponding value of R_{inv} for a spherical Gaussian source, and R_{th} is the expected HBT radius calculated from the empirical relation $R_{th} = 0.9(dN/dy)^{1/3}$.

We see from these results that, for multiplicities of interest in the 10^3 range, single-event 2-particle HBT analysis will always have better statistics than 3-particle HBT analysis for expected radii, as given roughly by R_{th}. Therefore we conclude that the greater number of triplets than pairs in an event is misleading because there are always fewer triplets than pairs with appropriately small momentum differences.

4.6 A fast temperature extraction algorithm for single event physics

J.G. Cramer

In CERN Experiment NA49 the 33 TeV Pb beam strikes a Pb target, producing thousands of pions and other particles that are tracked and momentum-analyzed in the four time-projection chambers of the experiment. In this environment the detected particle multiplicity of a single event is large enough to permit single-event physics. 'Single event physics' here means pre-selecting an event containing 1/100 to 1/1000 of the total events using a narrow range of values of a particular global variable (e.g., distribution temperature) and using this reduced ensemble in further physics analysis (e.g., strange particle ratios or HBT interferometry).

The distribution's 'temperature' (or inverse slope) is usually extracted by binning the particle transverse mass distribution function into a histogram, taking the logarithm of the vertical scale of this histogram, and then fitting a straight line to the resulting distribution. The inverse slope of the fitted line is the temperature. Here we present an algorithm which is a faster alternative to this procedure.

The transverse mass of a particle with rest mass m_0 and momentum components p_x and p_y in the directions transverse to the beam (z) direction is defined as: $m_t = \sqrt{m_0^2 + p_x^2 + p_y^2}$. In ultra-relativistic heavy ion experiments at CERN it has been found that the distribution of transverse masses of pions produced in a collision is well described by the probability density function (PDF):

$$P(m_t) = \frac{m_t e^{-(m_t - m_o)/T}}{T(T + m_o)}, \tag{1}$$

where $m_t \geq m_o$. We note the values of the following integrals over this PDF:

$$I_0 \equiv \int_{m_o}^{\infty} P(m_t)\,dm_t = 1 \tag{2}$$

$$I_1 \equiv \int_{m_o}^{\infty} P(m_t) m_t\,dm_t = \frac{2T^2 + 2Tm_o + m_o^2}{T + m_o} \tag{3}$$

$$I_2 \equiv \int_{m_o}^{\infty} P(m_t) \frac{1}{m_t}\,dm_t = \frac{1}{T + m_o}. \tag{4}$$

Therefore, $R_{12} \equiv I_1 / I_2 = 2T^2 + 2Tm_o + m_0^2$, and this quadratic equation can be solved for the distribution temperature, i.e:

$$T = \left[\sqrt{2R_{12} - m_0^2} - m_o\right] / 2. \tag{5}$$

This suggests that, given a set of tracked particles from a given event, the temperature can be extracted by computing sums over all tracks of the extracted values of m_t and $\frac{1}{m_t}$, taking the ratio R_{12} of these sums, and substituting this ratio into Eq. (5) above.

We have tested this procedure using a Monte Carlo simulation of NA49 events with particles having a Gaussian distribution of width of 3.2 in rapidity y, a uniform distribution in the azimuthal angle ϕ, and a transverse-mass PDF that is an order 2 gamma distribution as given by Eq. (1) above. We find that using this procedure the temperature of the PDF of a set of particles can be reliably extracted to a relative precision of about $\frac{1}{\sqrt{N}}$ where N is the number of particles in the event.

4.7 Fourier ripples in multiparticle Bose-Einstein correlations

J.G. Cramer

In Bose-Einstein interferometry, the correlation function C_n for n correlated particles is the Fourier transform of the smooth n-particle autocorrelation function in position space.[1] It is well known that when a function deviates slightly from a Gaussian distribution, its Fourier transform will show 'ripples' indicating this deviation. We propose to use such 'Fourier ripples' in Bose-Einstein interferometry with ultra-relativistic heavy ion collisions to search for non-Gaussian pion sources, perhaps arising from source shadowing effects.

To investigate this effect, we have written a Monte-Carlo program which performs a $3n$-dimensional integration in emission position over a fully symmetrized n-particle wave function to obtain C_n. We have compared n-particle correlation functions with n=2 to 6 for Gaussian sources with those for hemispherical sources with the same effective radius. Fig. 4.7-1 shows the observed Fourier ripples from the hemispherical source. We find that just as the correlation functions C_n have a peak value which increases with n as $n!$, the Fourier ripples are amplified in the higher order correlations by a factor of approximately $\sqrt{n!}$. This suggests that high order Bose-Einstein correlations may provide a tool for investigating non-Gaussian source shapes.

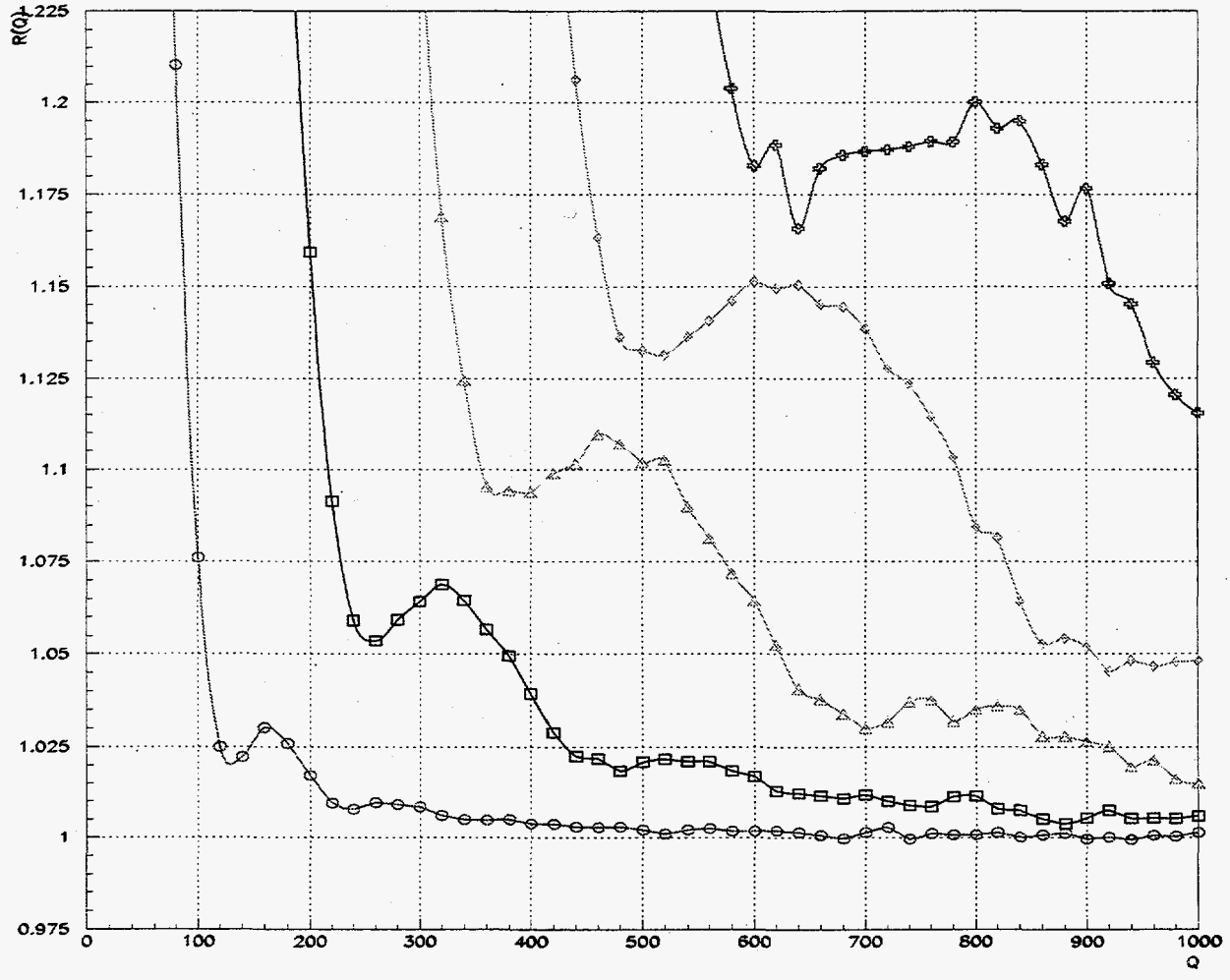

Fig. 4.7-1. Fourier ripples from a hemispherical source as found in correlations between 2,3,4,5 and 6 particles. Here $C_n(Q_{long})$ is plotted against (Q_{long}).

[1] W.A. Zahc, in Particle Production in Highly Excited Matter (NATO Conf. in Lucca, Italy), Gutbrod and Rafeleski, eds. (July 1992).

4.8 STAR trigger algorithms

J.G. Reid and T.A. Trainor

The purpose of this project is to create fast trigger algorithms which can identify 'interesting' events at different levels in the STAR data stream. For this purpose we have formulated a model-independent correlation analysis system using topological information and entropy measures. Rather than looking for features corresponding to a specific correlation model, we use the entropy and information measures of the data set to determine which events contain information which may be of interest.

Basic to our analysis is a binning of the data set. This yields a list of bin occupancies from which the entropy and information are calculated, but it can also contribute significant systematic errors. In using our analysis chain to find the scaled 'volume' of different simple loci we have observed that the orientation of our simple, square binning system biases our results. Fortunately, the density of STAR Electro Magnetic Calorimeter (EMCAL) data minimizes this effect. This error could be further reduced by use of a more complex binning system, but for triggering purposes the extra time required to use an exotic binning system is prohibitive.

Another element basic to our analysis is the reference entropy. Since topological information is by definition a relative quantity the choice of a baseline (or reference) entropy determines the results of the analysis. For most of the trigger software we have chosen to use the average event ensemble entropy as a reference, but we have found in some situations that it is desirable to use the entropy of a Poisson distribution as a reference since this can be considered to contain the maximum entropy for a given constraint system. This has led us to derive a closed form for the rank-q entropy of a Poisson distribution for use as a general reference in some of our analysis.

In applying our analysis to STAR EMCAL trigger data we have obtained promising results. Using the event generator HIJING and STAR GEANT to generate simulated STAR events we have analyzed EMCAL data for pp, CC, SiSi, pAu, and AuAu. The results look very promising for forming a space out of information values at different scale points. In this space we cut out the 'normal' events and trigger on the remaining 'interesting' events. We also rigorously tested a prototype version of our level-1 trigger software on a set of test events provided by BNL.

Our trigger algorithm shows excellent selection capability. However, there remain several issues in formulating a trigger from our general analysis system. The first and most obvious problem in developing a trigger is the essential issue of runtime. Since this analysis must be able to analyze an event in a time on the order of milliseconds we have developed an approach in which we use a subset of the full analysis which can still identify normal events for rejection (to reasonable accuracy) in a fraction of the time of the full analysis. We have further extended this idea so that this analysis is flexible enough to be applied in some form at every level of triggering (above level 0) and the full analysis can, of course, be used off-line as well.

We have recently begun to apply these techniques to data from CERN experiment NA49. We have created a simulator which gives us distributions in rapidity and transverse mass corresponding to a specified total multiplicity and slope parameter ('temperature'). By comparing our analysis of these events to the analysis of real events we have begun to form a space in which we can map out the systematics related to these thermodynamic quantities. This work has just begun, but it promises to be an important part of our activity in the future.

4.9 NA49 main TPC tracking software

S.J. Bailey, D.J. Prindle, S. Schönfelder* and T.A. Trainor

The large data volume recorded in December, 1994 was used for robust testing of the tracking software for the NA49 Main Time Projection Chambers (MTPCs). During 1995 these data were used to fine-tune the tracking parameters, test for distortions and inefficiencies, and make improvements in the software. In October of 1995 this software was used to begin production analysis of the 94 data.

During and after the analysis of the 94 data a number of improvements were made to the analysis chain. First, new data structures were introduced to allow a more global approach to the analysis. These allow the various TPCs to be treated simultaneously rather than segregating each one as a separate physics analysis. It is still more efficient to do the track finding process for the Vertex TPCs (VTPCs) separately from the MTPCs, but the resulting data files can be merged so that physics analysis may be done for all TPCs together.

The new data structures were also reorganized to reduce memory requirements. During the 94 production lack of memory per CPU was a perpetual problem and reduction of the size of the structures has been crucial for the stability of the software within the limited batch processing facilities available. The script for running the software was also entirely re-written in order to provide more robust error handling, flexibility, and debugging capabilities.

As part of the continued development of the tracking software we modified several algorithms and were able to improve the MTPC tracking speed by a factor of five without a loss of tracking efficiency. This established a precedent, and significant timing improvements were also made in gain calibrations, the MTPC momentum module, and VTPC tracking. The entire MTPC analysis chain for both MTPCs now takes less than 1.5 minutes per event whereas previously the tracking for one MTPC alone took 3-4 minutes.

During recent development of the MTPC software a number of general-use modules were created. These modules were initially written only for the MTPCs, but because of their utility they were converted for use by the VTPCs as well. The prime example is a drift speed module. Knowing the exact drift speed is crucial to the correct reconstruction of the y position (and thus momentum) of tracks. In NA49 numerous hardware methods were devised for determining the drift speed in the TPCs, including laser calibrations and drift speed monitors. But the most accurate method of determining the drift speed comes from looking at the TPC charge distribution itself. By counting the number of timebins in which data occurs and knowing the exact vertical dimensions of the TPCs, the drift speed can be determined with a precision of a few parts in 10^4. This module has become the standard against which other drift speed monitors are compared. Its use in the analysis chain has significantly improved the quality of the reconstructed tracks.

* Max Planck Institute, Für Physik (MPI), Föhringer Ring 6, D-80805 München, Germany.

4.10 NA49 geometry determination

T.A. Trainor and D. Weerasundara

During the 1995 fall run NA49 collected nearly 0.7 million nucleus-nucleus collisions using the 158 GeV/nucleon lead beam at the CERN SPS accelerator. A preliminary production analyses of these data is in progress at CERN. We describe below a correlation analysis that we performed to determine the geometry of the Time Projection Chamber (TPC) system of the NA49 experiment.

It is crucial to physics analysis, namely particle momentum determination and reconstruction of decay vertices, to know the locations and orientations of the TPCs relative to the standard NA49 coordinate system quite accurately. The design parameters of the NA49 experiment require the determination of relative TPC positions and their angles with an accuracy of order 100 μm and 100 μrad within a system that covers an area of nearly 15m by 7m. We have achieved this goal by carrying out an analysis of TPC tracking data to determine the geometrical positions of the four TPCs relative to each other, to the beam and to the magnet system. Tracking data for this analysis were collected for two different multi-target configurations. In one configuration, data were obtained from the simultaneous placement of four targets along the beam line. In the second configuration, data were collected with a single target in place along the beam for each of the four different targets. In both configurations, with the magnetic field turned off, each TPC sees straight tracks coming from these beam-target interaction points. TPC tracks are parametrized by four quantities: two slopes and two intercepts, in the horizontal (bend) and vertical planes.

By a correlation analysis of these straight tracks in an appropriately defined space, the location of the beam-target interaction point can be precisely reconstructed in each TPC local reference frame. A comparison of these relative positions generates a common registration of all of the TPCs with the beam-target system.

For the purpose of the TPC alignment we define an intercept space by $(\varepsilon_i,\varepsilon)$ where $\varepsilon_i = \varepsilon - z_i \cdot \varepsilon'$. z_i is the distance to target i from a TPC mid-plane, and ε and $\varepsilon' = d\varepsilon / dz$ are the intercept and slope of a TPC track in the (ε, z) plane in the internal coordinate system of each TPC ($\varepsilon = x, y$ for bending and vertical planes, respectively).

TPC tracks coming from a beam-target interaction form a straight-line correlation in this intercept space. Requiring the track correlation to be parallel to the track intercept axis determines the longitudinal (z) position, and the intercept of the correlation locates the transverse position of the beam-target interaction in the local coordinate system of each TPC. Simultaneous measurements of four of these beam-target interaction points uniquely determine the beam in each of the TPCs. Comparing the measured beam slopes and intercepts in each of the TPC local coordinate systems we are able to determine the relative positions and angles of the TPCs with the required accuracy.

4.11 NA49 event display

S.J. Bailey, J.G. Cramer, D.J. Prindle, T.A. Trainor, P. Venable and D. Weerasundara

The NA49 event display QCDisplay[1] was originally written to provide a visual verification that our main TPC tracking code worked. Because of the large number of tracks (about 300 per TPC) and the large number of measured space points (about 45,000 per TPC) it is very important to be able to easily choose and modify the viewpoint, scale and direction. By looking nearly along the direction of the tracks it is quite easy to see which points belong to tracks. By drawing the tracks at the same time we can see which tracks were missed, merged or suffered some other problem.

Briefly, QCDisplay can draw points and tracks reconstructed from raw data, and GEANT points and tracks. Each of these types of objects can be selected from and the selections can be assigned different colors. Movement, rotation and magnification can be done in a simple way, using the mouse for control. Individual points and tracks can also be selected by clicking on them with the mouse. QCDisplay knows the relationship between points and tracks and highlights the points on a selected track or the track of a selected point. Optionally, the point or track parameters can be displayed in a pop-up window. Pointers from the track or point to related objects can be followed and their parameters displayed in pop-ups.

During the past year we have made a number of enhancements to QCDisplay that make it a more generally useful tool. First, we added the capability of drawing curved tracks for particles bent by the magnetic field. This has made QCDisplay useful to persons working on the vertex TPC tracking code as well as to persons working to match vertex and main TPC tracks. A number of improvements have been made to make it easier to highlight tracking difficulties. With up to 1000 tracks per event and over 90% of the tracks fit very well it is inefficient to look for bad tracks by trial and error. If the event reconstruction program classifies a point or track as having a distinguishing characteristic it can set a bit in a variable. QCDisplay can map these bits to different colors. Optionally, each color can be displayed or not. This can be used to display only those points not assigned to tracks for example.

A more general method to select points or tracks has been provided by a tcl interface to QCDisplay. Within a **tcl** script one can get access to all information available to QCDisplay. This can be used to assign different colors to tracks depending on the track momentum or the number of points assigned to the track for example. The big advantage of the tcl interface is that it makes it possible for the user to extend the capabilities of QCDisplay without having to modify and relink the source code.

A few other additions have made QCDisplay more convenient to use. One of these is a color editor. This lets the user modify the colors interactively, useful to highlight certain features or just make the display more visually pleasing. The color palette can be saved and reloaded at a later time, making it possible to create sets of colors for different purposes. It is also possible to save the position, direction and magnification of the viewpoint and return to this view later. This is useful when one finds an interesting feature in an event and wants to be able to return. The option of saving the current display to a postscript file has also been added. This is more useful than a screen capture if one wants to enlarge or shrink the image later, for example when including the image within another postscript document.

---

[1]Nuclear Physics Laboratory Annual Report, University of Washington (1995) p. 45.

4.12 Experience with SControl in the 1995 NA49 run

J.G. Cramer and M.A. Howe

A paper describing the SControl system and program was presented in April at the AIHEN Conference held in Pisa, Italy.[1] The program SControl, written in C++ and operating on a dedicated HP-712 workstation, was used intensively during the November-1995 run of CERN Experiment NA49. The principal tasks of SControl were: (a) to collect experiment-status information from 6 satellite processors, (b) to maintain an archive of this information by updating an archive file, (c) to provide user-controlled displays of experiment parameters of interest, and (d) to generate and manage alarms.

The experiment is represented in the SControl display by pages organized in a hierarchical structure, with a 'home' page at the top level showing an orthographic representation of the whole experiment. On this diagram the major subsystems were outlined in white, and each of these outlined regions provided a hyper-link to the top-level page of the subsystem. The subsystem top-level pages typically showed a block diagram of the subsystem, with blocks outlined in red providing hyper-links to the appropriate sub-sub-systems. This pattern of diagrams with hyper-links was repeated at one or more levels until a page was reached that was designed to monitor several related functions of a particular subsystem.

In the period between the 1994 and 1995 runs, the program was reorganized and restructured, and the code was analyzed with the diagnostic program PURIFY to discover memory leaks and other problems. This resulted in a much more stable code. In the 1995 run the program, except for a few startup problems associated with interfacing to the Macintosh and PC systems, operated very stably and with few crashes or operating problems.

A number of improvements were also made to the user interface. For example, the modification of display pages is now password protected. This eliminates the problem of operators changing display pages by accident. Real-time controls were added to the chart objects to allow operators to change charting parameters without having to know the password. In addition, the cut and paste functions were expanded to included whole page deletion and duplication, and alignment tools were added to make it easy to line up groups of objects along their edges or centers.

For the 1995 run of NA49 the hierarchical paging structure was extensively modified to include the two new time projection chambers and the increase in monitor inputs, particularly temperatures and gas condition readouts. In addition, the alarm system was modified to enhance the transmission and display of messages when an alarm is generated, and complete on-line documentation was produced providing a detailed description of the condition which generates each alarm and the actions the should be taken when the alarm occurs.

---

[1] "SControl, an object-oriented program for the slow control of large physics experiments," M.A. Howe, J.G. Cramer, and P.B. Cramer, presented at AIHEN '95 - *4th International Workshop on Software Engineering and Artificial Intelligence for High Energy and Nuclear Physics*, Pisa, Italy, April 3-8, 1995, and to be printed in the Conference Proceedings.

4.13 STAR TPC fast simulator

D. Weerasundara

STAR TPC detector simulation software is required to simulate the response of the TPC detector volume and its electronics to the passage of charged particles through the TPC volume, including those from pp, pA and AA collisions. The STAR TPC Fast Simulator (TFS) has been designed to generate a large volume of event samples simulating the response of the TPC and the performance of the TPC hit reconstruction algorithm.

A GEANT Monte Carlo program takes tracks from an event generator and propagates them through the TPC, generating hits corresponding to each pad-row crossing. These GEANT hits are fed into the TFS as input. TFS assigns each GEANT hit a characteristic signal width (σ_{prf}) in the transverse plane and a spatial resolution (σ_z) in the drift direction. The parametrization of σ_{prf} and σ_z depend upon the intrinsic pad response, the drift length, track pad crossing angle, sense wire spacing, transverse and longitudinal diffusion of the TPC gas, electronics shaping time and sampling frequency. Then the hits are smeared about the known GEANT hit position according to a gaussian distribution function whose width is given by the σ_{prf} parametrization. Those hits which are then found to overlap in both the pad plane projection and the drift direction are merged to form larger single hit clusters. Hits in the same pad-row are merged when their separation Δ satisfies the condition

$$\Delta_{pad} < \sigma_{prf}(1) + \sigma_{prf}(2) + padwidth \qquad (1)$$

and

$$\Delta_z < \sigma_z(1) + \sigma_z(2) + 2 \cdot timebins \qquad (2)$$

This condition places a cut-off on the deconvolution of close hits related to the expected performance of the hit reconstruction algorithm. Merged hits whose combined spatial width is smaller than 10 pad widths and 20 time bins are preserved and written to the output along with the isolated hits. The output of TFS then forms the input of the STAR TPC tracking system.

TFS has been written with flexibility in mind. It is controlled by parameter files for easy modification of the TPC running parameters. In the past, TFS has been used extensively to optimize the STAR TPC design criteria, develop event reconstruction software and study the physics capabilities of the STAR TPC. TFS is also capable of merging events prior to and following the triggered event. This is particularly important in the high-luminosity environment of proton-proton collisions where non-triggered events will be registered during the time that the TPC volume is read out. We are now in the process of incorporating modifications to TFS in order to study STAR trigger algorithms.

4.14 STAR TPC high voltage regulation system

G.C. Harper and T.A. Trainor

A feedback regulation system has been developed at the University of Washington for the cathode high voltage power supply of the STAR TPC detector. The target software for a VME based Motorola microprocessor was developed using the Experimental Physics and Industrial Control System (EPICS)[1] software package on a SUN SPARC workstation. EPICS is a slow-controls software development package which uses a variety of graphics based tools to produce user displays, databases, and alarm structures in a simple and straightforward manner.

Variation in the pressure or density of the gas in the detector will produce undesirable variations in the electron drift speed. The feedback control scheme uses the drift speed of the electrons in the TPC as the controlled variable. Electrons are freed from the cathode surface by a short laser burst. The laser trigger signal is used as the start pulse for a LeCroy 1176 TDC. The stop pulse for the TDC is produced by a hit signal from one or more of the pad detectors of the TPC. The time delay between the two pulses is compared to a setpoint and an error signal is generated. The error signal is amplified by a gain element composed of a single sum-of-first-differences algorithm. The behavior of this algorithm, for simulations in which the drift speed is arbitrarily set equal to 1 μsec/kV, is effectively the same as a single time constant integrator with 9 dB/decade gain and a 0 dB crossing at 0.046 Hz. The amplified error signal is added to the quiescent setpoint for a Glassman 100 kV 6 mA high voltage power supply. The high voltage power supply is connected to the TPC cathode and its potential corrects the drift speed of the electrons as required.

Provisions are also made in the target software for a variety of interlock and safe start conditions. There are three conditions that must be met for operation of the high voltage power supply to proceed. The gas in the TPC must be at a satisfactory pressure, any personnel barrier must be secured, and the supply current must be below a prescribed level. Any failure of these conditions will turn off the high voltage, set the power supply to zero, open the feedback control loop, and alert the user with a large, red warning message on the display screen. The interlock conditions all have software latches so that the operator must take action before the system will restart.

The gain element is dynamically adjustable from the display. The correction signal is decomposed into high and low frequency components and the corner frequency for the decomposition is also dynamically adjustable from the display. A sinusoidal noise source with 0.001 Hz to 0.02 Hz frequency range and 0 to 0.5 μsec peak amplitude range is also available. All setpoints, control functions, and the interlock page are accessible from the display.

Interfacing between the VME crate and the power supply and hardware interlocks is through modules produced by the VMIC[2] corporation. The system uses a 4 channel DAC, a 16 channel differential input ADC, a 16 channel binary output module using form C contact closures, and a 32 bit differential binary input module. The timing signal is produced by the LeCroy 1176 TDC mentioned above. An interface card built in-house distributes the signals from the VME modules to the power supply and interlocks.

---

[1]Los Alamos National Laboratory and Argonne National Laboratory.
[2]VME Microsystems International Corporation, Huntsville, Alabama.

4.15 A vertex silicon detector (VSD) for CERN experiment NA49

J.G. Cramer, D.J. Prindle and G. Odyniec*

Much can be learned about the dynamics of ultra-relativistic nuclear collisions from the production of strange and charmed particles. The most interesting of these are multi-strange baryons (Ξ and Ω baryons with |S|=2 and |S|=3, respectively) and mesons having open charm (D mesons with |C|=1), because these are formed in the 'hot' early stages of the collisions and are expected to provide important information on possible formation of the conjectured quark-gluon plasma.

We have submitted a proposal to the National Science Foundation requesting funds for the design, fabrication, installation, testing and operation of a silicon-drift vertex detector to be added as an upgrade to CERN experiment NA49. This addition will give NA49, presently the 'flagship' experiment of the CERN heavy ion program, new capabilities which would make it the only CERN experiment capable of detecting charmed D mesons in heavy ion collisions and would also allow NA49 to efficiently detect and analyze multi-strange baryons.

The detector subsystem we propose, which we call NA49-VSD (Vertex Silicon Detector), will track charged particles very close to the target. Thanks to its excellent position and two-track resolution, this will permit separation of short-lived decay tracks from tracks originating at the primary vertex. This new capability of NA49 will allow the detailed study of multiple strangeness and charm production in the SPS ultra-relativistic energy regime, (33 TeV Pb beams on fixed targets). Together with the global characterization of the events already provided by the experiment, this should lead to unambiguous and definitive constraints on the reaction dynamics.

The NA49-VSD system, consisting of 20 p-type silicon drift detectors grouped into 5 planes (4 detectors/plane) will be read out by 3560 electronics channels. Entire thickness of the silicon wafers corresponds to only 1.5% of a radiation length. Therefore its contribution to multiple scattering is negligible.

The design of the detector, its construction, and testing will take place in FY96 and FY97. The detector will be ready for initial data taking for strangeness analysis in Fall-97 and will be refined for the more difficult open charm study in Fall-98.

*Lawrence Berkeley National Laboratory, Berkeley, CA and University of Washington.

4.16 Energy deposition by low energy electrons in Ar and other gases

H. Bichsel

In the collisions of ultra-relativistic heavy ions, the trajectory ('track') of thousands of emerging particles are measured in time-projection-chambers (TPC). An important datum for this purpose is the localization of segments of the particle tracks in small volumes. The localization in the plane perpendicular to the particle velocity is given by the extent of the cloud of ionization produced by the particles, typically averaged over segments of a few centimeters of track. For particles with charge ± 1, for about 80% of the segments ('pads' in current slang) the ionization cloud in gas at 1 atm has a diameter of less than 0.1 mm. For the others secondary electrons ('δ -rays') with energies exceeding 5 keV will produce ionization further from the track, and the position of such segments will be known with a larger uncertainty. In order to determine these uncertainties, the spatial distribution of the ionization by the δ -rays must be known. Also, we must know the spectrum of δ -ray energies. A fairly good approximation to this spectrum can be obtained with the Fermi-virtual-photon method, as outlined in earlier reports. This method is also known as the Weizsäcker-Williams or PAI method.[1] The spatial distribution of the energy deposited or, more appropriately, the ionization has been measured for electrons with energies up to about 5 keV in some gases, but not in Ar. A Monte Carlo program for the calculation of these distributions has been obtained from B. Grosswendt (at Physikalisch-Technische Bundesanstalt in Braunschweig), and is being investigated at present. Only preliminary results have been obtained so far, and need confirmation. Corresponding experiments would be very desirable.

[1] H. Bichsel, in Atomic and Molecular Physics Handbook, Ch. 87, G. Drake, ed., Amer. Inst. Phys. 1996.

5.0 ATOMIC AND MOLECULAR CLUSTERS

5.1 C_{60}^- beam by electron bombardment of C_{60} vapor

R. Vandenbosch and D.I. Will

Efforts to produce C_{60} anions directly from graphite in our General Ionex model 860 sputter ion source have proved fruitless. We have, however, seen nanoamp currents of C_{60}^- sputtered from C_{60} substrate in this source. These currents always decayed in less than an hour to unusable levels. As a result we undertook to develop a new C_{60}^- ion source. One of our colleagues, Adi Scheideman, was producing a neutral C_{60} beam from C_{60} powder placed in a quartz oven at 300 to 600° C. Reports that neutral C_{60} has a sizable capture probability for electrons impinging at energies from 2 to 20 eV induced us to try ionizing such a molecular beam by electron bombardment.

The geometry of our new C_{60}^- ion source is largely cylindrically symmetric about the C_{60} beam axis. A quartz oven emits C_{60} vapor from a 1 mm orifice into a drift tube where the vapor is ionized by electron capture from an electron beam crossing the C_{60} beam. The resulting C_{60}^- is accelerated forward by a potential of +200 V on the first electrode at the end of the drift tube. This beam is then focused by a second electrode at roughly +900 V (varied for best focus). Final acceleration is to a total energy of 6 kV (limited by the capability of our 90° analyzing magnet).

Some aspects of our design are unique to the C_{60}^- source (though the focus and final acceleration electrodes are unchanged from our direct extraction ion source). The quartz oven of 7 mm outside diameter by 50 mm length is heated by a nichrome coil wrapped tightly on the oven. An insulating blanket of alumina fiber felt is wrapped over the nichrome. A Pt-Pt13%Rh thermocouple monitors the oven temperature, and the oven heater power supply is then driven by a regulator circuit to maintain whatever constant temperature is preset. The C_{60} vapor leaves this oven through the 1 mm orifice (at one end of the oven) and immediately enters the drift tube made of 304 stainless steel which is 12 mm inside diameter by 50 mm long. A coiled tungsten filament is located in a hole in the side of the drift tube roughly 8 mm downstream of the oven. The potential of this filament is variable from 0 to -20 volts relative to the drift tube. In operation the filament is heated by roughly 6 amps DC from a voltage regulated supply and emits 1 to 2 mA of electrons directed crudely into the interior of the drift tube.

The C_{60}^- beam, once analyzed by the 90 degree magnet, is collected in a removable Faraday cup or can be accelerated off our injector deck by an additional 300 keV. To date we have observed up to 10 nA of analyzed C_{60}^- beam into our on-deck Faraday cup with oven temperatures around 650 degrees C. Of more interest, we can achieve stable beams of several hundred pA and maintain them for more than a day at oven temperatures around 500° C. On disassembly after a day's run we find most of the roughly 100 mg oven load of C_{60} deposited on the first electrode at the end of the drift tube. Based on rough integration of the beam seen on the Faraday cup over a day's time relative to the C_{60} load vaporized from the oven, our ionization efficiency is low, perhaps 1 part in 10^6. We find peak C_{60} electron capture for energies of 5 to 6 eV, in rough agreement with reported values.

5.2 A gas target for atomic cluster fragmentation

C.H. Cooper, J.F. Liang, R. Vandenbosch and D.I. Will

The motivation for constructing a gas target grew out of two studies reported last year. In an experimental study[1] of the yields of different RbC_n clusters, even n cluster anions were preferred (over odd n) by one to two orders of magnitude through n=8. Ab initio quantum mechanical calculations performed to elucidate the even n preference also suggested a linear structure for these anions with the Rb at one end. One method of checking this theoretical structure is to fragment the cluster anions to determine the chain lengths of pure C_n cluster fragments. The motivation for studying the fragmentation of C_{60} arises from conflicting interpretations of fragmentation mechanisms. For example, C_{50} might be formed by successive emission of C_2 fragments, or by emission of a C_{10} chain. We explored the latter mechanism in a model calculation[2] based on an unzipping mechanism suggested by deMuro *et al.* Our eventual goal is to perform definitive coincidence studies.

Initial calculations indicated a target of 10^{-1} to 10^{-3} Torr-cm of nitrogen would have the proper thickness. Such a target could consist of ~10 cm of N_2 gas at 10^{-2} to 10^{-4} Torr. Variation in the target thickness needed for different experiments, uncertainties in the cross sections, and uncertainties in the available pumping speed dictated a design in which the gas canal arms could be changed easily to alter gas loss and target thickness if needed. For ease of construction, 1/4" outside diameter stainless steel tubing of various wall thicknesses and lengths fitting snuggly into a central tee piece provides convenient variability. Endcaps with apertures smaller than tube inside diameter provide some decrease in gas loss while reducing the likelihood that breakup of ions by the tube inner wall will contaminate results. A pressure regulated supply of N_2 bled through a variable leak valve with a numerical turn counter gives repeatable target pressure. Finally a VRC Pirani gauge with capability down to 10^{-5} Torr was recently purchased to show actual pressure in the central tee piece of the target.

Our General Ionex model 860 sputter ion source and a new C_{60}^- source (see Section 5.1) both located on our injector deck produce anions of up to 300 keV. A 90° electrostatic deflector allows mass analysis of + and - ions after breakup. Our first test of the gas cell was with C_4^- clusters. Without gas we were able to focus 1/4 of the beam through the gas cell. With N_2 gas we found the optimum pressure for forming C, C_2 and C_3 charged fragments to be 10^{-2} Torr to 10^{-3} Torr. At these gas pressures the vacuum in the beam line was less than 10^{-5} Torr. Fragmentation of C_4^- at 180 keV gave mostly +1 fragments, although smaller yields of -1 and +2 charge states were observed. We also made a brief attempt to fragment CsC_{10}^-. The transmission through the cell was appreciably poorer and good external beamline pressure more critical. We did observe Cs^+ and C_{10}^- fragments. The latter observation confirms our earlier hypothesis that alkali polycarbide anions are chains with the alkali atom at the end of the chain.

Our principal goal for use of the gas cell is to study the fragmentation of C_{60}^-. We were able to transport 150 keV C_{60}^- ions through the gas cell. In this initial experiment we found several small-mass fragments with a target pressure of 10^{-2} Torr.

---

[1]Nuclear Physics Laboratory Annual Report, University of Washington (1995) p. 35 and J. Chem. Physics, in press.
[2]Nuclear Physics Laboratory Annual Report, University of Washington (1995) p. 38 and J. Phys. Chem. **99** 14686 (1995).

6.0 ELECTRONICS, COMPUTING AND DETECTOR INFRASTRUCTURE

6.1 Electronic equipment

G.C. Harper, T.B. Kalka, A.W. Myers and T.D. Van Wechel

Along with the normal maintenance and repair of the Nuclear Physics Laboratory electronic equipment, projects undertaken by the electronics shop this year included the following:

a. Three light pulsers were manufactured to support the new three-spectrometer setup and beamline for high energy gamma ray experiments (see Section 6.7).

b. A VME interface has been developed for the STAR TPC high voltage regulation system (see Section 4.14).

c. The SNO neutral current detector preamp reported in last years report as a prototype has been fabricated on hybrid circuits and tested satisfactorily (see Section 2.2).

d. The preamplifier for emiT has been constructed in a hybrid circuit and tested satisfactorily. We are currently designing the layout of the mother board for these preamps. The mother board will be approximately 2.5" by 13.5" and will contain 16 detectors, preamps and associated circuitry (see Section 1.9).

e. We have assisted in the design, layout and component placement of a shaper/ADC board with a VME interface to be used in the emiT experiment (see Section 1.10). This board is an 8 layer, .062" thick, 6U VME board with both surface mount and through hole components.

f. We have manufactured prototypes of the following for SNO: log amps, MUX and a fast shaper (see Section 2.2).

g. We manufactured an RS232 interface for use with a Lecroy HV4032A High Voltage power supply.

h. We designed and built a circuit to be used with a Pirani vacuum sensor. This circuit consists of a meter, a meter zeroing pot, a setpoint pot, an LED to indicate if the circuit is set to adjust the set point, a toggle switch to change between setpoint and sensor reading, an LED to indicate GOOD vacuum and an LED to indicate POOR vacuum. This circuit has been incorporated into 2 separate 5 1/4" chassis with 4 circuits per chassis. Each circuit has a corresponding relay on the back of each chassis to connect an external monitoring system if desired.

This past year we have upgraded our electronics shop capabilities to include surface mount rework and manufacturing circuit boards utilizing surface mount components. We received an OK Industries Pick and Place machine from the Super Conducting Super Collider closeout equipment. We have added our own video system to this equipment to aid in the placement of SMT components. We have purchased an OK Industries SMT rework/reflow station.

Recently we utilized both of these systems to populate the boards mentioned in item e above. We are further upgrading our SMT capabilities. This coming year we will purchase a reflow batch oven. This will significantly reduce the time required to manufacture and or populate circuit boards.

6.2 VAX-based acquisition systems

M.A. Howe, R.J. Seymour, D.W. Storm and J.F. Wilkerson

We now have four VAXstation 3200-based data acquisition systems. They consist of Digital Qbus-based VAXStation 3200s running VMS v4.7a using VWS/UIS as the "windowing" software. Each VAXstation supports a BiRa MBD-11 controlled CAMAC crate. Our primary system is attached to a dozen dedicated 200 MHz Tracor Northern TN-1213 ADCs. Those ADCs and other CAMAC modules are coincidence-gated by a UWNPL-built synchronization interface, which includes monitor (Singles) and routing-Or capabilities. The system also has a bank of 32 10-digit 75 MHz scalers.

Our principal VAXStation's small BA-23 cabinet is cabled into a second BA-23 CC expansion cabinet. That, in turn, has an MDB-11 DWQ11 Qbus-to-Unibus converter driving our old PDP 11/60's Unibus expansion bay. The system's Qbus peripherals include a CMD CQD-220/TM SCSI adapter for a Seagate ST41650 1.38 gigabyte disk and a TTI CTS-8210 8mm tape drive, a DEC IEQ11 IEEE-488 bus controller, and a DEC DRV11-J. The Unibus bay contains a DR11-C, our Printronix lineprinter controller and a Unibus cable to the MBD-11.

The other three acquisition systems consist solely of each VAXstation 3200's BA-23 using an Able Qniverter to provide a Unibus cable directly to a stand-alone MBD-11. Unlike the "principal" system, these do not control non-CAMAC-based equipment. The fourth "new" system is built from a Qniverter and MBD-11 graciously loaned by Russell Roberson at Duke upon Zhiping Zhao's request.

All three systems run acquisition software based upon TUNL's XSYS, with major modifications to their DISPLAY program.

TUNL's XSYS software includes an EVAL language compiler which generates VAX-native code. Our version of that compiler is limited to 1024 longwords of VAX sorting code per MBD channel. One Mass-8 experiment required far more space, so we completely replaced the EVL-generated code section by a pre-compiled Fortran subroutine set. Interface subroutines were created to provide easier access to the raw incoming event buffers. We still require an EVL routine to be used, but only for histogram storage coordination.

6.3 Analysis and support system developments

J.G. Cramer, M.A. Howe, R.J. Seymour, D.W. Storm, T.A. Trainor and J.F. Wilkerson

Our offline computing capacity is divided into five major groupings, with many resources shared across the entire system.

The oldest presence is that of the VMS cluster. It consists of ten VAXstations and a single Alpha 3000/400. The VAXstations are a mix of five 3100s and five 3200s holding from eight megabytes to sixteen megabytes each. Three are diskless. They are all running VMS v5.5-2.

The Alpha 3000/400 has 96 megabytes of memory, two 4-gigabyte (GB) disks, a 2-GB and a 1-GB disk. It also has a CDrom, a 19 inch color display, and two 8mm Exabyte tape drives attached to its external SCSI port. It is running OpenVMS v1.5. Digital's Fortran, C and C++ are the cluster's principal languages.

The entire VMS cluster shares seventeen gigabytes of disk space.

We use TGV's Multinet to provide our cluster with TCP/IP access to the Internet. Our primary Internet address is npl.washington.edu (128.95.100.10).

"NPL" is one of the VAXstation 3200s, with DHv11s driving our thirty-odd local rs232 terminals.

The second major computing presence is the Relativistic Heavy Ion's group of Hewlett Packard Unix systems. These are all HP 9000/7xx-family machines, ranging from our original pair of HP 9000/710s through four 9000/712/60s to the newest arrivals, a pair of 100 MHz dual-processor HP 9000/770s, also known as J200s or "Skyhawks". These eight machines use NFS to share fifteen disks for a total capacity of twenty-one gigabytes. The J200s are running HP-UX v10.01, the rest run versions ranging from 9.01 to 9.05.

Each November for the past two years has seen a number of our HP systems traveling to CERN to participate in the NA49 runs. In November 1995 four systems and a number of disks left, and the remaining two systems were reconfigured with respect to who had which disks and peripherals. A month after the four returned the two J200s were added to the group. Each of these cluster reconfigurations entailed making the travelling systems part of CERN's environment upon their arrival, and reintroducing them to the UW NPL environment upon their return. Much of the CERN configuration was preformed by Predrag Buncic.

One of the 9000/710s serves as the lab's World Wide Web server (www.npl.washington.edu).

The third major presence is the SNO group's collection of over fifteen networked Macintoshes. They also have a Sun SparcStation 20 running SunOS v1.4 to provide CADENCE circuit layout facilities to our electronics shop.

The fourth major presence are the ubiquitous Intel-based PCs. The Mass8 and gravity groups are the prime users of this platform, with another pair dedicated to AutoCAD service, and a pair in the front office performing administrative duties.

The fifth presence is the "miscellaneous" group, consisting of:

- Three VMS VAXstation 3200s providing Email and "surplus CPU cycles" for the Institute for Nuclear Theory and the Physics Nuclear Theory group.
- A Sun Sparc 5 for developing the Slow Controls software for STAR.
- Another VAXstation 3200 serving as the Linac's control and display system.
- The nine PDP-11s built into the Linac for cryogenics, vacuum and resonator control.
- Four PCs serving as controllers for the rest of the accelerator systems' interlocks, safety and vacuum system.

6.4 NSAC - a personal computer based data acquisition program

H.E. Swanson

NSAC is the data acquisition and control program developed for the neutron spin rotation experiment discussed in this annual report (see Section 1.8). It runs on a PC under the DOS operating system. The PC's interface to the experiment is an Analogic LDAS16 module providing 16 bit ADCs and DACs, and a parallel output port. NSAC was written in Microsoft FORTRAN so that students and faculty could more easily make modifications as the experiment evolved. To use FORTRAN in a real time environment, assembler routines were written to enhance FORTRAN as follows: (1) To allow subroutines to be called directly from an interrupt, (2) to allow hardware modules to be directly programmed, and (3) to intercept keyboard input as it is typed rather than waiting for the user to hit the Enter key. These routines follow the FORTRAN call convention and can be used in any FORTRAN program.

In operation a programmed sequence controls external fields and devices via digital output bits and DACs. The acquisition sequence is set up from a file which specifies the interface used to control external supplies and their states and timings. Detector currents for each state of the sequence are read with gated integrators and ADCs. We use the PC's clock to determine the timing for the sequence, but in principle any hardware interrupt will also work. The interrupt routines write data into a buffer and signal the main program using flags and variables in a shared common area. The main program writes data to disk and updates the plots.

Control of the program is from the keyboard. Typing BEGIN obtains a run number and title, and starts the normal acquisition sequence. After each pass through the sequence, the completed data cycle is written to disk. An END command stops acquisition at the end of a data cycle. Other acquisition modes provide for measuring the polarization product of the polarimeter, and scanning fields to determine their optimum settings. The PLOT command allows plotting both individual ADC readings as they are taken or asymmetries calculated from completed data cycles. A SETUP command modifies parameters within the program and provides control of the target while cooling down.

6.5 A high resolution particle detector using a PIN photodiode

E.G. Adelberger and H.E. Swanson

We built an integral module containing the detector, preamp and thermoelectric cooler element for use in an ultrahigh vacuum system. The module is shown in the following figure. The detector plugs directly into the front of the preamp box which accepts either 9mm X 9mm or 20mm X 20mm Hamamatsu PIN diodes. Both the detector and preamp are cooled by a thermoelectric element. Temperature is sensed at the detector and an external feedback circuit holds the temperature constant to better than 0.1 deg C. This is important for long term stability as the module runs in a cold shroud and the signals from both preamp and detector have a temperature dependence. The preamp electronics uses a small hybrid developed for the emiT PIN diode detector (see Section 1.9). It was necessary to reduce the gain so the dynamic range included 6 MeV protons. The preamp box seals the electronics from the vacuum. The copper rod conducts heat generated by the thermoelectric element to a heat sink external to the vacuum. The module is placed in an ion-pumped ultrahigh vacuum system to avoid condensing material on the detector surface.

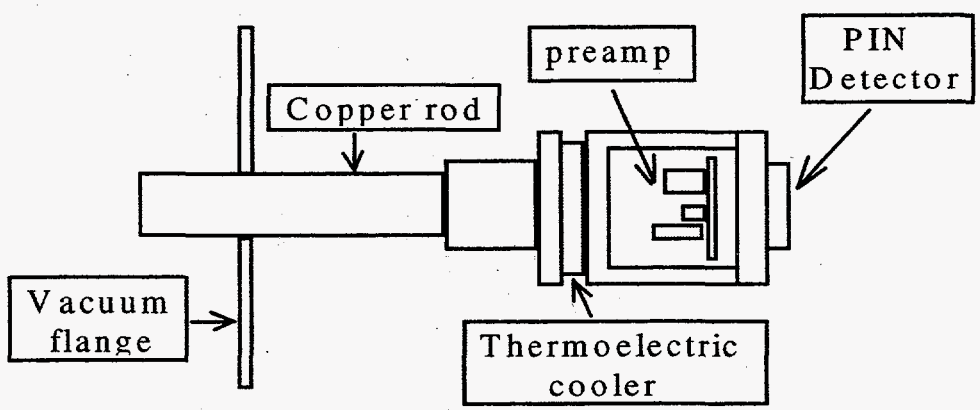

Fig. 6.5-1. Integral PIN diode detector.

The detector was operated at 10° C. which reduced the leakage current to less than 0.01 microamps. Under these conditions the resolution for 3 MeV Protons was about 6 keV, while the pulser resolution was about 5 keV.

6.6 Design of a long gas cell for measuring the gamma ray spectrum from ^{8}Be

K.A. Snover, D.W. Storm and D. Wright

In order to perform an accurate test of CVC by comparing the isovector M1 strength in the gamma decay of ^{8}Be with the weak magnetism determined from the analogue beta decays of ^{8}Li and ^{8}Be, it is necessary to determine the spectral strength of the gamma decay, because the final state is broad. For details see DeBraeckeleer, *et al.*[1] It is particularly important to be able to determine the gamma ray spectrum at energies considerably lower than the main transition energy of about 14 MeV. Since the excited state in ^{8}Be is made by a ^{4}He +^{4} He resonant collision, one uses a long gas cell with well shielded windows and does a measurement at 90°.

In preliminary measurements we found a background produced by He beam particles scattering in the windows and gas and then hitting the walls of the cell where they interacted and produced photons. This background depends on the kind of gas present, and is not well reproduced when we fill the cell with hydrogen. In order to reduce the background we plan to take two steps. First, we will line the cell with tantalum, so the Coulomb barrier will discourage interactions with beam ions that have already lost significant energy in gas scattering. Second, we can make a large enough diameter cell and can intercept the particles scattered from the windows with an aperture located in the cell behind the gamma ray shield. Thus, particles scattered from the window will not hit the cell wall in the visible region. The large diameter, combined with careful placement of the aperture, requires that any beam particles that scatter from the gas into the part of the cell wall that is visible to the detector will scatter through an angle large enough to reduce the energy of such particles from the 34 MeV beam energy to well below Coulomb barrier.

The details of the geometry are being worked out in order to build a cell that can be used as soon as the gamma ray detection system is ready.

[1] L. De Braeckeleer, *et al.*, Phys. Rev. C **51**, 2778 (1995).

6.7 New 3-spectrometer setup and beamline for high energy gamma ray experiments

J.F. Amsbaugh, J.H. Gundlach, M.P. Kelly C.E. Linder, K.A. Snover, D.W. Storm and J.P.S. van Schagen

An upgrade of the '10-inch' beamline designed to enhance our capability for high energy gamma ray experiments is nearing completion. Two large NaI spectrometers have been obtained on long-term loan, one from Ohio State University and the other from the University of Illinois. These spectrometers are similar in design and performance to the Seattle NaI spectrometer, with high-quality NaI scintillators and both active and passive shielding. All three spectrometers will be located in Cave 2 on a refurbished beamline previously used with the Seattle spectrometer.

In order to accommodate the extra weight and surface area requirement of the three spectrometers, a new 13' by 14' platform has been constructed consisting of six reinforced concrete slabs supported by a flat framework of steel I-beams sitting on 18 steel support posts which rest on the 12" thick concrete basement floor. After some unsuccessful experimentation with fast-setting concrete-type products, the requirement of a superflat floor, flat to 20 mils, was achieved by pouring a thin epoxy layer over the slabs with the use of a leveling bar.

The NaI spectrometers, each weighing 2.5 to 3.5 tons, will be mounted on carts with air pads, and positioned on radially mounted rails, one for each detector, which rotate about the platform center on a pivot which also serves as the support for the target chamber. The NaI gains will be stabilized using LED's and computer controlled feedback via a programmable HV supply.

The vacuum system is being upgraded as well. The old oil diffusion pump has been removed and replaced by two 360 liters/sec turbomolecular pumps, one located at the collimator box just upstream of the target chamber and the other located at a new station on the beam dump, which has been enlarged from 4" to 8" diameter. Liquid nitrogen cold traps will be employed at the target chamber and upstream of the collimator box.

7. VAN DE GRAAFF, SUPERCONDUCTING BOOSTER AND ION SOURCES

7.1 Van de Graaff accelerator operations and development

D.T. Corcoran, G.C. Harper, C.E. Linder, A.W. Myers, T.D. Van Wechel and W.G. Weitkamp

This year we found a leak in an old, five-minute epoxied half-inch NPT joint in a stripper box flange. This joint did not noticeably leak below 140 psig tank gas pressure, but above 140 psig tank gas pressure the HE ion gauge reading increased linearly with tank gas pressure up into the 10^{-6} Torr range. When the NPT hole was filled and welded closed, the beam tube vacuum stayed well down in the 10^{-7} Torr range to 225 psig tank gas pressure.

We developed unstable operation at 8.5 MV during an experiment this year. Local, small-scale sparking seemed to occur around the LE chain pellets as they left the terminal for a distance of 5 or 10 feet (as seen from a top port). When the LE chain charge was increased this sparking increased in brightness and frequency, and tank sparks were triggered. Upon opening we found that the upper LE pick-off pulley[1] had thrown its rubber tire, and the aluminum rim was being rubbed by the pellets. There were tiny metal chips dusted over the terminal, beam tube, and column. Replacement and cleanup allowed normal, high-voltage terminal operation.

During another experiment, a 1.5 Hz ripple with amplitude 1 to 4 μamp was observed on the high energy chain current meter. Visual inspection of the chain showed a side-to-side harmonic oscillation coincident with this ripple. The low energy chain seemed to have a smaller oscillation at twice the frequency. The frequency of the HE chain was strongly affected by added manual downward pressure on the counterweight. The carriage seemed to be sticking, so that the counterweight could not move it freely, and the chain had some link-joints that moved stiffly. LPS2 was applied to all bearings and links of both chains. After this treatment there was absolutely no observable ripple on either LE or HE chain current meters at 10 kV charge (in air).

Tank sparks have repeatedly taken out the pelletron charging resistors, high voltage charging supplies, and RG-8/U cables at the low energy end, with the negative supply being the most frequent victim. Spark bar gaps were measured to be within tolerance. High-power, high-surge, ceramic composition resistors were installed in place of the wire wound series charging resistors provided with the pelletron. These have withstood repeated tank sparks without being destroyed. Additional transient suppression has been added to the charging supplies at both ends of the machine. This is in the form of series impedances and shunt clamps attached to wires from the high voltage sections of the supplies into the electronics.

Current sensors for both high and low energy columns were connected to the ADC card of the terminal computer as a diagnostic. This extra column current measurement helps us to see whether the beam is hitting one of the beam tubes.

The stripper canal actuator was driven past its limit due to a faulty diode in the motor circuit. This destroyed the special, high-pressure bellows seal. The high cost of an equivalent bellows necessitates re-engineering of the motion feedthrough mechanism. The canal has been left out, as no current experiments require gas stripping.

The Leybold TMP-450 turbo-molecular pump at the low energy end, which has failed twice in the past, failed for a third time this year. We installed a greased bearing TMP-360 on this line. This allowed us to eliminate a 90° elbow, giving us about the same pumping speed at the beam tube.

Detailed, illustrated procedures were written this year for several of the gas handling operations and vacuum system operations involving the tandem. These have been included in the general operations manual for ion sources and beam transport and also posted at the appropriate systems.

---

[1] NEC part number 2DA007251.

We are experimenting with the use of corona points made from Thoriated Tungsten TIG welding electrode material ground with a toolpost grinder to a long taper. As there has been no observable degradation in sharpness since their installation ultimate point life cannot be accurately estimated, but it appears to be very long.

The terminal ^{3}He ion source was installed, used, and removed, and the Van de Graaff was restored to tandem operation successfully three times during the last year.

During the year from March 1, 1995 to February 29, 1996 the tandem pellet chains operated 3162 hours. Additional statistics of accelerator operations are given in Table 7.1-1.

Table 7.1-1. Tandem Accelerator Operations
March 1, 1995 to February 29, 1996

Activity	Days Scheduled	Percent
A. Nuclear Physics Research, Ion Sources Alone	42	11
B. Nuclear Physics Research, Tandem Alone		
Light Ions	32	9
^{3}He Terminal Ion Source	40	11
Subtotal	72	20
C. Nuclear Physics Research, Booster and Tandem Coupled		
Heavy Ions	72	20
D. Other Operations		
Tandem Development	38	10
Tandem Maintenance	83	23
Unscheduled Time	59	16
Subtotal	180	49
Total	366	100

7.2 Booster operations

J.F. Amsbaugh, D.T. Corcoran, G.C. Harper, M.A. Howe, D.W. Storm, D.I. Will and J.A. Wootress

During the period March 1, 1995 to February 29, 1996, the booster was operated for 69 days. This is a decrease from the last two years, but is the same as the average annual operation for the five year period ending February 28, 1994.

Beams ranged in mass from ^{11}B to ^{60}Ni, and included ^{12}C, $^{16,18}O$, and ^{40}Ca, as well. This year the most popular beam was ^{12}C.

During the entire period there have been three resonators which were inoperable, for a variety of reasons that require opening the cryostats to repair. As the desired energies were available without these resonators, we did not repair them.

We continue to operate the low beta resonators at an average field of 3.0 MV/m and the high beta ones at average of 2.4 MV/m.

A substantial improvement in operation resulted from the new high-energy buncher, which is described in a subsequent section of this report.

The Leybold-Hereaus turbomolecular pumps with greased ceramic bearings provided reliable service, without any failures. They are a substantial improvement over the pumps with greased steel bearing that we had originally.

The helium compressors continued to run with no failures this year. Our oldest compressor now has run for 80k hours, and the other two have run for 50k hours in one case and 21k hours in the other case.

7.3 High energy buncher operating at 13/12 the linac frequency

D.T. Corcoran, G.C. Harper, D.W. Storm and K.B. Swartz

The concept of using a high energy buncher operating at a frequency equal to the sum of the linac frequency and the low energy buncher frequency was presented last year.[1] The construction of the new resonator by modifying one of our low-β resonators was described in that report. The resonator was successfully plated with a lead-tin mixture (1.8% tin by weight) using a technique similar to that used at Stony Brook.[2] This resonator exhibited substantially more severe multipacting than the low beta resonators used in the linac. We were able to overcome this multipacting using the freon conditioning technique first described by Noé.[3] The resonator has a low-field Q of 1.8×10^8 and can reach 2.5 MV/m at 10 W. This is not as good as most of our low-β resonators, but is more than sufficient for the buncher.

In order to operate the resonator in the linac, new electronics were developed which produce a clock signal at 13/12 times the linac frequency f_0. The same unit produces the signal for the low energy buncher at $1/12 \times f_0$. The power rf electronics we use in the linac are sufficiently narrow-band that they will not operate with this buncher, so we obtained an appropriate 100 W amplifier and circulator. The resonator control electronics are the same as was used with the previous high energy buncher.

With the previous high energy buncher operating at f_0, the linac pulses between the bunches produced by the low energy buncher had small amounts of beam present, typically 1% of the main bunch in each of the 11 intermediate bunches. These small bunches resulted from the high energy buncher acting on the continuous beam that lies between the bunches produced by the low energy buncher. Because the new buncher is only in phase with the linac when the main bunch is present, much less beam is captured into the intermediate bunches. The reduction is typically a factor of 10 or more, as is illustrated in the figure. We thank Felix Liang for the figure.

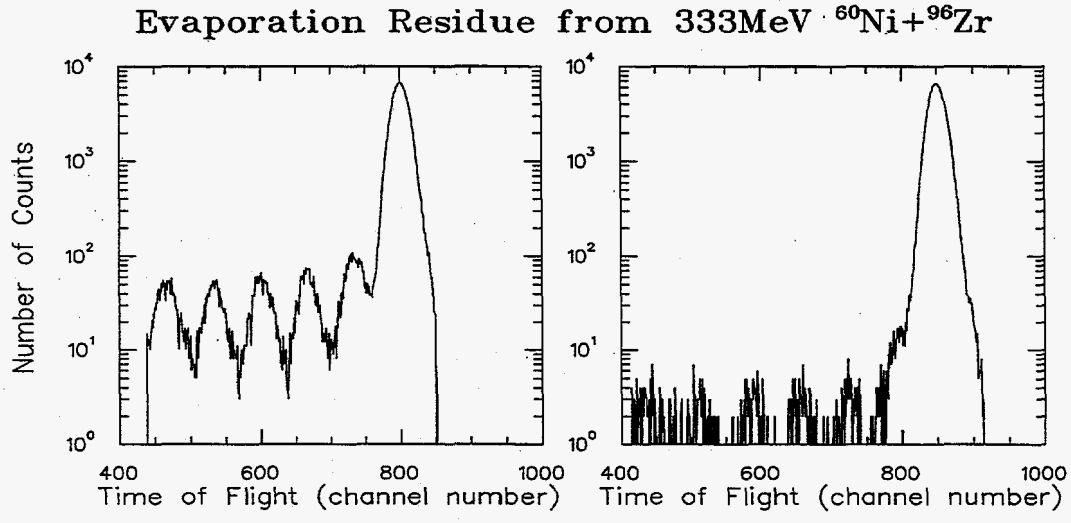

Fig. 7.3.1. Time of flight spectra for elastically scattered ^{60}Ni ions, showing the main bunch at channel 800 or 850 with 5 or 6 of the 11 small bunches at lower channels. The left hand spectrum was taken with the old buncher running at f_0, while the right hand spectrum was taken with the new buncher running at $13/12 \times f_0$.

---

[1] Nuclear Physics Laboratory Annual Report, University of Washington (1995) p. 65.

[2] J.W. Noé, J. Rico and H. Uto, Nucl. Instrum. Methods A **328**, 285 (1993).

[3] J.W. Noé, Nucl. Instrum. Methods A **328**, 291 (1993); D.W. Storm, D.T. Corcoran and G.C. Harper, *Proc. of Seventh Conf. on Heavy Ion Accel.* (1995), to be published in Nucl. Instrum. Methods.

7.4 13/12 buncher electronic upgrade

G.C. Harper and T.D. Van Wechel

The 13/12 buncher required the construction of a 13/12 clock generator as well as changes in the way that the LE buncher is phase locked to the linac. The original LE buncher clock generator divided the linac frequency of 148.8 Mhz by three to 49.6 MHz. The LE buncher operates at the linac frequency divided by 12, or 12.4 MHz, producing a bunched beam that harmonically excites the resonant phase detector near the entrance to the HE buncher. The resonant phase detector produces a 49.6 MHz signal. The signal from the resonant phase detector was compared to the LE buncher clock to phase lock the bunched beam from the LE buncher to the linac clock. The frequency of the phase shifted signal was divided by 4 to 12.4 MHz to drive the LE buncher. The problem with this method was that there were 4 phase relationships between the LE buncher and the linac clock to which the LE buncher could phase lock.

The LE buncher clock generator circuit was changed to divide the frequency of the linac clock by 12 so that the LE buncher clock is now 12.4 MHz. The 12.4 MHz clock is now frequency multiplied by 4 to produce a 49.6 MHz reference using two frequency doublers and this signal is compared in phase to the signal from the resonant phase detector. The circuit was modified so that the corrections in the buncher phase are now done by phase shifting the signal at 12.4 MHz instead of 49.6 MHz as was done previously. Now there is only one phase relationship between the LE buncher and the linac where phase lock can occur. There are still 4 phase relationships between the resonant phase detector and the 49.6 MHz reference where lock will occur but the 12.4 MHz buncher signal is not affected by this.

The simplest way to generate the 13/12 clock for the HE buncher is to mix the linac frequency and the LE buncher clock using a double balanced mixer (DBM). This generates frequencies of 11/12 f and 13/12 f, where f is the linac clock frequency, at the output of the DBM. The problem is that since 11/12 f and 13/12 f are relatively close in frequency it is difficult to provide much attenuation of the 11/12 f term without introducing phase shift in the 13/12 f term. The concern here is that the phase shift of the 13/12 f term will not be stable with time or temperature. The solution to this problem is to use an image canceling mixer. The image canceling mixer consists of two DBMs that have their outputs summed together with a power combiner. The RF input of DBM 1 is the linac clock and the RF input of DBM 2 is the linac clock in quadrature phase. The LO input to DBM 2 is the 12.4 MHz clock and the LO input of DBM 1 is the 12.4 MHz clock in quadrature phase. When the outputs of the two DBMs are summed the 11/12 f terms cancel and the 13/12 f terms add constructively.

We investigated the jitter in the LE buncher waveform that has been present for several years. This jitter was synchronous to the reference DACs being updated by the DECK computer. This was traced to the way that the DACs were grounded. The DACs are located in a chassis separate from the controllers, but were grounded only at the controller chassis to avoid ground loops. However, it was found that also grounding the DACs to the DAC chassis eliminated the computer noise that was causing the jitter.

7.5 Tandem terminal ion source

G.C. Harper

Tests of the RF discharge source for use in the tandem terminal were completed this year, and two experiments were run using the source.

Bench tests last year[1] with a 1 mm diameter canal produced 32 μamps of unanalyzed beam using ^4He as the gas with a measured gas load of 2.0 mTorr-l/sec and a focused FWHM of 1.3 mm. The emittance of the $^4He^+$ beam from the 1 mm canal was estimated to be about 1.1 π mm mrad $\sqrt{MeV}$. The source was then installed in the terminal of the Van de Graaff. An unanalyzed beam of 22 μamps using ^3He gas was measured before the magnet. An analyzed beam of 3 μamps of $^3He^+$ was measured on a flap just after the magnet. The size and shape of the beam spot on this flap indicated some problem with the magnet. The source and magnet were removed and tested in the 24 inch chamber.

The strange beam spot repeated itself on a faraday cup inside the 24 inch chamber. Several possible causes were investigated. Ultimately, a more careful measurement of the dipole magnetic field indicated that the vertical component of the fringe field was extremely irregular. It was determined that the 8C permanent magnet material has a very low relative permeability and is unable to produce uniform fields in the fringe regions. Pole faces of soft steel with high permeability were attached to the 8C poles. The edge of the steel was beveled by 45° to avoid saturation in that region. This produced a beam profile, intensity, and diameter as originally expected. Electrostatic deflectors were also built and tested and these proved to be a usable alternative to the dipole magnet if the need ever arose for applications involving heavier beams.

The source and magnet were again installed in the terminal. The source ran uninterrupted with a steady output of 32 μamps for 15 days in an experiment that ran from 15 April to 30 April. The source produced 32 μamps of analyzed beam with a measured gas load of 0.76 mTorr-l/sec. At the 5.5 MV terminal voltage required by the experiment, 90% of the beam was transported through the spiral inclined field tubes. In the terminal voltage range of 1.8 MV to 7.5 MV over 50% of the beam was transported. The source was not disassembled or cleaned after this experiment.

A second experiment was scheduled from 1 December to 21 December. After the installation just prior to this experiment an electrolytic capacitor in the RF power supply collapsed under tank pressure. A new capacitor was purchased and both capacitors for the RF supply were potted in thin-wall stainless steel tubes with epoxy. During the experiment the source sparked on a regular basis but ran with satisfactory beam output. The source was disassembled after this experiment and the pyrex bottle was found to be coated with a metallic film. The canal was partially sputtered away. The coating was believed to be the cause of the sparking.

---

[1] Nuclear Physics Laboratory Annual Report, University of Washington (1995) p. 61.

7.6 Cryogenic operating experience

D.I. Will and J.A. Wootress

The booster linac is cooled by liquid helium which is thermally shielded by liquid nitrogen. This liquid nitrogen is delivered in lots of ~6,000 gallons by semitrailer tanker. In 1995 liquid nitrogen consumption of 198,200 gallons was 12% less than that in pre-1994 years because a precool heat-exchanger leak now prohibits the use of liquid nitrogen assist in our Koch Process Systems 2830 Helium Refrigerator.[1] Helium is purchased as high purity, bulk gas and liquified by our helium refrigerator. Usage of 107,200 Standard Cubic Feet (SCF) in 1995 was down 52% from that in the peak use year, 1993, when the leaky heat exchanger caused substantial loss. Usage was down 27% from the mean for 1989 through 1992, more typical years.

The following table summarizes our maintenance from January 1, 1995 to December 31, 1995:

Item	In Use	Major Services	Times Performed
Refrigerator			
Cold Box	94%	warm/pump/purge	1
Main Dewar	100%	warm/pump/purge	0
Top Expander	~7859 Hrs	warm/pump/purge	7
	~120 RPM	valve rod and valve seals	1
		wristpin, crank, and cam follower brngs	2
		main seals, flywheel bearings and belts	2
		replaced alternator	1
Middle Expander	~7714 Hrs	warm/pump/purge	7
	~105 RPM	valve rod and valve seals	1
		wristpin, crank, and cam follower brngs	2
		main seals, flywheel bearings and belts	2
Wet Expander	~4685 Hrs	warm/pump/purge	4
	~58 RPM	main seals	1
Distribution System	99%	warm, pump, purge lines	9

This final table shows screw compressor history here as of March 12, 1996:

Item	Total	1995	Status	Maintenance
RS-1	80,151 hours	8731 hours	running	none
RS-2	55,958 hours	0 hours	phases shorted	core removed 1993
RS-2a	20,923 hours	8735 hours	running since 1993	none
RS-3	22,752 hours	0 hours	shorted to ground	core removed 1990
RS-3a	49,283 hours	8737 hours	running since 1990	none

Excluding the RS-2 compressor pump core which was stopped and started often to adjust compressor capacity to refrigeration needs (before we learned that such compact 100 HP motors have only a limited number of starts before failure), mean pump core lifetime is 51,597 hours with three of these four cores still running.

[1] Nuclear Physics Laboratory Annual Report, University of Washington (1994) p. 75.

8. NUCLEAR PHYSICS LABORATORY PERSONNEL

Faculty

Eric G. Adelberger, Professor
John G. Cramer, Professor
Hans Bichsel, Affiliate Professor
Ludwig De Braeckeleer, Research Assistant Professor
Peter J. Doe, Research Professor
Steven R. Elliott, Research Assistant Professor
George W. Farwell, Professor Emeritus
Jens H. Gundlach, Research Assistant Professor
Isaac Halpern, Professor Emeritus
Blayne R. Heckel, Professor
John P. Lestone, Research Assistant Professor
R.G. Hamish Robertson, Professor
Kurt A. Snover, Research Professor
Derek W. Storm, Research Professor; Director, Nuclear Physics Laboratory
Thomas A. Trainor, Research Associate Professor
Robert Vandenbosch, Professor
William G. Weitkamp, Professor Emeritus
John F. Wilkerson, Professor

Research Staff

Marcus Beck, Research Associate
Joseph V. Germani, Research Associate
Jun Jien (Felix) Liang, Research Associate
Reena Meijer Drees, Research Associate
Steven D. Penn, Research Associate
Thomas D. Steiger, Research Associate
Josephus P. van Schagen, Research Associate
Dhammika Weerasundara, Research Associate
Zhiping Zhao, Research Associate

Predoctoral Research Associates

Qazi Rushdy Ahmad
Stephen Bailey
James C. Beck
Jeffery D. Bierman[1]
Michael Browne
Pakkin Chan[2]
Christopher Cooper
Alexander D. Cronin[3]
Charles Duba
Melanie Felton
Michael Harris
Karsten Heeger
Rebecca Hoffenberger
Michael P. Kelly
Diane M. Markoff
Alan W.P. Poon
Jeffrey Reid
Andrew Sharp
Gregory L. Smith
Alejandro Sonzogni
Kenneth Swartz
David Wright[4]

---

[1] Now at Green River Community College, Auburn, WA.
[2] Now at AT&T Wireless.
[3] Now at Physics Department, University of Washington, Seattle, WA.
[4] Now at Physics Department, University of Washington, Seattle, WA.

Professional Staff
John F. Amsbaugh, Research Engineer
Thomas Burritt, Research Engineer
James Franklin, Research Engineer
Gregory C. Harper, Research Engineer
Mark A. Howe, Research Engineer
Carl E. Linder, Research Engineer
Duncan Prindle, Research Scientist
Richard J. Seymour, Computer Systems Manager
H. Erik Swanson, Research Physicist
Timothy D. Van Wechel, Electronics Engineer
Douglas I. Will, Research Engineer

Technical Staff
Dean T. Corcoran, Engineering Technician
James Elms, Instrument Maker
Allan Myers, Electronics Technician
Hendrik Simons, Instrument Maker, Shop Supervisor
John A. Wootress, Accelerator Technician
Steve Zsitvay, Instrument Maker

Administrative Staff
Barbara J. Fulton, Administrative Assistant
Karin M. Hendrickson, Office Assistant

Part Time Staff
Ryan Allen
Brandon Allgood
Michael Beard
Vassilious Bezzerides
Sara Chanthaseny[5]
Ralph Chestine
Jaime Freeman
Jennifer Harvilla
Karsten Isaacson
Tim Kalka
Hadley Lawler
Steve Martin
Kim Maudlin
John McGrath
John O'Meara[5]
Erik Power
Curtis Reynolds
Christina Scovel
Michael Strombach
Amy Supple
Matthew Wilson
Benjamin Wood[5]

[5] No longer associated with NPL.

9. DEGREES GRANTED, ACADEMIC YEAR, 1995-1996:

"Experimental determination of the distribution of fusion barriers for the systems $^{40}Ca + {}^{192}Os.\ {}^{194}Pt$," Jeffrey Dean Bierman, University of Washington (1995).

"Measurement of the $\beta - \alpha$ angular correlation in the decay of ^{8}Li;" Kenneth Bradley Swartz, University of Washington (1996).

10. LIST OF PUBLICATIONS FROM 1995-96

Published papers:

"Ultradipole radiation in $^{12}C + ^{24,26}Mg$ collisions at E/A = 6-11 MeV/u," M. Kicinska-Habior, K.A. Snover, A. Maj, Z. Drebi, D. Ye and M. Kelly, *Proceedings of the XXIX Zakopane School of Physics* (Zakopane, Poland, 1994) Acta Phys. Pol. B **26**, 439 (1995).

"Charged particle-matter interactions," H. Bichsel, in Atomic and Molecular Physics Handbook, Ch. 87, G. Drake, ed., Amer. Inst. Phys., 1996.

"Atomic and molecular data for radiotherapy and radiation research," H. Bichsel *et al.*, IAEA-TECDOC-799, IAEA, Vienna, Austria, May 1995.

"Stopping powers and ranges for heavy ions," T. Hiraoka and H. Bichsel, Jpn. J. Med. Phys. **15**, 91 (1995).

"Large odd-even effect in RbC_n^- cluster size distributions," R. Vandenbosch and D.I. Will, J. Chem. Phys. **104**, 5600 (1996).

"High-energy fragmentation of C_{60}," R. Vandenbosch, J. Phys. Chem. **99**, 14686, (1995).

"Calculated Bragg curves ionization chambers of different shapes," H. Bichsel, Med. Phys **22**, 1721 (1995).

"Progress and prospects in neutrino astrophysics," J.N. Bahcall, K. Lande, R.E. Lanou, J.G. Learned, R.G.H. Robertson and L. Wolfenstein, Nature **375**, 29 (1995).

"'No-background' maximum likelihood analysis in HBT interferometry," J.G. Cramer, Nucl. Instrum. Methods A **370**, 516 (1996).

"A solenoidal spectrometer for positron-electron pairs produced in heavy-ion collisions," I. Ahmad *et al.*, (APEX Collaboration), Nucl. Instrum. Methods **370**, 540 (1996).

"A wire probe as an ion source for an electron beam ion trap," S.R. Elliott and R.E. Marrs, Nucl. Instrum. Methods B **100**, 529 (1995).

"Positron production in heavy ion collisions: current status of the problem," I. Ahmad *et al.*, (APEX collaboration), Nucl. Phys. A **583,** 247 (1995).

"Antibaryon production in sulfur-nucleus collisions at 200 GeV per nucleon," T. Alber *et al.*, (the NA35 Collaboration), Phys. Lett. B **366**, 56 (1996).

"Measurement of the 3d-4f transition in Ni-like Er for use in a photo-pumped x-ray laser scheme," S.R. Elliott, P. Beiersdorfer and J. Nilsen, Phys. Rev. A **51**, 1683 (1995).

"Measurements of line overlap for resonant spoiling of x-ray lasing transitions in nickellike tungsten," S.R. Elliott, P. Beiersdorfer, B.J. MacGowan and J. Nilsen, Phys. Rev. A **52**, 2689 (1995).

"Structure and Lamb shift of $2s_{1/2}$-$2p_{3/2}$ levels in lithiumlike Th^{87+} through neonlike Th^{80+}," P. Beiersdorfer, A. Osterheld, S.R. Elliott, M.H. Chen, D. Knapp and K. Reed, Phys. Rev. A **52**, 2693 (1995).

"Measurement of two-electron contributions to the ground-state energy of helium-like ions," R.E. Marrs, S.R. Elliott and Th. Stohlker, Phys. Rev. A **52**, 3577 (1995).

"^{36}Ca β decay and the Isobaric Multiplet Mass Equation," A. Garcia, E.G. Adelberger, P.V. Magnus, H.E. Swanson, F.E. Wietfeldt, O. Tengblad and the ISOLDE Collaboration, Phys. Rev. C **51**, 3487 (1995).

"Spin-induced shape changes in light-medium mass compound nuclei," Z.M. Drebi, K.A. Snover, A.W. Charlop, M.S. Kaplan, D.P. Wells and D. Ye, Phys. Rev. C **52**, 578 (1995).

"Evaporation residue, fission cross sections, and linear momentum transfer for ^{14}N induced reactions from 35A to 155A MeV," A.A. Sonzogni, A. Elmaani, C. Hyde-Wright, W. Jiang, D. Prindle, R. Vandenbosch, *et al.*, Phys. Rev. C **53**, 243 (1996).

"Temperature dependence of the level-density parameter," J.P. Lestone, Phys. Rev. C **52**, 1118 (1995).

"Cumulants, coherence, and contamination in multiparticle Bose-Einstein interferometry," J.G. Cramer and K. Kadija, Phys. Rev. C **53**, 908 (1996).

"Inclusive positive pion photoproduction," K.G. Fissum, H.S. Caplan, E.L. Hallin, D.M. Skopik, J.M. Vogt, M. Frodyma, D.P. Rosenzweig, D.W. Storm, G.V. O'Rielly and K.R. Garrow, Phys. Rev. C **53**, 1278 (1996).

"Transverse momentum dependence of Bose-Einstein correlations in 200A GeV/c S + A collisions," D.T. Alber *et al.* (the NA35 collaboration), Phys. Rev. Lett. **74**, 1303 (1995).

"Search for narrow sum-energy lines in electron -positron pair emission from heavy-ion collisions near the Coulomb barrier," I. Ahmad *et al.*, (APEX collaboration), Phys. Rev. Lett. **75**, 2658 (1995).

"Transverse energy production in ^{208}Pb+Pb collisions at 158 GeV per nucleon," T. Alber *et al.*, (The NA49 Collaboration), Phys. Rev. Lett. **75**, 3814 (1995).

"Experimental fusion barrier distributions reflecting projectile octupole state coupling to prolate and oblate target nuclei," J.D. Bierman, P. Chan, J.F. Liang, M.P. Kelly, A.A. Sonzogni and R. Vandenbosch, Phys. Rev. Lett. **76**, 1587 (1996).

"Two-pion Bose-Einstein correlations in nuclear collisions at 200 GeV/nucleon," T. Alber *et. al.* (the NA35 Collaboration), Z. Phys. **66**, 77 (1995).

Papers submitted or to be published:

"Energies of neon-like n=4 to n=2 resonance lines," J. Nilsen, P. Beiersdorfer, K. Widmann, V. Decaux and S.R. Elliott, submitted to Phys. Rev. A.

"Search for 1s2s $^3S_1$ - 1s2p $^3P_2$ decay in U^{90+}," P. Beiersdorfer, S.R. Elliott, and others, accepted by Phys. Rev. A.

"Nonstatistical γ emission in ^{3}He and α – induced reactions," J.A. Behr, K.A. Snover, C.A. Gossett, G. Feldman, J.H. Gundlach and M. Kicinska-Habior, Phys. Rev. C, in press.

"Analysis of α-particle emission from ^{19}F + ^{181}Ta reactions leading to evaporation residues," J.P. Lestone, Phys. Rev. C, to be published.

"Structure of ^{18}Ne and the breakout from the hot CNO cycle," K.I. Hahn, A. Garcia, E.G. Adelberger, P.V. Magnus, A.D. Bacher, N. Bateman, G.P.A. Berg, J.C. Blackmon, A.E. Champagne, A.J. Howard, J. Liu, B. Lund, Z.Q. Mao, P.D. Parker, M.S. Smith, E.J. Stephenson, K.B. Swartz, S. Utku and R.B. Vogelaar, Phys. Rev. C, to be published.

"A new technique for measuring Newton's Constant *G*," J.H. Gundlach, E.G. Adelberger, B.R. Heckel and H.E. Swanson, submitted to Phys. Rev. D.

"Disappearance of entrance channel dependence of fission fragment anisotropies at well-above barrier energies," R. Vandenbosch, J.D. Bierman, J.P. Lestone, J.F. Liang, D.J. Prindle, A.A Sonzogni, S. Kailas, D.M. Nadkarni and S.S. Kapoor, submitted to Phys. Rev. Lett.

"Trapped-ion technique for measuring the nuclear charge radii of highly charged radioactive isotopes," S.R. Elliott, P. Beiersdorfer and M.H. Chen, Phys. Rev. Lett., accepted for publication.

"Neutrino," J.F. Wilkerson, McGraw-Hill Encyclopedia of Science and Technology, Eighth Edition, to be published.

"Giant Resonances," K.A. Snover, McGraw-Hill Encyclopedia of Science and Technology, Eighth Edition, to be published.

Abstracts and other conference presentations by NPL personnel:

"Solar neutrinos and G. Garvey," J. F. Wilkerson, *Symposium in Honor of G.T. Garvey*, Los Alamos, NM, Jan. 1995.

"APEX and the e^+/e^- puzzle: recent results," I. Ahmad *et al.*, (APEX collaboration), presented by T.A. Trainor, *Proceedings of the 12th Winter Workshop on Nuclear Dynamics*, Snowbird, UT, Feb. 1996, eds. W. Bauer and G.D. Westfall.

"The Russian-American Gallium solar neutrino experiment," S.R. Elliott, J.F. Wilkerson and others, *Proceedings. of the XXXth Rencontres de Moriond, Electroweak Interactions and Unified Theories*, Les Arcs, Savoie, France, March 1995.

"Experimental neutrino physics, advancing beyond the standard model?" J.F. Wilkerson, Invited paper, *1996 PASCOS Meeting*, Baltimore, MD, March 1995.

"Progress in the search for time reversal invariance violation in neutron decay," J.F. Wilkerson, R.G.H. Robertson, S.R. Elliott *et al.*, Bull. Am. Phys. Soc. **40**, 2 (1995).

"Recent results of neutrino experiments," J.F. Wilkerson, Invited Review talk, *SNO Collaboration Meeting*, Toronto, April, 1995.

"An object-oriented software Bus," F. McGirt and J.F. Wilkerson, Invited paper, *Ninth Conference on Real-Time Computer Applications in Nuclear, Particle and Plasma Physics*, Michigan State University, East Lansing, MI, May 1995.

"The Sudbury Neutrino Observatory data acquisition system," J.F. Wilkerson, Q.R. Ahmad, S.R. Elliott *et al.*, Invited Talk, *Ninth Conference on Real-Time Computer Applications in Nuclear, Particle and Plasma Physics*, Michigan State University, East Lansing, MI, May, 1995.

"Solar neutrinos: The next generation," J.F. Wilkerson, Invited Talk, *Gordon Research Conference on Nuclear Physics,* Tilton, HN, July, 1995.

"Preliminary results from the Russian-American Gallium Experiment Cr-neutrino Source measurements," S.R. Elliott, J.F. Wilkerson and others, *Proceedings of the IV International Workshop on Theoretical and Phenomenological Aspects of Underground Physics*, Toledo, Spain, Sept. 1995.

"A beat frequency buncher," D.W. Storm, D.T. Corcoran and G.C. Harper, *7th International Conference on Heavy Ion Accelerator Technology*, Canberra, Australia, Sept. 95, to be published in Nucl. Instrum. Methods.

"Terminal ion source for an FN tandem," G.C. Harper, *7th. International Conference on Heavy Ion Accelerator Technology*, Canberra, Australia, Sept. 95, to be published in Nucl. Instrum. Methods.

"Search for fundamentally new interactions with ranges down >1cm," J.H. Gundlach, *Proceedings of the 7th Marcel Grossman Meeting on General Relativity*, eds. R. Ruffini and M. Kaiser, World Science Publishing Inc. (1995).

"Monte Carlo calculation of track structure," H. Bichsel, Invited paper presented at *Int. Rad. Res. Conf.* in Wuerzburg, Germany, Aug. 1995.

"Precise measurements of energy loss of heavy ions," H. Bichsel and T. Hiraoka, Contributed paper, *Sympmosium on Radiation Therapy with Heavy Ions*, GSI, Darmstadt, Germany (1995).

"The solar neutrino deficit - principle and interest (a modern problem)," R.G.H. Robertson, to be published in Proc. *7th International Conference on the Structure of Baryons* ("Baryons '95"), Sante Fe, NM, Oct. 1995.

"Solar neutrinos measurements: current status and future experiments," J.F. Wilkerson, *Orbis Scientiae 1996*, Jan. 1996.

"A new torsion balance technique for measuring Newton's Constant *G*," J.H. Gundlach, talk given at the *XXXI Recontres de Moriond on Dark Matter in Cosmology, Quantum Measurements and Experimental Gravitation*, Les Arcs, France, Jan. 1996.

"Solar neutrinos: remarkable measurements, surprising implications," J.F. Wilkerson, Invited Talk, *Pacific Northwest Association of College Physics Meeting*, Auburn, WA, March, 1996.

"Overview of the current spectroscopy effort on the Livermore electron beam ion traps," P. Beiersdorfer, S.R. Elliott and others, *Proceedings of the 1st Euroconference on Atomic Physics with Stored Highly Charged Ions*, Heidelberg, Germany, March 1995, to be published.

"Results from the Russian-American Gallium experiment Cr-neutrino source measurement," S.R. Elliott for the SAGE Collaboration, Spring meeting of American Physical Society, Bull. Am. Phys. Soc. **41**, 897, (1996).

"The problem of the missing solar neutrinos," R.G.H. Robertson, Invited paper, Spring meeting of American Physical Society, Bull. Am. Phys. Soc. **41**, 904 (1996).

"The emiT experiment - a search for time reversal invariance violation," S.R. Elliott, R.G.H. Robertson, T.D. Steiger, J.F. Wilkerson and others, Spring meeting of American Physical Society, Bull. Am. Phys. Soc. **41**, 963, (1996).

"A polarized cold neutron beam for fundamental physics," J.F. Wilkerson and others, Spring meeting of American Physical Society, Bull. Am. Phys. Soc. **41**, 964, (1996).

"Entrance channel effects in the ^{156}Er compound nucleus decay," J.F. Liang, J.D. Bierman, M.P. Kelly, A.A. Sonzogni, R. Vandenbosch and J.P.S. van Schagen, paper, Spring meeting of American Physical Society, Bull. Am. Phys. Soc. **41**, 965, (1996).

"Spin assignments in ^{37}K and B(GT) distribution in the A. = 37 system," E.G. Adelberger and others, Spring meeting of American Physical Society, Bull. Am. Phys. Soc. 41, 986, (1996).

"An apparatus to measure the PNC spin rotation of transmitted cold neutrons in a liquid heliulm target," D.M. Markoff, E.G. Adelberger, J.H. Gundlach, B.R. Heckel, S.K. Lamoreaux, S.D. Penn, H.E. Swanson and others, Spring meeting of American Physical Society, Bull. Am. Phys. Soc. 41, 1034, (1996).

Conference presentations by collaborators of NPL personnel:

"First results from NA49 on Pb+Pb collisions at 158 GeV/nucleon," S. Margetis for the NA49 Collaboration, *Invited paper presented at Quark Matter '95*, Monterey, CA, Jan. 1995 and to be printed in the Conference Proceedings.

"First results from experiment NA49 from the study of Pb-Pb collisions at 158 GeV per nucleon projectile energy," P. Seyboth for the NA35 Collaboration, *Proceedings of the 1995 International Symposium of Multiparticle Dynamics*, Stara Lesna, and to be printed in the Conference Proceedings.

"First Pb+Pb results from experiment NA49 and a comparison with S+A results from NA35," T. Alber for the NA49 Collaboration, *Proceedings of the 'Recontres de Moriond'*, (1995).

"First results from Experiment NA49," H. Rudolph for the NA49 Collaboration, *Presented at 11th Winter Workshop on Nuclear Dynamics*, Key West, FL, Feb. 1995, and to be printed in the Conference Proceedings.

"FT-ICR mass spectrometry of very highly charged atomic ions," L. Schweikhard, B. Beck St. Becker, P. Beiersdorfer and S.R. Elliott, *Proceedings of 43rd Conference of the Amer. Soc. of Mass Spectrometry*, Atlanta, GA, May 1995, to be published.

"A new look at positron production from heavy-ion collisions: results from APEX," I. Ahmad *et al.*, (APEX collaboration), Invited talk presented by F.L. H. Wolfs, *Proceedings of the IV International Symposium on Weak and Electromagnetic interactions in Nuclei*, Osaka, Japan, June, 1995, to be published by World Scientific, Singapore, eds., H. Ejiri, T. Kisimoto and T. Sato.

"The positron peak puzzle - recent results from APEX," I. Ahmad *et al.*, (APEX collaboration), presented by R. Betts, *Proceedings of the XXIV Mazurian Lakes School of Physics*, Piaski, Poland, Aug. 1995, Acta Physica Polonica, in press.

"Results from SAGE," J.N. Abdurashitov, S.R. Elliott, J.F. Wilkerson and others, *Proceedings of the IV International Workshop on Theoretical and Phenomenological Aspects of Underground Physics*, Toledo, Spain, Sept. 1995.

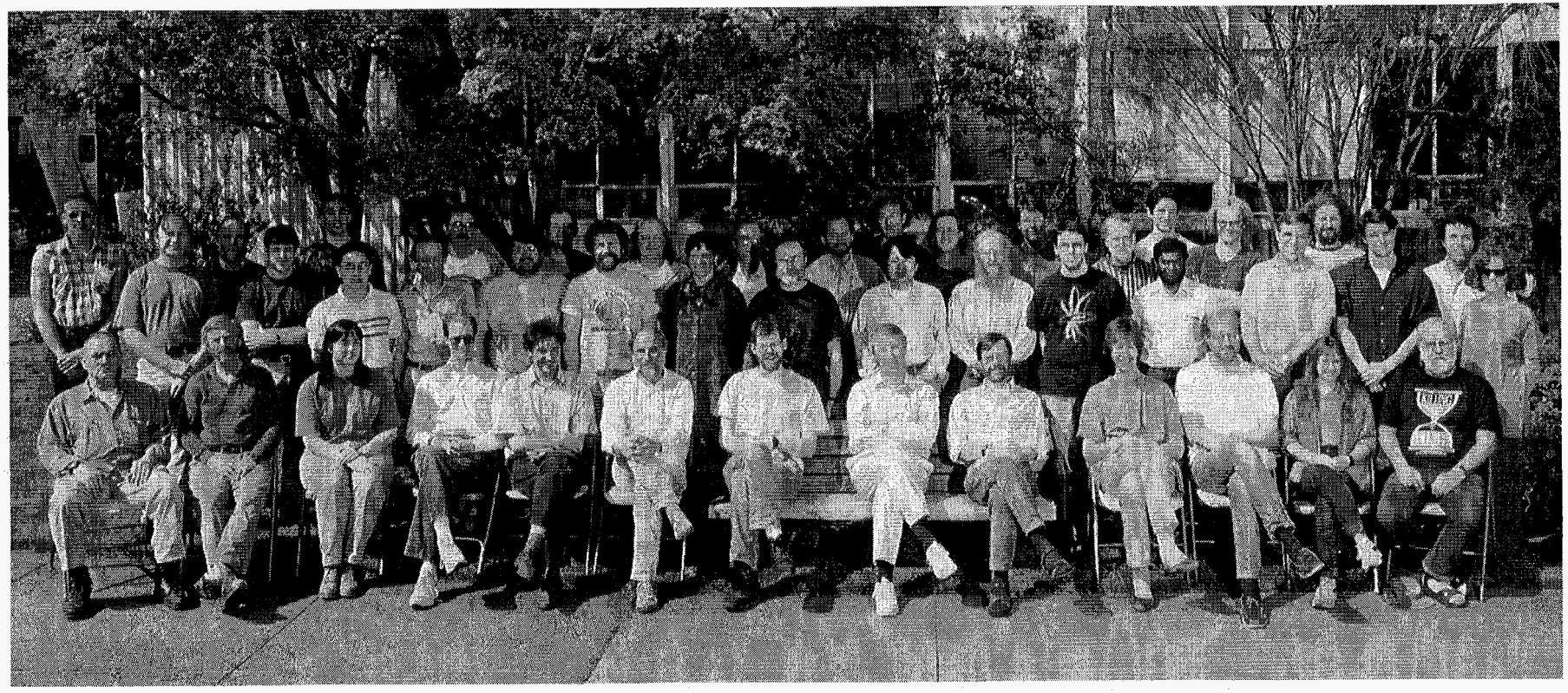

FRONT ROW: JOHN WOOTRESS, KURT SNOVER, MELANIE FELTON, STEVE ELLIOTT, JENS GUNDLACH, ERIC ADELBERGER, GREG SMITH, HAMISH ROBERTSON, TOM TRAINOR, BARB FULTON, MARK HOWE, DIANE MARKOFF, CARL LINDER

SECOND ROW: TOM STEIGER, KEN SWARTZ, FELIX LIANG, MARCUS BECK, ALLAN MYERS, STEVE PENN, REENA MEIER DREES, DOUG WILL, ALAN POON, DICK SEYMOUR, JEFFREY REID, DHAMMIKA WEERASUNDARA, DEAN CORCORAN, CHARLES DUBA, KARIN HENDRICKSON

THIRD ROW: JIM BECK, DEREK STORM, MIKE KELLY, JOHN MCGRATH, STEVE ZSITVAY, DUNCAN PRINDLE, JOHN CRAMER, TIM VAN WECHEL, MIKE HARRIS, STEPHEN BAILEY, KARSTEN HEEGER, ERIK SWANSON, ANDREW SHARP, JOS VAN SCHAGEN, GREG HARPER, JOE GERMANI